Manning Diversified Forest Products Research Trust Fund
FDRP9/95

Quantifying Extreme Winds in Experiments Aimed at Reducing Wind Damage to Released White Spruce Understories – **Final Report**

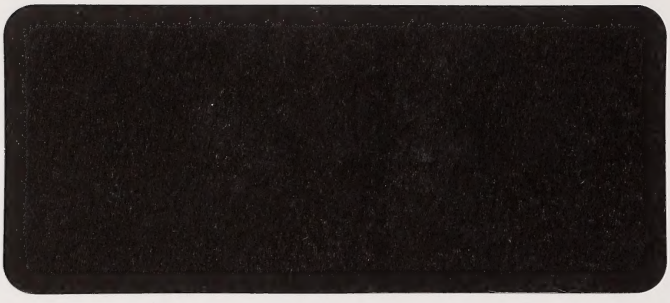

Manning Diversified Forest Products
Research Trust Fund
FDRP9/95

Quantifying Extreme Winds in Experiments Aimed at Reducing Wind Damage to Released White Spruce Understories – **Final Report**

October 1998

By Drs. Thomas K. Flesch and John D. Wilson
Department of Earth and Atmospheric Sciences
University of Alberta
Edmonton, Alberta
Canada

Pub. No. T/329
ISBN: 0-7732-5054-9

DISCLAIMER

The study on which this report is based was funded by the Environmental Protection and Enhancement Fund (EPEF). The views, statements and conclusions expressed and the recommendations made in this report are entirely those of the authors and should not be construed as statements or conclusions or expressing the opinions of the Manning Diversified Forest Products Integrated Technical Sub-Committee.

EXECUTIVE SUMMARY

Within the next 60 to 80 years, spruce that has developed under the protection of hardwoods will be the main source of spruce timber in the boreal mixedwoods of western Canada. However, much of the inventoried hardwood stands are scheduled for harvest using conventional methods that destroy the spruce understory. An effort is being made to develop procedures to protect the associated spruce understory during this harvest. A difficulty is that even if the understory survives the hardwood harvest, it is susceptible to wind damage. Project 8032, "Harvesting options to favour immature white spruce and aspen regeneration in boreal mixedwoods", is a project[1] to test harvest methods that may reduce wind damage in the "released" spruce understory. Conventional logging equipment is used, but with innovative approaches to cutblock design, including different cut widths, and different harvest levels. The study is located at Hotchkiss River, northwest of Manning, Alberta.

Critical to the assessment of these new harvest methodologies is an understanding of wind climatology at the study site. In particular it is necessary to know: i) the ambient wind characteristics encountered during the lifetime of the Hotchkiss silvicultural study; and ii) the effect of the different harvest designs on wind flow, and windthrow risk, within harvest cutblocks. We have just finished a four-year project that attempts to provide answers to these two questions. The following report documents our results. This work is divided into five distinct, stand-alone chapters (Chapters 2 through 5 have been written in a form suitable for publication in technical, scientific journals).

In Chapter 1 we examine the wind record as measured over 4 ½ years at a weather station adjacent to the Hotchkiss site. These observations are used to determine how the ambient winds at Hotchkiss relate to the historic climatology of the region. In Chapter 2 our focus changes toward a detailed examination of the winds *within* two cutblocks at Hotchkiss. Because windthrow is not simply a matter of wind -- tree mechanical properties are also important -- we investigate how cutblock wind patterns relate to tree sway (we believe tree sway to be a better indicator of windthrow than the wind). This work is described in mathematical detail in Chapter 3. In Chapter 4 we detail our construction of a computer model to predict the wind flow within different cutblock designs (this chapter is also highly mathematical in form). Finally, in Chapter 5 we apply our wind flow model to identify shelterwood designs that minimize the likelihood of remnant spruce windthrow. The following are brief summaries of each of these chapters.

Summary of Chapter 1, "Monitoring and Interpretation of Maximum Windspeeds at Hotchkiss River, Alberta"

This chapter describes, and interprets, the maximum wind events which we measured at the Hotchkiss silviculture site from 9 October 1993 to 19 March 1998. Over this period there were 28

---

[1] A joint project including Forestry Canada, Forest Engineering Research Institute of Canada, Daishowa-Marubeni International, and Alberta Environmental Protection.

days in which wind gusts exceeded 60 km/hr, with most of these extreme events having a southwest-west-northwest direction. The maximum windspeed recorded at Hotchkiss was 81 km/hr from the west. The highest wind events occurred overwhelmingly in the spring (with March being the windiest month). The most "active" year was 1994, with 13 days of winds above 60 km/hr. The "quietest" year was 1995, with three days over 60 km/hr.

Based on historic climatology, we conclude that the wind experienced at Hotchkiss during this period did not depart substantially from the climatological average for the region. We saw no evidence of catastrophic (or even unusually strong) events at Hotchkiss that would substantially alter the interpretation of Project 8032 results.

A secondary issue examined in our study was the spatial representativeness of wind data collected at weather stations. We compare the maximum winds measured daily at Hotchkiss with those measured at the Manning airport (30 km apart). Based on this comparison, we conclude that distant weather stations can be used to infer the long-term wind climatology of an area (if the terrain is not too extreme). However, trying to use remote weather stations to estimate the windspeed on specific days is not advisable.

Summary of Chapter 2, "Measured Wind in Experimental Cutblocks"

In this chapter we characterise the winds across two shelterwood cutblocks at Hotchkiss: a narrow cutblock whose width was 1.7 forest heights (40 m), and a wide cutblock whose width was 6.1 forest heights (140 m). Wind and turbulence measurements were made at height of 9 m, representing the wind affecting understory trees. Our measurements occurred when the wind direction was across the cutblock width.

In both cutblocks the best wind shelter was near the upwind forest edge, where the average windspeed and turbulence were reduced to approximately 20% of their corresponding large-clearing values. The average windspeed increased slowly with downwind distance (x) across the cutblocks. The pattern of turbulence was different. Turbulence increased rapidly with x immediately downwind of the forest, then attained near-constancy beyond 70 m downwind of the forest edge (in the wide cutblock), at a level above its clearing value. Based on these observations, we conclude that effective cutblock wind shelter (for understory trees) occurs within three forest heights of the upwind forest edge, where both the average wind velocity and the turbulence are reduced relative to their levels in larger clearings.

Summary of Chapter 3, "Relating Measured Tree Sway to Wind Statistics".

In this chapter we describe our attempts to quantify wind shelter in terms of tree sway (we believe tree sway to be a better indicator of windthrow than wind statistics). We investigate the relationship between wind statistics and tree sway in two shelterwood cutblocks at Hotchkiss: a narrow cutblock whose width was 1.7 forest heights (40 m), and a wide cutblock whose width was 6.1 forest heights (140 m). We focus on the case of winds oriented across the cutblock width. A simple mass-spring-damper tree displacement model, calibrated to tree sway measurements, is used to infer the windthrow protection in the sheltered cutblocks.

Our approach is to predict a threshold average wind velocity in the open (U_w, essentially an *average* weather station windspeed -- not a gust speed) which correlates with the occurrence of windthrow of remnant spruce in the cutblocks. Our assumption is that an average velocity of 10 m s^{-1} (36 km/hr) will cause windthrow of unprotected trees in the open. Larger windspeeds (U_w) are needed to cause windthrow in the cutblocks.

In the wide cutblock, U_w varies from 13 m s^{-1} (47 km/hr) near the downwind forest edge to 25 m s^{-1} (90 km/hr) near the upwind edge. In the narrow cutblock U_w varies from 19 m s^{-1} (68 km/hr) at the downwind edge to 30 m s^{-1} (108 km/hr) at the upwind edge. The most effective wind shelter, as given by the highest U_w, is within 70 m of the upwind forest. Given these values, and local wind climatology, we conclude that windthrow would occur only in the downwind portion of the wide cutblock, and not at all in the narrow cutblock. Our results reinforce the speculation of Chapter 2: in designing cutblocks to reduce windthrow, cutblocks should not exceed three forest heights in width.

Summary of Chapter 4, "A Wind Flow Model to Diagnose Spatial Variation in Cutblock Winds".

In Chapter 3 we demonstrated that tree sway can be related to simple wind statistics. Therefore, the spatial pattern of wind statistics over the landscape, if known, arguably maps the relative risk of windthrow - suggesting a computer wind model can provide the basis to interpret spatial patterns of windthrow, and guide strategies with respect to that concern.

To test this idea, we adopt a simple flow model able to describe both the average wind and kinetic energy of the turbulence. We first compare this model with others' measurements of wind near forest edges, then simulate our own observations at Hotchkiss. We show that the model predicts well the spatial variation of the mean windspeed and turbulent kinetic energy, these being the wind statistics having greatest impact upon tree sway.

Summary of Chapter 5, "Using a Wind Flow Model to Identify Harvest Designs that Reduce Windthrow"

In this, the culmination of our work, we demonstrate how a computer wind flow model can be used to determine the windthrow risk associated with a harvest design. Here we have collaborated with Canadian Forest Service scientists Dan MacIsaac and Stan Lux to examine the "optimum" configuration of a shelterwood harvest system.

In shelterwood design (more precisely a one-pass modified uniform shelterwood design), forest strips provide wind shelter for immature spruce in the cutblocks. We define an optimum shelterwood design as one minimizing windthrow, but at the same time minimizing the percentage of forest retained as windbreak strips (maximizing aspen harvest), and maximizing the width of the individual cutblocks. Our wind model is used to search for an optimum design (for the circumstances at Hotchkiss).

While delineation of a truly optimal design requires economic and engineering judgements to supplement our "environmental" calculations, our results lay out likely bounds to an optimum design. We show that 10% forest retention does not provide adequate wind protection, while retaining more than 30% is unnecessary. Cutblocks wider than three forest heights (70 m at Hotchkiss) are at significantly higher risk than narrower cutblocks, while little benefit comes from using cutblocks narrower than two forest heights (45 m at Hotchkiss).

Study Conclusions

The first objective of our study was to determine the ambient wind climatology encountered at the Hotchkiss silvicultural study (as opposed to the small-scale wind features found within specific harvest cutblocks). We found that:

i) The wind experienced at Hotchkiss from October 1993 to March 1998 did not depart substantially from the climatological average for the region. We saw no evidence of catastrophic (or even unusually strong) events that would substantially alter the interpretation of Project 8032 results.

The second, and more substantial objective of our study was to determine the effect of the different cutblock designs on wind flow, and therefore windthrow potential. We found that:

ii) Wind sheltering in a long and narrow rectangular cutblock is greatest when the wind is oriented across the narrow width of the cutblock, as opposed to along its length. This simply confirms earlier assumptions that cutblocks should be oriented perpendicular to the expected direction of maximum winds. In northern Alberta, this means cutblocks should be oriented in a north - south direction.

iii) A "quiet" zone/"wake" zone picture provides a good description of cutblock winds. When the wind is oriented across a cutblock, the quiet zone, where the average windspeed and turbulence are reduced from values in a large clearing, extends from the upwind forest to three forest heights downwind of the forest (for an understory spruce which is half the full overstory height). Downwind of this quiet zone will be a wake zone (if the cutblock extends this far), where the turbulence will be above the level seen in very large clearings. We believe this pattern exists across a wind range of cutblocks (with different dimensions, different upstream features, and different forest architectures).

iv) Our field observations at Hotchkiss strongly suggest that cutblocks whose width is less than three forest heights provide very good shelter for remnant understory spruce (at least for cutblocks that have an upwind forest border greater than two forest heights in width). This is because trees in these cutblocks are not exposed to the "wake" zone. While larger cutblocks will provide some wind shelter, those trees farther than three forest heights from the forest edge will be exposed to turbulence as energetic as found in very large clearings.

v) A high resolution wind flow model, based on physical principles, can be constructed to accurately predict wind statistics across a range of different forest cutblock types.

vi) Based on wind model simulations, we speculate that an optimum shelterwood design (i.e., a one-pass modified uniform shelterwood design minimizing understory windthrow) would retain 10 to 30% of the forest in shelterwood strips that separate cutblocks which are between two and three forest heights in width.

ACKNOWLEDGEMENTS:

We are grateful for the help of Dr. Stan Navratil and Lorne Brace in initiating this work, and Stan Lux for his help in the field. Dan MacIsaac's ideas were also appreciated. Thanks also to J.P. Bielech and Clarence at Manning Diversified Forest Products for helping us stay clear of chainsaws. A special thanks to Terry Thompson: this work would not have been possible without him.

TABLE OF CONTENTS:

LIST OF TABLES:

CHAPTER 1

CHAPTER 2

CHAPTER 3

CHAPTER 5

LIST OF FIGURES:

CHAPTER 1

CHAPTER 2

CHAPTER 3

CHAPTER 4

CHAPTER 5

CHAPTER 1

MONITORING AND INTERPRETATION OF MAXIMUM WINDSPEEDS AT HOTCHKISS RIVER

Thomas K. Flesch

1. Introduction

Large portions of the Canadian boreal forest have a predominately aspen (Populus tremuloides) overstory with a white spruce (Picea glauca) understory. In some cases a selective harvesting of the mature aspen may be commercially worthwhile, leaving the "released" spruce understory for future harvest. This "two-stage" harvest system is also ecologically attractive, as it better maintains "mixedwood" diversity compared with the traditional alternative of aspen clear-cutting. An obstacle to a two-stage harvest is the susceptibility of the remnant spruce to windthrow (uprooting). Developed under a sheltered aspen canopy, individual spruce trees have poor wind stability, making them vulnerable to the increased wind exposure that accompanies aspen removal.

Project 8032, entitled "Harvesting options to favour immature white spruce and aspen regeneration in boreal mixedwoods", is a joint project by Forestry Canada, the Forest Engineering Research Institute of Canada, Daishowa-Marubeni International, and Alberta Environmental Protection. The project tests different harvest methods that may be useful in minimizing wind damage in the spruce understory. Conventional logging equipment is used, but with innovative approaches to cutblock design, including different cut widths, and different harvest levels. The project is located at Hotchkiss River, northwest of Manning, Alberta.

Critical to the assessment of new methodologies in this project, is an understanding of the wind climatology. In particular it is necessary to know whether the extreme wind characteristics encountered at Hotchkiss during the period of Project 8032 are typical given the long term climatology of the region. Is the success, or failure, of a harvest scheme at Hotchkiss due to unusually strong, or unusually weak winds? A secondary question we will examine is whether wind observations taken in the climatological network can be used to characterise the winds at distant forest locations?

2. Wind Measurements

Windspeeds were measured at two sites in support of Project 8032. One was adjacent to the silviculture trials (hereby referred to as the "Hotchkiss site"). The other was at the Manning, Alberta airport. The Hotchkiss location was selected to give the "ambient" wind conditions experienced on-site. The Manning airport location was chosen as representing a typical regional weather station.

2.1. Hotchkiss site

In consultation with Forestry Canada, harvest site CC4 was selected as our Hotchkiss site. This cutblock borders the northwest edge of the silviculture trials, located immediately west of harvest treatment F7 (Figure 1.1). Cutblock CC4 is an irregularly shaped, clear-cut section. A tower was placed near the centre of the section. The tower is located approximately 60 m from the service road that runs through the cutblock. At its closest point, the forest edge is approximately 275 m from the tower. The distance from the tower to the forest edge by direction is approximately: North - 275 m; East - 400 m; South - 300 m; West - 500 m. The surrounding forest is approximately 25 m in height.

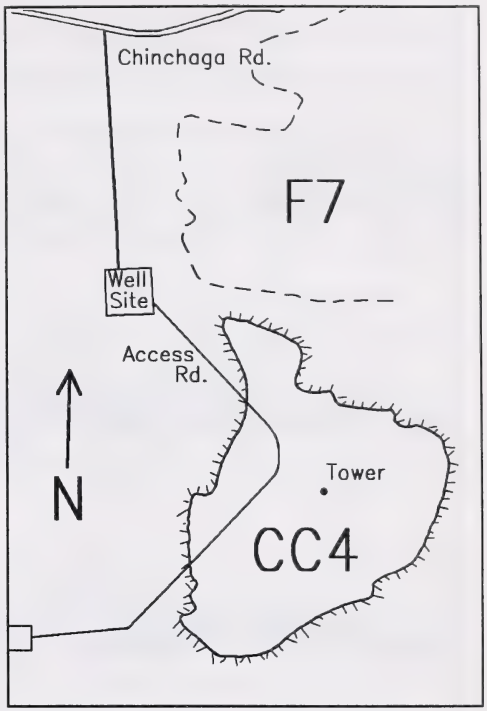

Figure 1.1. Tower location at the Hotchkiss site (not drawn exactly to scale).

The terrain in CC4 is relatively flat, sloping gently downward toward the Hotchkiss River to the south. The ground is rough, strewn with tree debris and aspen seedlings. Larger trees are isolated throughout CC4; the nearest is 48 m to the west-southwest of the tower, with another 51 m to the southwest. We believe that they have an insignificant effect on the wind measurements.

The meteorological tower consisted of a 12 m tall Delhi triangular tower with a 3 m pipe extension. Two wind sensors were deployed on the tower. An R.M. Young propvane (model 05103-10) was installed at a height of 15 m. This propvane is a combination anemometer (for measuring windspeed) and wind vane (giving wind direction). Important specifications of the R.M. Young propvane are:

Windspeed:	Threshold	3.6 km/hr
	Range	0 - 216 km/hr
	Gust Survival:	360 km/hr
	Distance Constant:	2.7 m for 63% recovery
Direction:	Threshold:	3.6 km/hr
	Delay Distance:	1.3 m for 50% recovery
	Damping Ratio:	0.25

The second sensor was a Met-One (model 013A) cup anemometer, which was installed at a height of 9 m. Our intent was to use the two anemometers to compare the gust characteristics at two different heights. In the end, we concluded that the difference in measurement characteristics of the

two anemometers was significant enough to confound any examination of the slight differences between the winds at the two heights. Although we monitored windspeeds from the Met-One anemometer throughout the study, we will not report on these windspeeds.

A Campbell Scientific CR10-55 datalogger remotely recorded the wind measurements. The datalogger was mounted on the tower in a white fiberglass-reinforced enclosure, at a height of 2.5 m above the ground. The wind measurements filled the datalogger memory roughly every 3.5 months. A 10-Watt solar panel was used to power the datalogger.

Instrumentation was placed at the site during October 1993, with the first full day of measurements starting on 9 October, 1993. The following information was recorded:

- *Hourly* maximum windspeed (2 second average) and associated wind direction
- *Hourly* average windspeed and direction for each hour.
- *Daily* maximum windspeed which occurred for each of the 8 cardinal points of the compass (N, NE, E, SE, S, SW, W, NW).

This information was recorded without interruption up to 19 March 1998.

2.2. Airport site

Permission was received from Environment Canada and Alberta Transportation to place instruments on the meteorological tower at the Manning Airport. This tower is located over short grass (mowed regularly), and is approximately 50 m west of the airport office. The expansive grass surrounding the airport tower represents the ideal for weather stations in Canada.

An R.M. Young propvane, as described above, was installed at a height of 8.5 m on the tower. A Campbell Scientific CR10 datalogger was used to record the wind measurements. The measurements filled the memory of the datalogger roughly every 4 months. Every 3 months we downloaded the data. A car battery was initially used to power the datalogger, but was replaced by a solar panel in 1995. The same wind information as was collected at the Hotchkiss site was collected at the airport beginning on 8 October, 1993.

3. Summary of Extreme Winds from October 93 to March 98

3.1. Hotchkiss site

Daily maximum windspeeds at Hotchkiss are illustrated in Figure 1.2 for the 1623 days from 9 October 1993 to 19 March 1998. Over this period there were 28 days in which winds exceeded 60 km/hr at the measurement height of 15 m (1.7% of the days), or 78 hours with gusts exceeding 60 km/hr (0.2% of the hours). Table 1.1 lists the days where the wind exceeding 60 km/hr, with the maximum daily windspeed and associated wind direction. The maximum windspeed recorded at Hotchkiss was 80.8 km/hr, recorded at 2:26 p.m. on 14 November 1993.

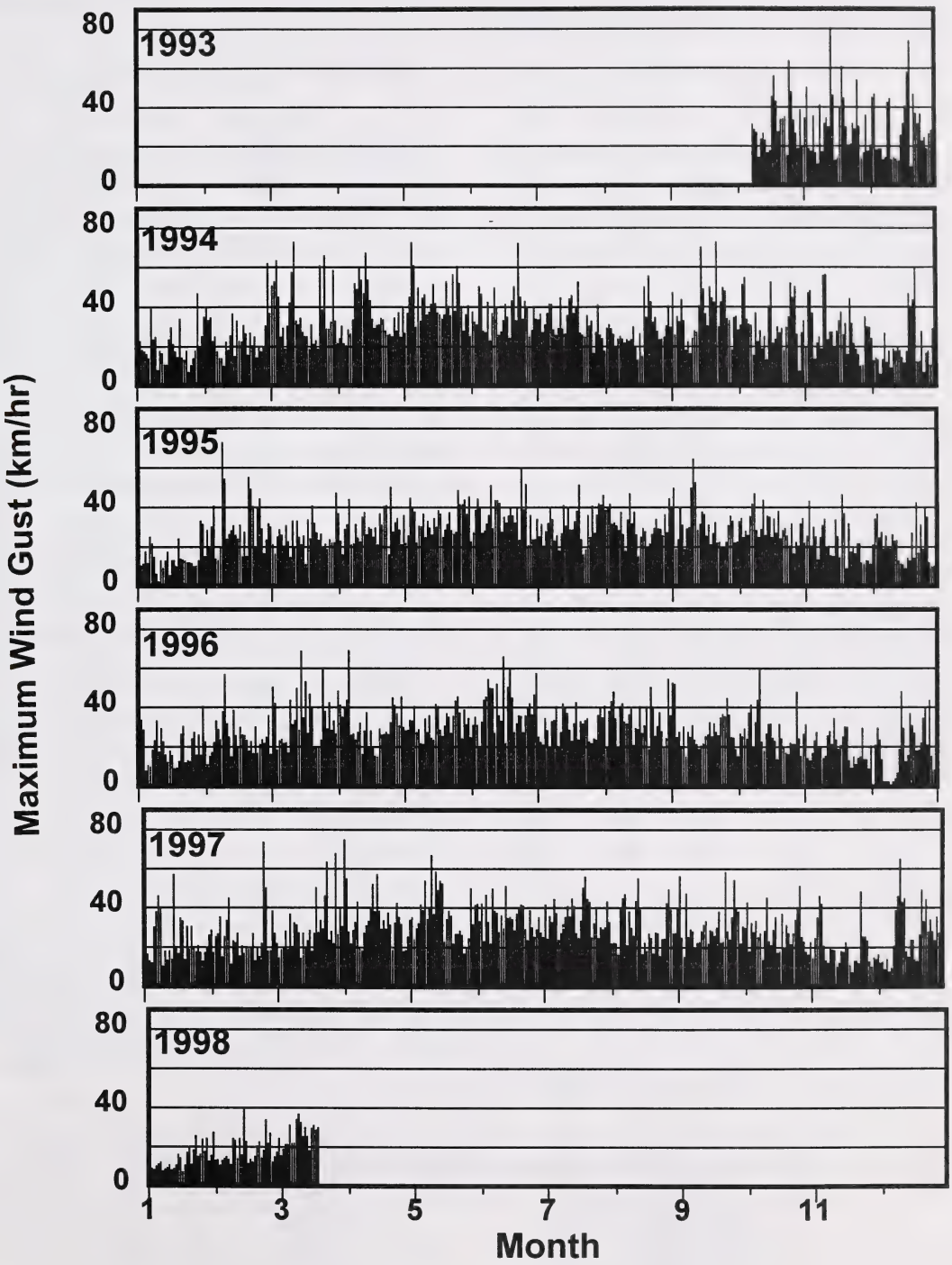

Figure 1.2. Daily maximum windspeeds recorded at the Hotchkiss site northwest of Manning, Alberta, from October 1993 through March 1998.

Table 1.1. Dates when the wind exceeded 60 km/hr at either Hotchkiss or the Manning airport during the period October 93 through March 98.

Date	Hotchkiss		Manning Airport	
	Windspeed (km/hr)	Dir	Windspeed (km/hr)	Dir
93/10/26	63.9	SW	73.7	W
93/11/14	80.8	W	96.7	W
93/11/19	61	W	74.1	SW
93/11/20	44.8	N	72.7	SW
93/12/11	44.5	W	64.9	W
93/12/19	58.2	NW	60.7	NW
93/12/20	74.1	NW	77.3	NW
94/3/1	62.1	W	65.3	W
94/3/5	63.5	W	57.9	SW
94/3/13	73	SW	78	W
94/3/25	61	NW	71.3	NW
94/3/27	66	NW	49	NW
94/4/12	60	W	53.3	SW
94/4/13	53.6	W	64.5	W
94/4/15	67.4	W	67.4	W
94/5/6	72.7	W	70.2	W
94/5/7	61	W	69.2	NW
94/5/27	60.7	SW	65.6	SW
94/7/13	44.8	NW	91	NW
94/8/14	23.7	NE	69.2	W
94/9/15	70.2	SW	64.5	SW
94/9/22	73	W	82.2	SW
94/12/22	59.8	SW	63.5	SW
95/2/8	72.9	W	69.3	NW
95/2/9	54.5	W	63.3	NW
94/6/24	72.3	SW	53.3	NW
95/6/25	60	W	52.2	W
95/9/11	64.5	W	61.2	W
96/3/15	69	N	58.9	NW
96/3/25	60.5	N	58.2	NW
96/4/6	69.3	N	86.4	SW
96/6/16	66.1	SW	59.3	SW
96/6/18	50.6	NW	64.2	NW
96/6/19	59.3	NW	72	N
96/6/26	36	SE	65.6	SW
96/7/14	40	SW	75.9	W
96/10/11	59.6	W	62.8	W
97/2/24	73.7	W	71.3	W
97/3/20	50.4	W	62.5	W
97/3/25	63.5	W	66	W
97/3/29	67.9	SW	82.2	SW
97/4/2	75	SW	66	SW
97/5/12	67	NW	73.7	NW
97/5/14	58.6	S	75.1	S
97/5/16	53.8	SW	60.7	SW
97/7/20	50.4	SW	65.3	SW
97/8/14	55.2	N	60.3	NW
97/9/27	54.3	W	67.4	W
97/12/11	45.9	SW	60.7	SW
97/12/12	65.1	W	75.5	W
97/12/22	49.4	SW	62.5	SW

A visually obvious trend in Figure 1.2 is that the number of "quiet days", days in which the maximum windspeed was below 20 km/hr, was greater in the winter (Nov - Feb) than at other times. There is another more important feature hidden in the "noise" of Figure 1.2: the highest wind events occurred overwhelmingly in the spring. Using the four complete years from 1994-97, we looked at the number of days with winds exceeding 60 km/hr by season:

Season	Days where windspeed > 60 km/hr
Winter (Dec - Jan)	3 (12%)
Spring (Mar - May)	17 (65%)
Summer (Jun - Aug)	3 (12%)
Fall (Sep - Nov)	3 (12%)

If we further separate extreme events by month, we see that 35% occurred in March, with 15% in each of April and May. There was also yearly variability. In 1994 there were 13 days in which the windspeed exceeded 60 km/hr. This dropped to 3 days in 1995 (with 4 and 6 days in 1996 and 1997 respectively).

One means of summarizing the frequency of extreme wind events is by looking at the number of days with windspeeds above a threshold value. Figure 1.3 gives the percentage of days in the measurement period with winds above 40, 50, 60, 70 and 80 km/hr. It is interesting that with every 10 km/hr increase in the threshold, the number of days exceeding that threshold drops by roughly two-thirds.

Using the "number of days with windspeeds above a threshold" as the basis for analysis, we grouped the extreme gust events by direction. Figure 1.4 shows this grouping, and illustrates that most of the extreme gusts are from the SW-W-NW direction. For example, whenever the windspeed exceeded 60 km/hr, there was only a 20% chance the wind was not from the SW-W-NW. The only other direction from which we recorded extreme winds was N. The directional distribution of the gusts are similar no matter what the threshold windspeed. .

One useful means of characterising the wind is with a gust factor. The gust factor G is the ratio of the gust wind speed to the corresponding average hourly windspeed. The utility of G is that it allows an estimation of the infrequently measured maximum gust from the more often known average windspeed. While we do not utilise G in this study, it may prove useful to other researchers. For instance, current models of wind flow through forests calculate only the average windspeed, not gust events. Therefore G may prove useful in applying flow models to estimate gust speeds. We calculated G by looking at those hours in which the maximum gust exceeded 40 km/hr. In these conditions, at our 15 m measurement height, G was 2.16. This is in good agreement with values reported by Milne over a Sitka Forest in Scotland.

3.2. Airport site

Over the 1623 complete days of the study period, we recorded 43 days (2.6%) at the Manning airport when the maximum windspeed was greater than 60 km/hr (these are listed in Table 1.1). The airport location was clearly a windier site than Hotchkiss, with 50% more days above this threshold windspeed. That trend continued for higher wind thresholds as well (Figure 1.3). The maximum windspeed recorded at the airport was 96.5 km/hr at 2:43 p.m., 14 November 1993 (about 20 minutes after the highest gust measured at Hotchkiss).

Using the reduced sample of "days with gusts above a threshold" as the basis for analysis, we grouped the gust windspeeds by direction. Figure 1.4 shows such the grouping for the airport. This analysis shows that most of the large gusts are from the SW-W-NW direction. Except for more high wind events, the directional characteristics of the airport gusts are similar to those at the Hotchkiss site.

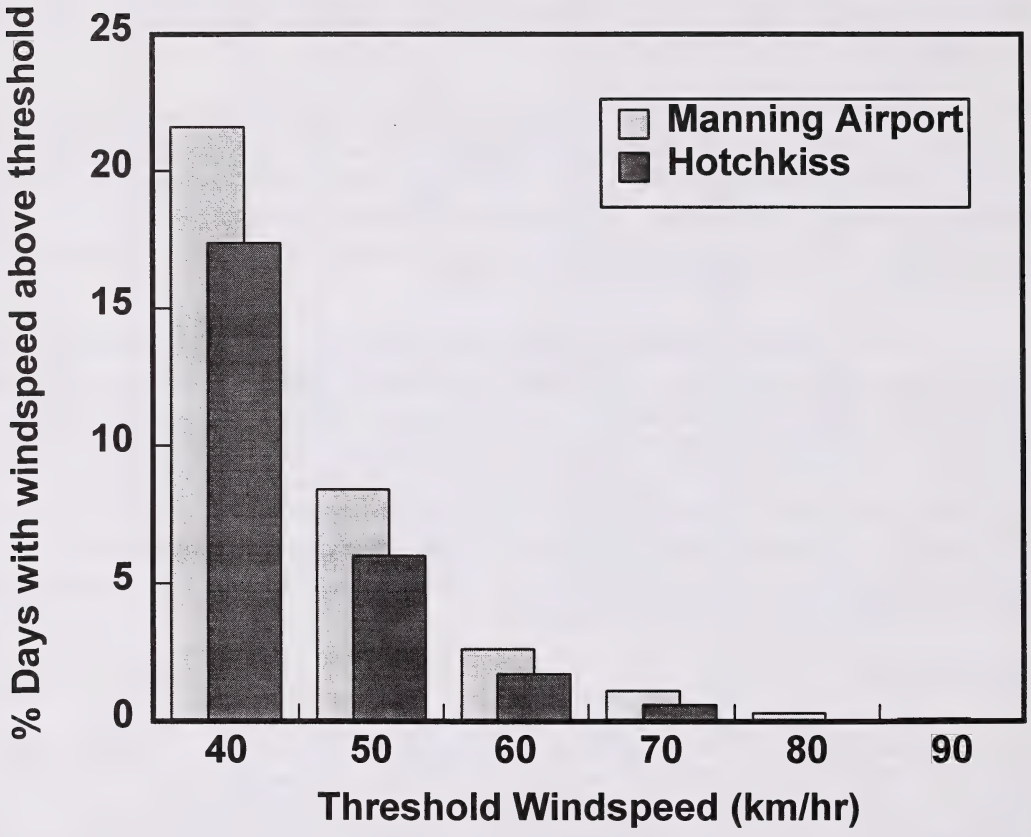

Figure 1.3. Percentage of days with windspeeds above various threshold values at the Hotchkiss site and the Manning airport. There were 1623 days in the period.

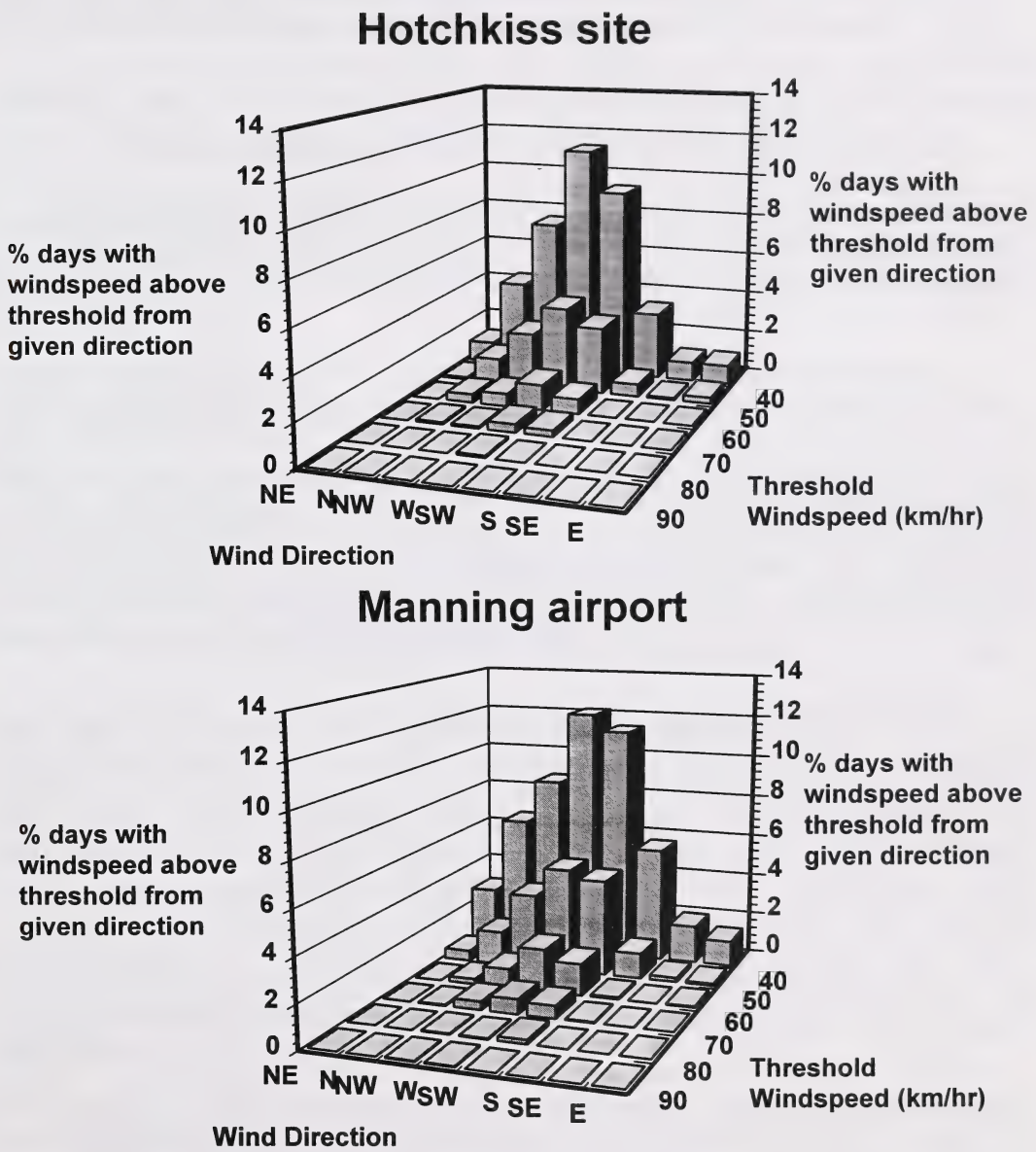

Figure 1.4. The percentage of days with a maximum windspeed above various threshold values, grouped by wind direction, for the Hotchkiss site (top) and the Manning airport (bottom).

The gust factor (G) calculated at the airport was 1.84, lower than at Hotchkiss. This was not surprising, given that the value of G increases in areas with greater turbulence. We would expect that the expansive grassy areas at the airport would lead to less turbulence than at Hotchkiss, where uneven terrain, and dramatic changes in surface roughness would contribute added turbulence to the wind flow.

4. A Climatological Perspective of Hotchkiss Winds (Were the winds unusual?)

The central objective of this phase of our study is whether the winds experienced at Hotchkiss were unusual: e.g., is the success, or failure, of a harvest scheme at Hotchkiss due to unusually strong, or unusually weak winds? Here we compare the extreme winds at Hotchkiss with the historic wind climatology of the region.

Flesch and Wilson (1993) examined the extreme wind climatology at a number of sites in Alberta. They preformed an extreme value analysis of maximum windspeeds to assess the future likelihood of extreme winds. This likelihood was expressed in terms of return periods, which represents an average length of time between gusts of a given windspeed. One of the weather stations examined in that study was High Level, Alberta. We believe that this site is comparable to Hotchkiss. While the two sites are separated by approximately 150 km, this is close considering the scale at which wind climatology changes (outside mountain regions). Both locations also share a similar surrounding: a relatively small clearings surrounded by forest. Peace River is another location studied by Flesch and Wilson. While closer to Hotchkiss than High Level, the weather station (airport) is located on a more open landscape than Hotchkiss.

The maximum windspeed ever recorded at High Level was 120 km/hr (up until 1988). While this is higher than the maximum 81 km/hr recorded at Hotchkiss, the data record at High Level extends 18 years, compared with less than 5 years for Hotchkiss -- so High Level was more likely to see a very extreme event. A more valid comparison between the two sites is the value of the return period for an 81 km/hr wind. From the information provided in the Flesch and Wilson (1993) report, we calculated a return period of 2.3 years for this windspeed at High Level. This means that on average, an 81 km/hr wind occurs once every two to three years at High Level. At Hotchkiss, we would say that an 81 km/hr wind occurs once every 4.5 years (as this was the length of our windspeed record at Hotchkiss). The return period for a 90 km/hr wind at High Level is 4.7 years. In other words, the long-term climatology from High Level would say that we should have observed a 90 km/hr wind over this period (we observed 81 km/hr). While it is tempting to conclude that the period 1993-98 at Hotchkiss was less windy than expected, it would be unwise to do so. Given the short wind record at Hotchkiss, and the different instruments used at the sites (the anemometer used at Hotchkiss is the more accurate, and our electronic recording system is more precise), we would conclude that these differences in return periods between Hotchkiss and High Level are not significantly different.

The seasonal pattern of extreme winds is somewhat different between the two sites. Flesch and Wilson (1993) defined their seasons differently than we did. The windiest season at High Level was winter, which they defined as from November to March. If we do the same at Hotchkiss, winter

would also be the windiest season. Summer (Jul - Oct) would be the next windiest season at High Level, followed by spring (Apr - Jun). However at Hotchkiss we would say that spring is much more windy than summer.

The predominant wind direction for extreme events at High Level is westerly, much like Hotchkiss. A more detailed comparison of directional characteristics is not possible because official weather stations do not measure extreme wind directions to the same level of detail we did.

We would conclude that the wind experienced at Hotchkiss over the period October 1993 to March 1998 did not depart substantially from the climatological average for the region. We saw no evidence that there were catastrophic (or even unusually strong) events at Hotchkiss, events that might alter the interpretation of Project 8032 results. However, the period was not particularly benign either.

5. A Comparison of Winds Between the Airport Site and Hotchkiss

Over the complete study period, the maximum windspeed recorded at the Manning airport averaged 3.5% higher than at the Hotchkiss site. This results in our classifying more days as having extreme wind events at the Manning airport than Hotchkiss (Figure 1.3). For example, the airport reported 43 days in which the maximum windspeed was greater than 60 km/hr (as listed in Table 1.1), while the Hotchkiss site saw 28 days. The maximum windspeed recorded at the airport was about 15 km/hr higher than that recorded at Hotchkiss.

Even though the airport site is clearly windier than Hotchkiss, when daily maximum wind gusts at the airport site are plotted against those at Hotchkiss (Figure 1.5), we see relatively good agreement between the two sites. Although there is a good deal of scatter in the data, the observations clearly fall close to the one to one line -- except for some of the highest wind events at the airport site that correspond to much lower winds at Hotchkiss. One conclusion we can draw from Figure 1.5 is that the weather factors that resulted in daily gust events usually affected both the airport and Hotchkiss, as there was a strong correlation between the two. The most obvious outliers, indicated with a circle around the data in Figure 1.5, occurred during the summer. We believe these outliers illustrate that summer extreme events, which we believe are often the result of thunderstorms, do not have the large spatial extent as do extreme storms seen during the rest of the year (where extreme events are caused by large winter storms, or frontal passages, both of which will affect large areas).

We would conclude that over a period of months and years, the winds at the Manning airport will be highly correlated with the winds at Hotchkiss -- although the airport site will average 3.5 % higher windspeeds than Hotchkiss. On a day to day basis the agreement in windspeed between the two sites is not so good -- especially for summer events (thunderstorms).

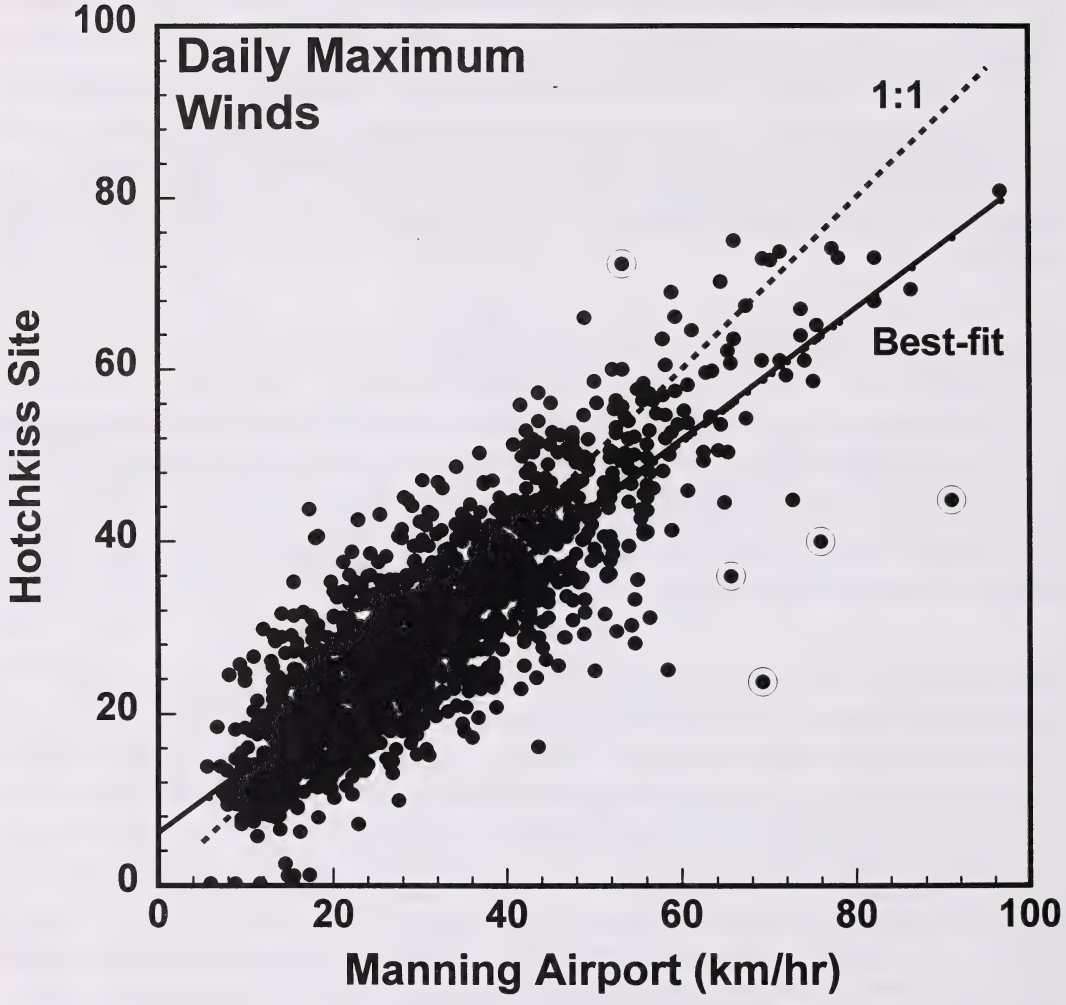

Figure 1.5. Comparison of the maximum daily windspeed recorded at the Hotchkiss site with that recorded at the Manning airport for the same day. The two sites are separated by approximately 30 km. Summer outliers discussed in the text are circled.

The relatively good long-term agreement between maximum windspeeds at the two sites was slightly surprising, given that they are approximately 30 km apart, the measurement heights differ, and the surrounding terrain differs. This would seem to indicate that extreme wind climatology, as measured at a weather station, will be spatially representative, even for different observation heights and different terrain. This is encouraging for those trying to estimate the wind characteristics at locations where there are no wind observations. If the terrain is not too extreme (mountains and foothills), then weather stations some distance from the location of interest can be used to infer the wind climatology. However, trying to use the wind at remote weather stations to estimate the windspeed on specific days is not advisable.

6. Summary and Conclusions

Wind measurements were made at the site of the Hotchkiss silvicultural project (Project 8032) from October 1993 to March 1998. The maximum windspeed recorded at Hotchkiss was 80.8 km/hr, recorded on 14 November 1993. Over this period there were 28 days in which wind gusts exceeded 60 km/hr, with most of these events having a SW-W-NW direction.. The highest wind events occurred overwhelmingly in the spring (with 35%of the events occurring in March). 1994 was a windy year, with 13 days in which the windspeed exceeded 60 km/hr. The quietest year was 1995, with 3 days of winds over 60 km/hr.

Based on the comparison of Hotchkiss winds with the winds at High Level, Alberta, we would conclude that the wind experienced at Hotchkiss over the period October 1993 to March 1998 did not depart substantially from the climatological average for the region. We saw no evidence that there were catastrophic (or even unusually strong) events at Hotchkiss that would substantially alter the interpretation of Project 8032 results.

We compared maximum winds measured daily at Hotchkiss with measured winds at the Manning airport (30 km distant). Over the period of study, the winds at the Manning airport were highly correlated with the winds at Hotchkiss, although the airport site had windspeeds that were 3.5% greater than Hotchkiss (on average). This is encouraging for those trying to estimate the wind characteristics at locations where there are no wind observations. If the terrain is not too extreme (e.g., mountains and foothills), then weather stations some distance from the location of interest can be used to infer the wind climatology. However, trying to use the wind at remote weather stations to estimate the windspeed on specific days is not advisable.

7. References

Milne, R., 1992, Extreme winds over a Sitka spruce plantation in Scotland. Agric. For. Meteorol., 61:39-53.

Flesch, T.K., and Wilson, J.D., 1993. Extreme value analysis of wind gusts in Alberta. Partnership Agreement in Forestry (PAR) Report 107. Nat. Resour. Can., Can. For. Serv., Northwest Reg., Edmonton, Alberta.

CHAPTER 2

MEASURED WINDS IN EXPERIMENTAL CUTBLOCKS

Thomas K. Flesch and John D. Wilson

1. Introduction

Large portions of the Canadian boreal forest have a predominately aspen (Populus tremuloides) overstory with a white spruce (Picea glauca) understory. In some cases a selective harvesting of the mature aspen may be commercially worthwhile, leaving the "released" spruce understory for future harvest. This "two-stage" harvest system is also ecologically attractive, as it better maintains "mixedwood" diversity compared with the traditional alternative of aspen clear-cutting.

An obstacle to a two-stage harvest is the susceptibility of the remnant spruce to windthrow (uprooting). Developed under a sheltered aspen canopy, individual spruce trees have poor wind stability, making them vulnerable to the increased wind exposure that accompanies aspen removal. Navratil et al. (1994) described the results of a two-stage harvest trial in western Canada, where aspen were harvested in large cutblocks, with dimensions of approximately 20 forest canopy heights (h). On average, 15 to 25% of the remnant spruce taller than 0.4 h were lost to windthrow within three years of aspen harvest. These trials were on dry soils, and higher losses would be expected on the wetter soils common to the mixedwood region of Canada. Therefore, the development of silvicultural techniques to provide wind protection is deemed essential for the success of two-stage harvest systems.

One proposed solution to the windthrow problem is a modified shelterwood harvest system. In this shelterwood design (Figure 2.1) the aspen is harvested in a series of narrow cutblocks, separated by unharvested forest strips (shelterwood). The cutblocks are oriented perpendicular to the expected direction of maximum wind. The forest strips are then analogous to agricultural windbreaks, and the expectation is that they will provide wind shelter for the remnant spruce in the cutblocks.

McNaughton (1989) described the general features of wind flow behind a thin windbreak of height h. Immediately downwind of the windbreak is a "quiet zone", where the average wind velocity and the turbulence (conveniently characterised by the turbulent kinetic energy, TKE) are reduced relative to the "ambient" levels far upwind. This quiet zone lies below a line that extends roughly from the top of the windbreak to the ground about 8h behind the windbreak. Further downwind, and above the quiet zone, lies a "wake zone", where the TKE is enhanced over ambient levels (although the average wind velocity is still reduced from ambient). Still further downwind there is an eventual recovery to the ambient (i.e., upstream wind conditions).

Does this pattern exist in forest cutblocks? The observations of Gash (1986), Raupach et al. (1987), and Liu et al. (1996) suggest it does -- if "ambient" in these cases is defined by the wind condition in the clearing far *downwind* of the forest. In these studies one can observe a quiet zone immediately downwind of the forest, followed by a wake zone. This is encouraging from a windthrow protection standpoint, as it suggests that narrow cutblocks will experience wind shelter, particularly if their width is limited to the dimensions of the quiet zone. However, a series of forest-cutblock strips has a more complicated geometry than either an isolated windbreak, or an isolated forest-clearing interface. It is possible to imagine complex flow patterns where the quiet and wake zones are altered in location, or are no longer appropriate descriptions of cutblock flow.

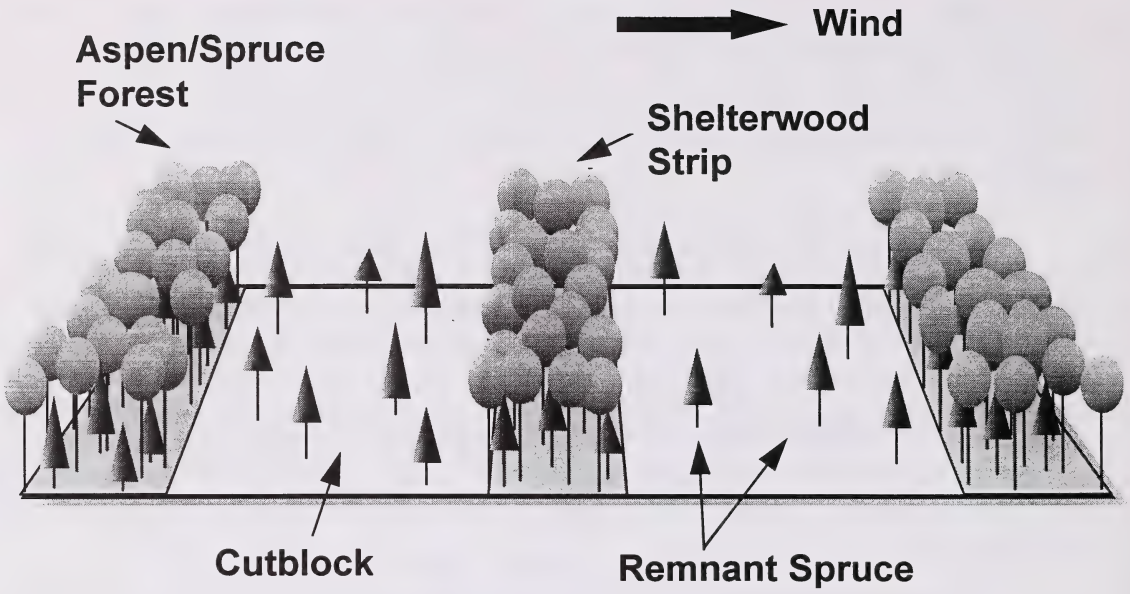

Figure 2.1. Idealised view of shelterwood harvest system. Cutblocks are created by selectively harvesting the mature aspen overstory, leaving the spruce understory intact. Forest strips (shelterwood) separate the cutblocks, providing wind shelter.

A micrometeorological field experiment was undertaken with the goal of providing a theoretical basis for understanding the windthrow protection afforded by shelterwood cutblocks. Our objective was quite specific: to quantify windthrow protection available for an isolated remnant understory spruce, when winds are oriented across the cutblock. In this phase of the study, we describe winds across two differently sized cutblocks. We were particularly interested in whether a common flow pattern exists across cutblocks of different dimensions and across cutblocks having different upwind and downwind forest features. The second phase of the work (Chapter 3) relates wind velocity statistics to remnant tree sway, so that cutblock wind shelter can be quantified in terms of tree sway. In the third phase of the study, a wind flow model (Chapter 4) was developed to generalise our measurements in a way that allows spatial mapping of windthrow hazard for arbitrary cutblock designs.

2. Field Measurements

2.1. The Hotchkiss silviculture experiment

A silvicultural experiment in Alberta, Canada is examining shelterwood designs for effectiveness at reducing remnant spruce windthrow. The project site is approximately 30 km northwest of Manning, at a location called Hotchkiss River. The area is classified as boreal mixedwoods, having a predominately aspen overstory of 20 to 25 m in height, with a significant white spruce understory averaging 10 m in height. The terrain is gently rolling.

During the initial harvest, aspen and mature spruce were removed from long rectangular cutblocks, whose width ranged from approximately 40 to 150 m, and whose length varied from approximately 500 to 1000 m. The cutblocks were oriented perpendicular to the direction of the expected maximum winds (westerly). Remnant spruce density in the cutblocks varied according to the density of the original understory.

2.2. Wind measurements

Two cutblocks were selected for intensive study (Figure 2.2a and 2.2b): a wide cutblock with width (X_c) = 140 m (studied in 1994 and 1995), and a narrow cutblock with X_c = 40 m (studied in 1996 and 1997). These cutblocks were 500 and 700 m in length, respectively. Each was the furthest east in a series of nominally identical cutblocks, which were separated by forest strips of about the same width (X_f) as the cutblocks (e.g., the 140 m wide cutblock was bordered upwind by a 140 m wide forest strip: $X_c = X_f = 140$ m). We defined x as the across-cutblock coordinate (very nearly east-west), y as the along-cutblock coordinate, and z as a vertical coordinate. The origin x = 0 lies at the westward edge of the test cutblock, with x increasing toward the east (downwind for most of our discussion). Wind measurements were made in each test cutblock, along east-west transects sited where the residual spruce density was low (we cut down the few trees that might otherwise have created wind anomalies along the transect). The canopy height (h) was approximately 23 m.

In 1994 towers were placed at x/h = -0.8, 1.0, 2.1, 3.2, 4.3, 5.4, and 7.2 in a transect across the wide cutblock (Figure 2.2a); the cutblock boundaries lying at x/h = 0 and 6.1. Cup anemometers (Climet Instruments Co., model 011B) were placed on each tower at z = 9 m (z/h = 0.4) to measure

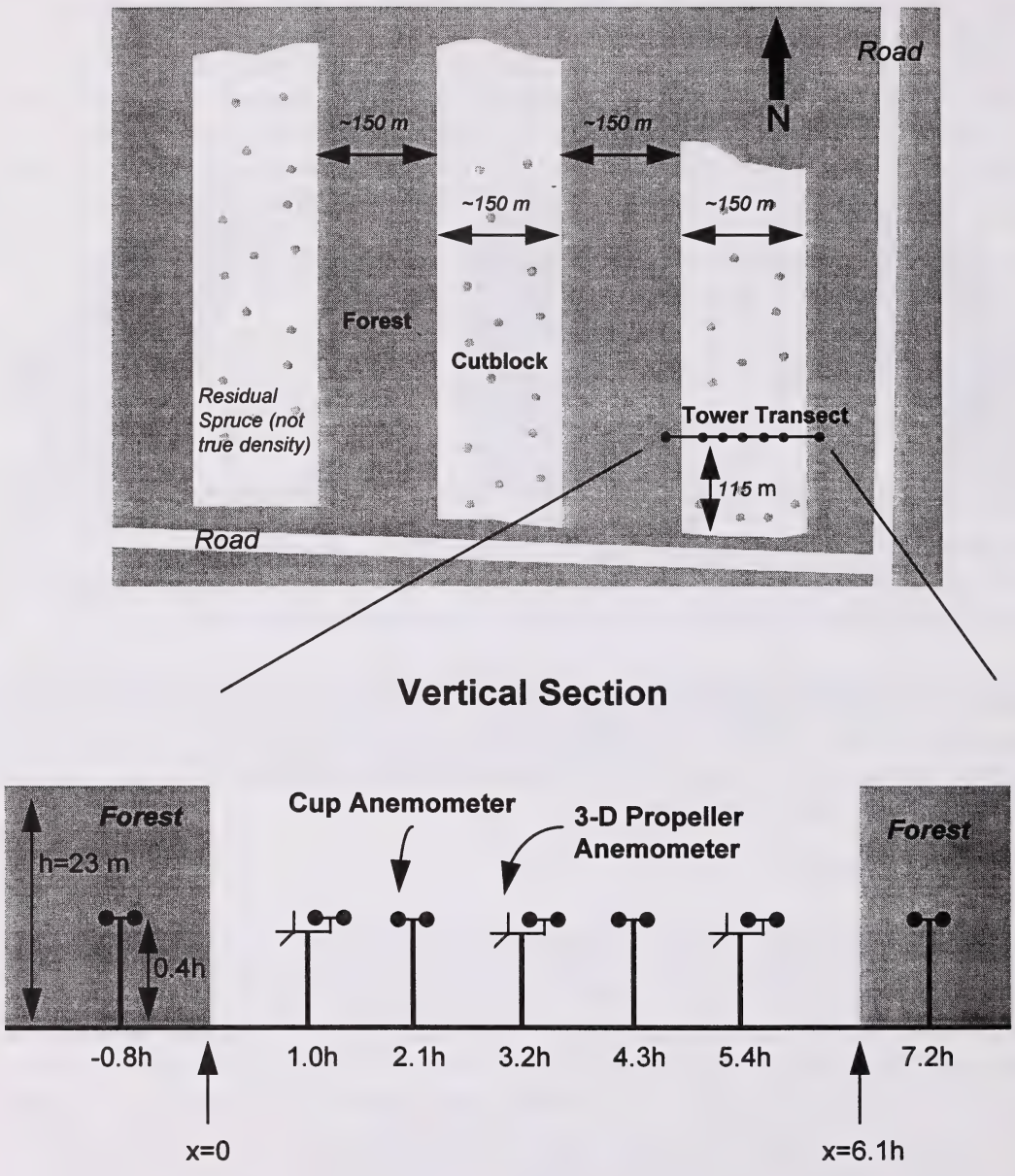

Figure 2.2a. Location of wind measurements in the wide cutblock. We have illustrated cup anemometers on all towers, and the 3-D propellers at x/h = 1.0, 3.2, and 5.4.

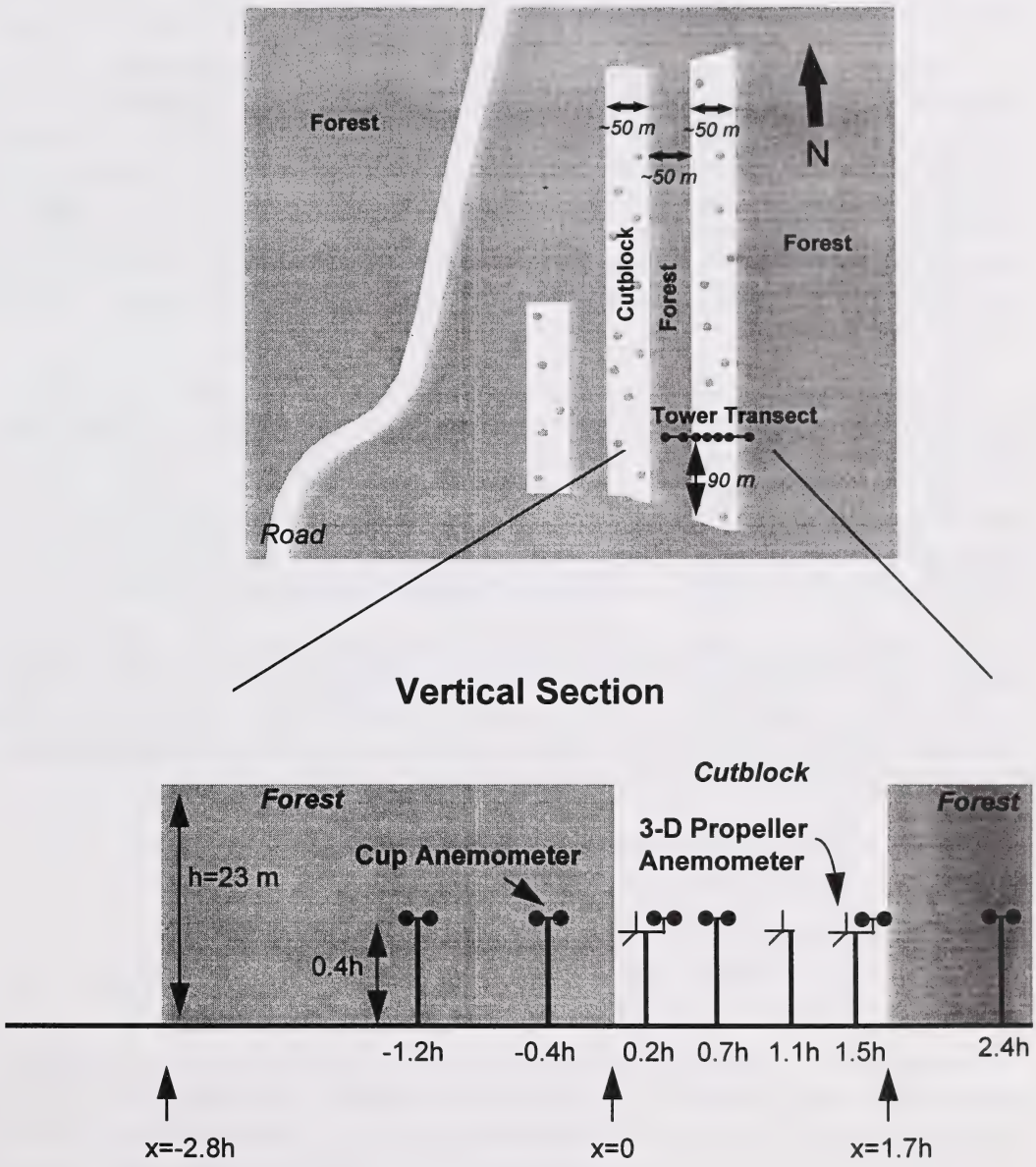

Figure 2.2b. Location of wind measurements in the narrow cutblock.

the average cup windspeed (S). From October to November in both 1994 and 1995, hourly averages (S) were recorded, encompassing a range of wind directions and speeds. The S measurements were corrected for cup overspeeding (see Appendix).

Three-dimensional (3-D) propeller anemometers (R.M. Young Co., Gill UVW anemometer) were also operated during periods of high winds oriented across the cutblock (westerly winds). In 1994 the propellers were placed at x/h = 1.0, 3.2, and 5.4 (at z = 9 m). In 1995 they were placed at x/h = -0.8, 3.2, and 7.2. Average windspeed and direction at x/h = 3.2 were used to trigger propeller sampling, which lasted 15 minutes with a 5 Hz sampling frequency. A datalogger (Campbell Scientific Inc., CR-7X) recorded the measurements. Propeller data were recorded as a voltage time series, and later converted to velocities according to Horst (1972), correcting for the imperfect cosine response of these anemometers. Six measurement periods were selected for analysis in 1994, and five in 1995 (Table 1.1).

In 1996 the towers were moved to the narrow cutblock and placed at x/h = -1.2, -0.4, 0.2, 0.7, 1.1, 1.5, and 2.4 (Figure 2.2b); the cutblock boundaries lying at x/h = 0 and 1.7. Cup anemometers were placed on six of the towers (excluding x/h = 1.1), and hourly S were recorded in October and November 1996. The 3-D propeller anemometers were placed at x/h = 0.2, 1.1, and 1.5. Propeller measurement periods lasted 30 minutes (the increased duration from 1995 was due to increased data storage capability). Five periods were selected for analysis (Table 1.1). In the fall of 1997, the propellers were placed at x/h = -1.2 and 0.7, and two 30-minute periods were recorded.

We used u, v, w to denote the instantaneous across-cutblock velocity (x direction), along-cutblock velocity (y direction), and the vertical velocity, respectively. We will write, for example, an instantaneous velocity $u = U + u'$, where U is the time average velocity, and u' is the instantaneous departure from average. For each velocity time series measured with the propellers, we calculated the following statistics (the angle brackets $< >$ denote a time average):

- average velocities, denoted U, V, and W;
- average cup windspeed, $S = <(u^2 + v^2)^{1/2}>$;
- velocity standard deviations, denoted σ_u, σ_v, and σ_w;
- turbulent kinetic energy, $TKE = (\sigma^2_u + \sigma^2_v + \sigma^2_w)/2$;
- velocity skewness, denoted Sk_u, Sk_v, and Sk_w (e.g., $Sk_u = <u'u'u'>/\sigma_u^3$);
- velocity kurtosis, denoted Kt_u, Kt_v, and Kt_w (e.g., $Kt_u = <u'u'u'u'>/\sigma_u^4$);

Simultaneous with our cutblock measurements, average cup windspeed and wind direction (hourly averages) were measured in a large "reference" clearing 5 km from the cutblocks. This clearing was irregularly shaped, with a diameter of roughly 1 km. A cup anemometer (Met-One, model 013A) was placed at z = 9 m on a tower that was 12 - 30 h from the forest edge. The case in which we were most interested (west winds) put the tower 20h downwind of the forest edge, with the clearing extending approximately 20h further downwind of the tower. Throughout this work we will use the clearing cup windspeed (S_{clr}) as a velocity scale to normalise our in-cutblock data, to permit an assessment of the windiness of the cutblocks *relative to* an essentially open region (presumably the worst case scenario for windthrow). We will also use S_{clr} and the wind direction in the clearing to derive a reference across-cutblock wind velocity (U_{clr}). During November 1995,

Table 1.1. Propeller anemometer measurement periods used in the study.

No.	Cutblock Width	Date	Time	S_{clr} (ms^{-1})	Wind Direction (0 is across the cutblock)	Gill UVW locations
W-1	6.1h	27 Oct. 1994	1345-1400	6.41	3 deg	x/h = 1.0, 3.2, 5.4
W-2	6.1h	28 Oct. 1994	1015-1030	4.85	4 deg	x/h = 1.0, 3.2, 5.4
W-3	6.1h	28 Oct. 1994	1145-1200	4.97	16 deg	x/h = 1.0, 3.2, 5.4
W-4	6.1h	28 Oct. 1994	1200-1215	5.86	25 deg	x/h = 1.0, 3.2, 5.4
W-5	6.1h	4 Nov. 1994	1100-1115	6.21	3 deg	x/h = 1.0, 3.2, 5.4
W-6	6.1h	18 Nov. 1994	1615-1630	5.21	-16 deg	x/h = 1.0, 3.2, 5.4
W-7	6.1h	26 Oct. 1995	1145-1200	3.69	10 deg	x/h = -0.8, 3.2, 7.2
W-8	6.1h	26 Oct. 1995	1200-1215	3.70	24 deg	x/h = -0.8, 3.2, 7.2
W-9	6.1h	26 Oct. 1995	1545-1600	4.21	-7 deg	x/h = -0.8, 3.2, 7.2
W-10	6.1h	26 Oct. 1995	1615-1630	3.47	-14 deg	x/h = -0.8, 3.2, 7.2
W12	6.1h	26 Oct. 1995	1730-1745	4.39	-15 deg	x/h = -0.8, 3.2, 7.2
N-1	1.7h	7 Oct. 1996	1100-1130	4.71	4 deg	x/h = 0.2, 1.1, 1.5
N-2	1.7h	11 Oct. 1996	900-930	7.50	-13 deg	x/h = 0.2, 1.1, 1.5
N-3	1.7h	11 Oct. 1996	1000-1030	7.06	-10 deg	x/h = 0.2, 1.1, 1.5
N-4	1.7h	11 Oct. 1996	1200-1230	6.89	-3 deg	x/h = 0.2, 1.1, 1.5
N-5	1.7h	11 Oct. 1996	1400-1430	7.82	0 deg	x/h = 0.2, 1.1, 1.5
N-6	1.7h	26 Sep. 1997	1300-1330	4.94	-26 deg	x/h = -1.2, 0.7
N-7	1.7h	26 Sep. 1997	1330-1400	4.94	-26 deg	x/h = -1.2, 0.7

a 3-D propeller was placed in the reference clearing (at z = 9 m), and ten 15-min measurement periods were used to characterise the turbulence there.

3. Measured winds in forest cutblocks

3.1. Average cup windspeed

Average cup windspeed (S) within our study cutblocks was significantly reduced from that in the nearby reference clearing (S_{clr}), as illustrated in Figure 2.3. During windy periods ($S_{clr} > 3$ m s^{-1}) S/S_{clr} ranged from 0.12 to 0.64, depending on the wind direction and on location in the cutblock. As expected, S/S_{clr} increased with increasing distance from the upwind forest edge. The most effective sheltering (lowest spatial average S/S_{clr} along our transect) occurred when the wind was oriented directly across the width of the cutblock, which at any location, minimized the distance to the upwind forest. For example, when the wind was oriented across the wide cutblock (along the x direction, ± 30 deg) S/S_{clr} in the cutblock ranged from 0.23 at the upwind tower to 0.51 at the downwind tower, but when the winds were oriented along the cutblock length, this speed range increased to between 0.47 and 0.53 (Figure 2.3). This seems to confirm the premise of the Hotchkiss silviculture trials: that maximum shelter occurs when the wind is oriented across the cutblocks. There was a concern, in terms of windthrow, that wind channelling might occur when winds are oriented along the cutblock length, with $S/S_{clr} > 1$. We saw no sign of this. From now on, our focus will be on the case where the wind is oriented directly across the cutblock width -- the optimum case for wind shelter.

With the wind oriented across the cutblocks, the pattern of S was qualitatively the same as found behind an isolated windbreak: S was at a minimum near the windbreak, and it increased slowly with downwind distance (Figure 2.3). In the forest immediately upwind of our cutblocks, we observed an average S/S_{clr} of approximately 0.17. We cannot say whether the minimum S was at the forest edge (x = 0), or just upwind or downwind of the edge. We saw an almost linear increase in S with distance from the forest edge, so that S/S_{clr} reached approximately 0.5 at x/h = 5.4 in the wide cutblock, and 0.3 at x/h = 1.5 in the narrow cutblock. In each cutblock the maximum S occurred at the farthest downwind measurement location.

3.2. Average wind velocity

When we restrict our attention to winds oriented across the cutblocks (V = 0), we might expect the average along-wind velocity (U) to be very similar to S. But since $S = \langle (u^2 + v^2)^{1/2} \rangle$, it follows that S increasingly exceeds U as σ_v increases, or the proportion or magnitude of flow reversal (i.e., $u < 0$) increases. Far above a homogeneous surface, the difference between S and U is generally small. We observed a different situation in the cutblocks.

In the wide cutblock, U/U_{clr} ranged from approximately 0.1 in the upwind forest to 0.42 at the downwind cutblock tower (Figure 2.4). These values were smaller than the corresponding S/S_{clr} ratios, although the spatial pattern was similar. This was not the case for the narrow cutblock. While S was at a minimum near x = 0, U was near its maximum there. And while S almost doubled across the cutblock, U showed less change. These differences were the result of a large rise in the

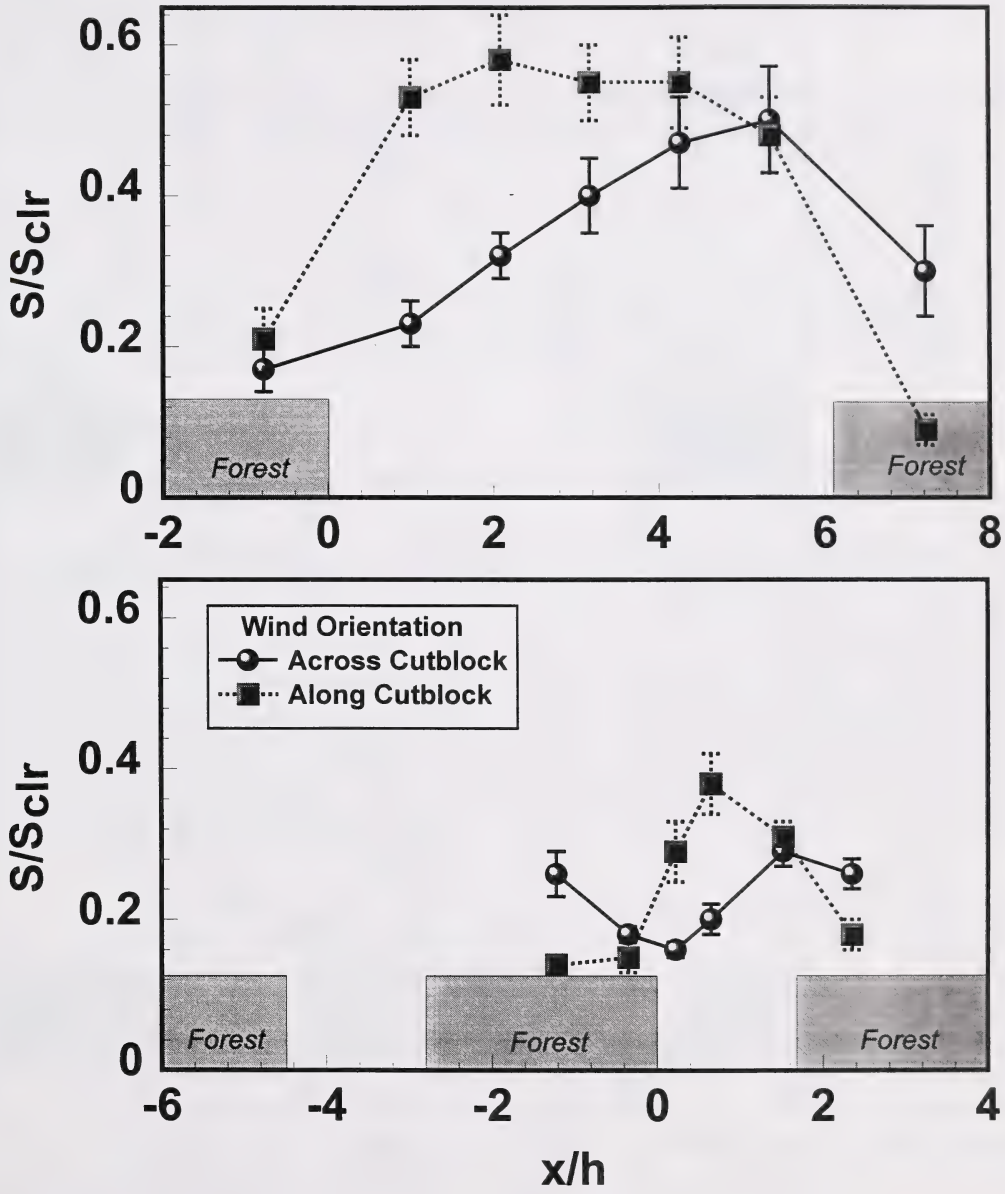

Figure 2.3. Average cup windspeed (S), scaled on windspeed in the nearby reference clearing (S_{clr}), and plotted versus position (x/h) in the wide cutblock (top) and the narrow cutblock (bottom). The two lines are for ambient winds oriented across the cutblock (average wind direction along x, ± 30 deg) and along the cutblock length (average wind direction along y, ± 30 deg). The "error bars" surrounding each observation are ± one standard deviation.

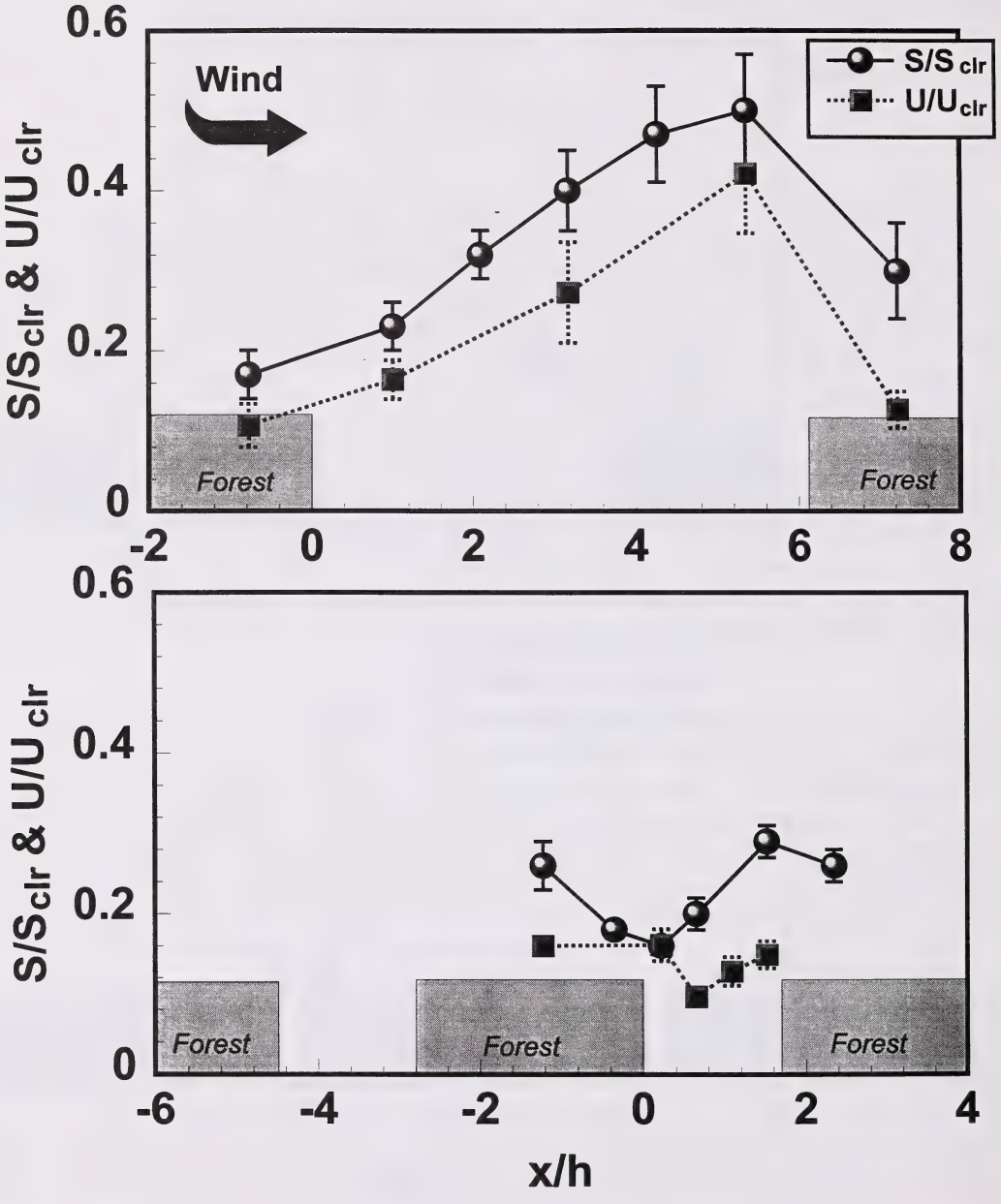

Figure 2.4. Average cup windspeed (S) and across-cutblock velocity (U), scaled on their values in the reference clearing (S_{clr} and U_{clr}), plotted versus position (x/h) in the wide cutblock (top) and the narrow cutblock (bottom). Winds were oriented across the cutblock (along x direction, ± 30 deg). The S are from 9 hours (wide cutblock) and 6 hours (narrow cutblock) of cup anemometer measurements. The U values are from 1 to 2.5 hours of 3-D propeller measurements. The "error bars" surrounding each observation are ± one standard deviation.

turbulence intensity with increasing x, and intermittent flow reversal. Figure 2.5 shows the time fraction when $u < 0$ in the cutblocks ($\tau_{u<0}$). This varied from 0 to 0.17 in the wide cutblock, and from 0.06 to 0.23 in the narrow cutblock.

The U deceleration in the upwind portion of the narrow cutblock indicated mass convergence, and in view of the continuity equation (in its 2-D form, assuming $\partial/\partial y=0$)

$$\frac{\partial U}{\partial x} + \frac{\partial W}{\partial z} = 0$$

suggested updrafts on average over the upwind portion of the cutblock. Our observations did show $W > 0$ at the upwind tower locations, particularly in the narrow cutblock (although our W observations are prone to uncertainty due to the difficulty in levelling the anemometers).

3.3. Turbulence statistics[1]

3.3.1. Turbulent wind velocities and TKE

Besides providing shelter in terms of the *average* windspeed, the cutblocks provided an environment of reduced wind-*variability* (turbulence) compared with large clearings-- at least over part of the cutblocks. Figure 2.6 shows the normalised standard deviations of wind velocities (σ_u/S_{clr}, σ_v/S_{clr}, σ_w/S_{clr}) across the two cutblocks. Values of σ_u and σ_v were statistically identical in the cutblocks, with σ_w being about 60% of σ_u and σ_v. The spatial patterns of σ_u, σ_v, and σ_w were similar, and naturally the turbulent kinetic energy ($TKE = (\sigma^2_u + \sigma^2_v + \sigma^2_w)/2$) also shows this pattern (Figure 2.7). The TKE in the wide cutblock rose from 19% of the reference clearing value at the upwind forest edge, to plateau at more than 100% of the clearing value for $x/h > 3$. In the narrow cutblock, the steep increase in TKE was sustained all the way across the cutblock, although the TKE never reached the level found in the reference clearing.

This pattern of turbulence generally corresponds to that found behind a typical thin windbreak (see review by McNaughton, 1989). The region from $0 < x/h \lesssim 3$ can be labelled a "quiet zone", where the turbulence was reduced from clearing levels. Downwind of this was a "wake zone", where the turbulence level exceeded that found in the clearing. The enhanced turbulence originates with the strong vertical wind shear concentrated near the top of the canopy at the upwind forest edge (which results in enhanced TKE production). Raine and Stevenson (1977) broadly divided the quiet and wake zones behind a thin windbreak with a line running from the top of the windbreak to the ground at $x/h = 8$. Based on this general rule, we should have found the transition from quiet to wake zones occurring at $x/h = 4.8$ (at $z/h = 0.4$), not at $x/h \approx 3.0$. This is consistent with McNaughton's (1989) speculation that the quiet zone behind a forest edge may be less extensive than that behind a typical thin agricultural windbreak, because the greater level of turbulence over a rough forest (compared with over typical agricultural land) increases the rate of vertical spread of the wake zone from the forest edge.

---

[1] Statistics from propeller anemometers are subject to errors from poor high frequency response and stalling. We believe these errors are small in this experiment (see Appendix).

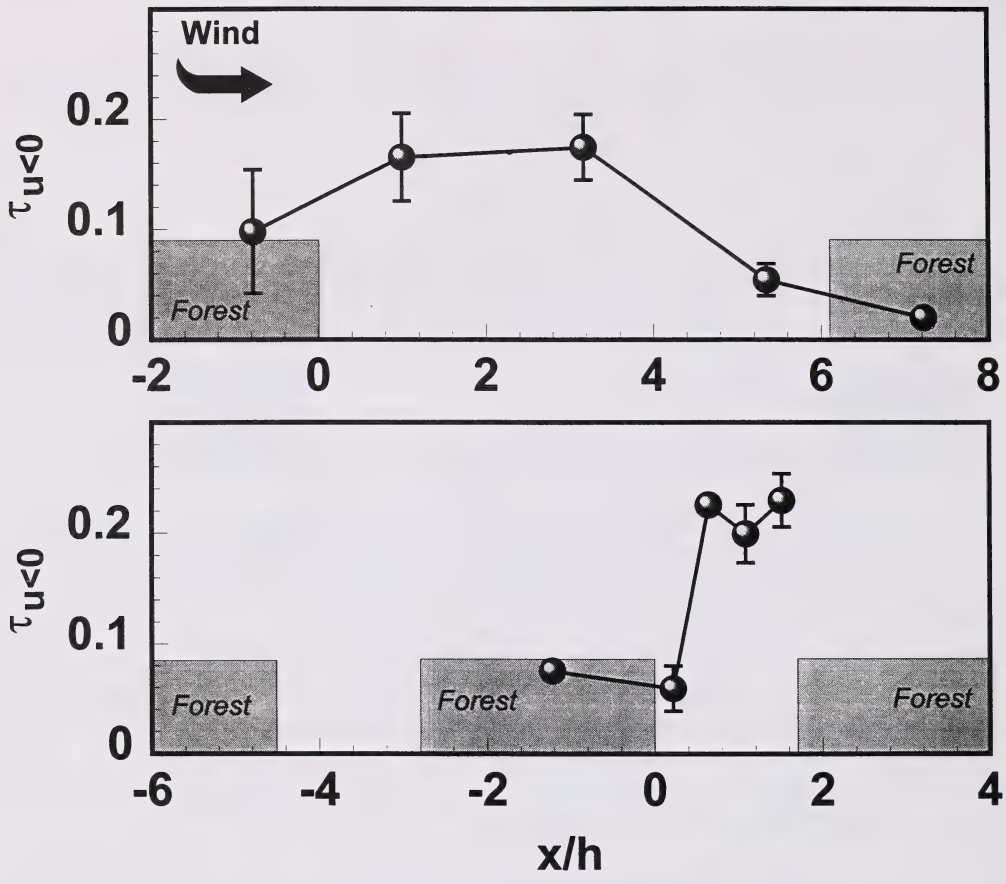

Figure 2.5. Average time fraction of flow reversal ($\tau_{u<0}$) in the wide cutblock (top) and the narrow cutblock (bottom). The "error bars" surrounding each observation are ± one standard deviation.

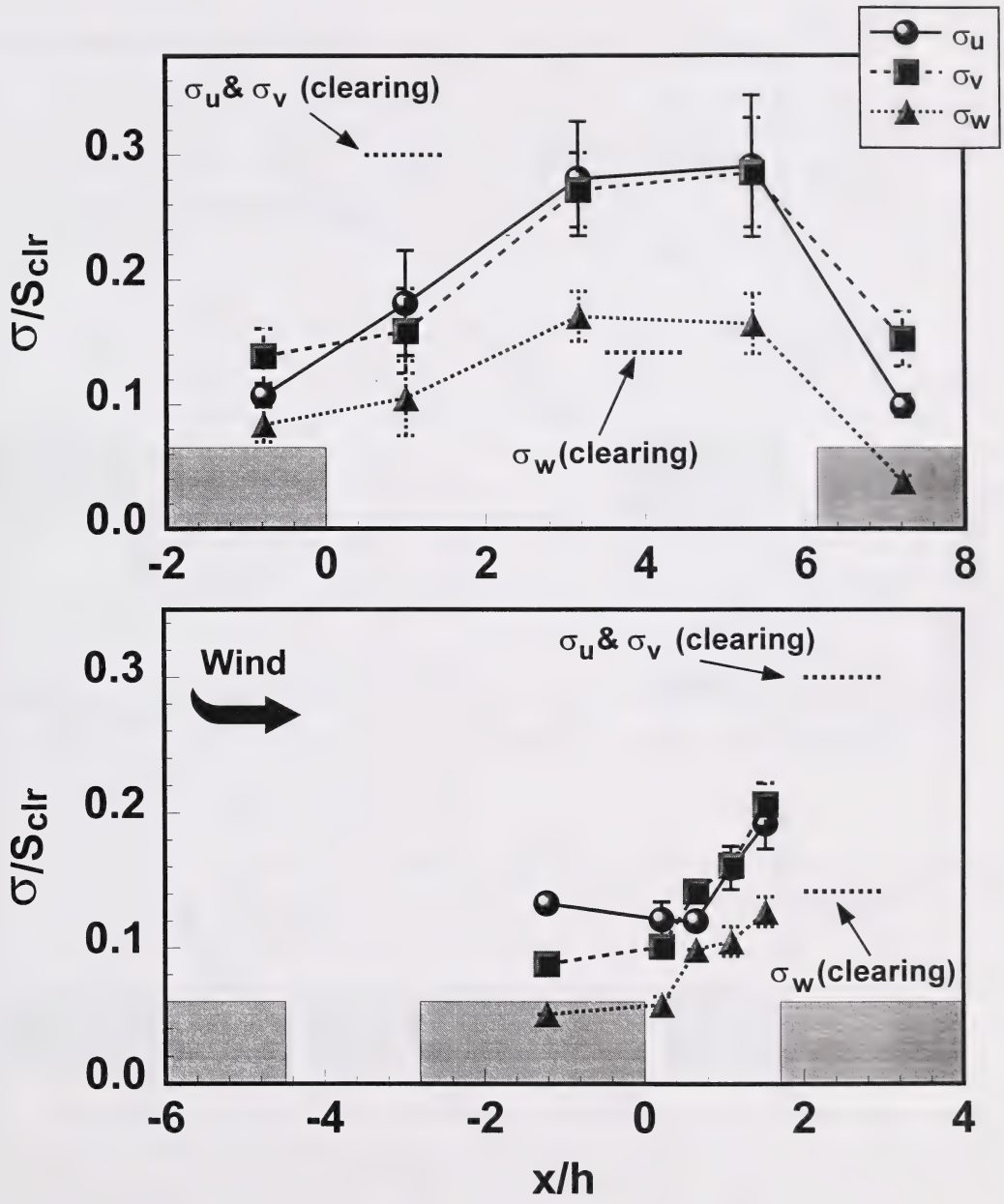

Figure 2.6. Velocity standard deviations (σ_u, σ_v, σ_w), scaled on cup windspeed in the nearby reference clearing (S_{clr}), plotted across the wide cutblock (top) and the narrow cutblock (bottom). The "error bars" surrounding each observation are ± one standard deviation. Values of σ_u/S_{clr}, σ_v/S_{clr}, and σ_v/S_{clr} in the reference clearing are shown by the level dashed lines (which are not at their proper location on the x axis).

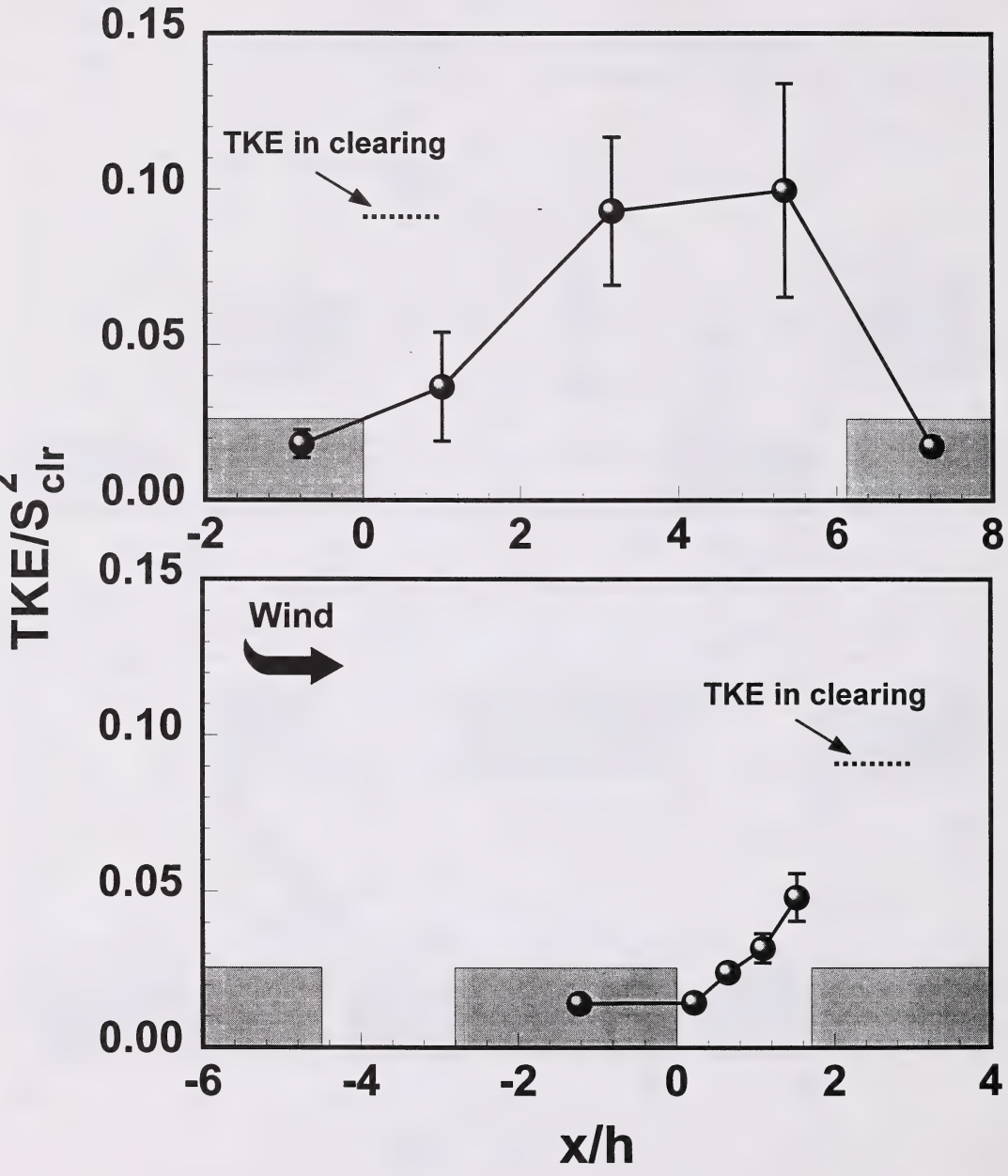

Figure 2.7. Average turbulent kinetic energy (TKE), scaled on cup windspeed in the nearby reference clearing (S_{clr}), across the wide cutblock (top) and the narrow cutblock (bottom). The "error bars" surrounding each observation are ± one standard deviation. Also shown (by the level dashed line) is TKE/S^2_{clr} in the reference clearing.

3.3.2. Skewness and kurtosis

Wind flow in plant canopies is often characterised as a temporally dominant "quiescent" regime with intermittent gusts (Finnigan and Raupach, 1987). Velocity skewness (Sk) is often taken as indicative of gust intermittency. A positive Sk_u, which is characteristic of canopy flow, is the result of an asymmetric probability density function (PDF), with a long "tail" toward large u values (gusts). If windthrow is the result of short duration gusts, Sk may be useful in identifying areas prone to wind damage: a larger Sk_u will correspond to greater extreme u values for a given σ_u.

Figure 2.8 illustrates Sk_u and Sk_w in our study cutblocks. We have less confidence in these statistics compared with averages and standard deviations, due both to propeller errors (discussed in the Appendix), and to the known need for longer averaging intervals to determine higher-order statistics. Within the cutblocks the average Sk_u varied from 0.5 to 0.8, while Sk_w fell between -1.2 and 0. These were within the range commonly observed within forest canopies (e.g., Baldocchi and Meyers, 1989; Amiro, 1990), indicating the occasional occurrence of high speed gusts originating above the canopy (with $u > 0$, $w < 0$). Flow was also marked by Kt exceeding 3 (Figure 2.8), which is the value for a Gaussian PDF. A large Kt indicates a narrow PDF peak (near zero velocity). This is consistent with a "two-state" canopy flow, dominated by a quiescent regime, but punctuated by infrequent gusts, giving a broad PDF tail. The "scatter" in our Sk and Kt observations, and the likelihood of measurement errors, makes it difficult to discern any spatial pattern across the cutblocks. The apparently modest spatial variation in Sk_u and Kt_u seems to rule out the possibility of hidden "hot spots" in the cutblocks: there is little reason to suspect the existence of cutblock locations more prone to intense gusts than is indicated from an assessment merely of U and σ_u.

3.4. Throughflow or recirculating flow?

Observations by Bergen (1975), Weiss and Allen (1976), and Raupach et al. (1987) suggest that the wind pattern across a forest clearing varies temporally between direct throughflow and recirculating flow. In throughflow, clearing streamlines everywhere are oriented with the above canopy streamlines, and the wind flows *into* the downwind forest at all height levels. Recirculating flow is marked by a standing vortex (rotor) within the clearing, with reverse flow near the ground. In smaller clearings this rotor may span the full width of the clearing, while it may be confined to the areas near the forest edge in large clearings.

The time spent in throughflow- and recirculation-states appears to depend on forest porosity, with increased porosity leading to increased dominance of the throughflow-state, and more intermittent recirculation (Raupach et al., 1987). Did recirculation occur in our cutblocks? Our limited observations make this question difficult to answer. Bergen (1975) examined wind flow across a narrow pine clearing ($X_c = 1$) and classified the flow as recirculating 25% of the time. Our leafless aspen forest was almost certainly less dense that Bergen's, and on that basis we might expect less frequent recirculation.

What would recirculation "look" like in our observations? We focused on our narrow cutblock, where rotors were expected to have features similar to those observed by Bergen: they

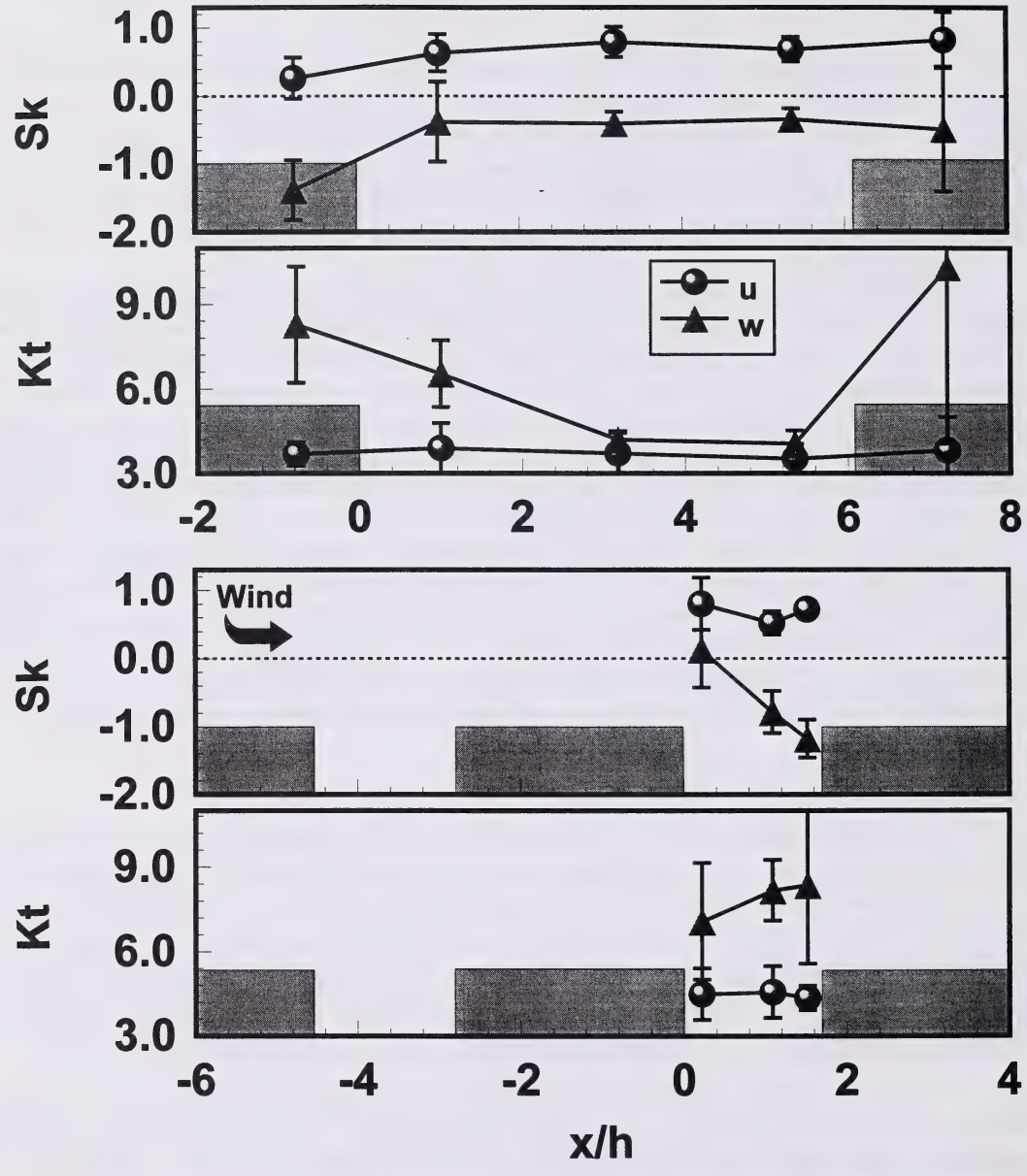

Figure 2.8. Average skewness (Sk) and kurtosis (Kt) for u and w across the wide cutblock (top two graphs) and the narrow cutblock (bottom two graphs). The "error bars" surrounding each observation are ± one standard deviation.

would span the width of the cutblock, and have an average duration of 10 to 20 s before a return to throughflow. Our data was broken into 10 s blocks, and the fraction (τ_{recir}) of these blocks having possible recirculation was calculated: the recirculation-state was characterised by the requirement of having updrafts at the upwind cutblock tower, and downdrafts at the downwind tower (10 s blocks were classified as having updrafts or downdrafts when $|W| > 0.2$ m s^{-1}). We calculated $\tau_{recir} = 0.12$. If we invoked a more conservative recirculation signature, which was consistent with Bergen's observations of 1) updrafts at our upwind tower, 2) downdrafts at the downwind tower, 3) $U < 0$ at the upwind tower, and 4) a near-zero U at the downwind tower (defined as having a block-average U less than the overall period average). Using these criteria, we calculated $\tau_{recir} = 0.02$. Although both of the above classification schemes are unsophisticated, we believe they show that the wind pattern in the cutblocks was dominated by throughflow.

4. Comparisons With Other Experiments

In this study we were particularly interested in whether common flow patterns exist in cutblocks of different dimensions and cutblocks having different upwind and downwind forest features. This is an important question when considering silvicultural designs that differ from the situation of our study cutblocks. When the wind statistics from our two different width cutblocks are plotted together versus x/h (Figure 2.9), they show surprisingly good agreement with each other. The greatest difference was the U deceleration ($\partial U/\partial x < 0$) observed upon "entering" the narrow cutblock, which was not seen in the wide cutblock (where, however, our anemometer spacing may have been too great to reveal this). The overall agreement in the wind statistics between the two cutblocks was surprising, given differences in upwind conditions. For instance, the narrow cutblock had an upwind forest border (entry-region) of approximately 2h, while the wide cutblock had an entry-region border of approximately 6h. This suggests that upwind features have a limited influence on the flow in a cutblock[2]. The agreement also shows that the effects of the downwind forest edge do not propagate very far upwind. If it is true that upwind and downwind conditions have limited influence on cutblock winds, we might then expect that wind observations from other forest-clearing interfaces would show similarities with our data.

4.1. Experiment of Gash (1986)

Gash (1986) measured winds near a forest-heath interface (the forest was a mix of pine and larch, the heath of heather and shortgrass). Because these data, which were taken mostly at a height $z/h = 0.33$, were scaled on above forest wind velocities (for which we did not have an equivalent observation), we were not able to fully compare Gash's observations with our data. We can say that Gash observed a larger S/S_{clr} at $x/h = 5$ than we found at more or less that same location at Hotchkiss (Figure 2.9). We do not know if this marked difference is due to differences in forest density and/or forest architecture, upwind geometry, or place of observation. However, we do know that our values

---

[2] However, in Chapter 4 we describe model results which suggest that the amount of upwind forest can have a large impact on U and TKE in the cutblock.

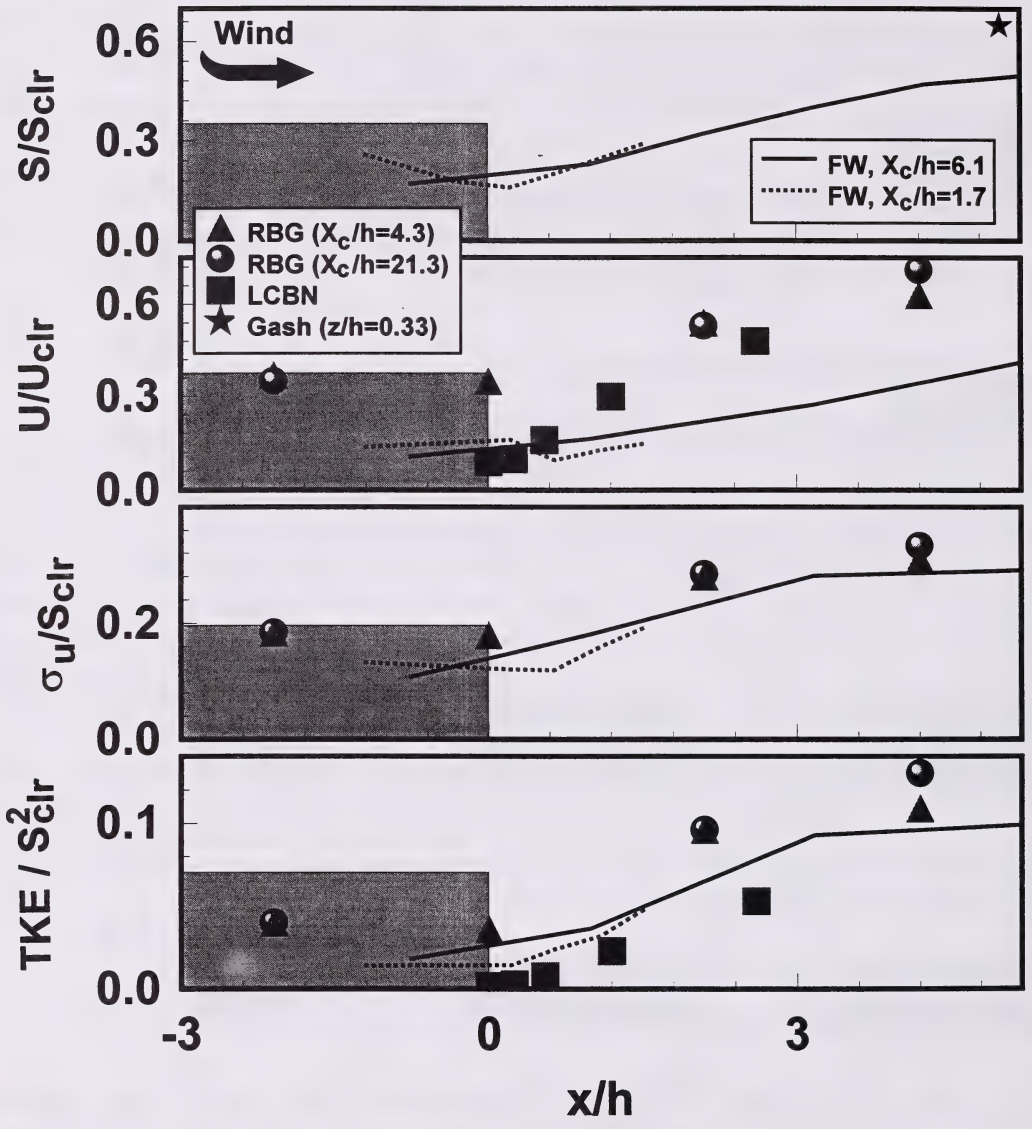

Figure 2.9. Multi-experiment comparison of average cup windspeed (S), average across-cutblock velocity (U), u velocity fluctuations (σ_u), and turbulent kinetic energy (TKE), plotted versus distance from the upwind forest (x/h). These statistics are scaled on clearing values of S or U (S_{clr} and U_{clr}). Our observations, denoted FW, are shown as lines. Other observations are plotted using the symbols described in the legend: RBG denotes Raupach et al. (1987), LCBN denotes Liu et al. (1996), and Gash denotes Gash (1986).

of S/S_{clr} and U/U_{clr} stand out as low relative to comparable data we have examined (as will be demonstrated in the comparisons that follow).

From Gash's observations we can also surmise that a narrow quiet zone existed in the heath immediately downwind of the forest. Gash observed that both σ_u and σ_w at $x/h = 5$ were larger that values further downwind of the forest. Therefore a quiet zone, in which σ_u and σ_w were below their far-downwind values, must have been confined to $x/h < 5$. This is consistent with our results.

Gash's observations also raise a question mark about whether the winds at our reference clearing typify a "generic" large clearing. Even as far downwind as $x/h = 40$, Gash observed $\partial S/\partial x > 0$: which suggest our observations at $x/h = 20$ have not reached an equilibrium clearing state. However, because the change in S seen by Gash was small beyond $x/h = 20$, and because σ_u and σ_w had apparently reached an equilibrium at $x/h = 20$, we feel comfortable that our observations at $x/h \approx 20$ can be interpreted as representing the winds in a generic large clearing.

4.2. Experiment of Raupach et al. (1987)

The wind tunnel study of Raupach et al. (1987), referred to as RBG, may more easily be compared with our observations. RBG examined two model forest clearings ($X_c/h = 4.3$ and 21.3), bordered upwind and downwind by forest, and made wind measurements at locations nearly equivalent to our observations. Their measurement at $x/h = 21.3$, at the downwind boundary of the large clearing, roughly corresponds in terms of distance downwind from the nearest shelter, to the location of our reference clearing observation (unfortunately, we must accept that this velocity is affected to some extent by the forest edge nearby). We compared our measurements with RBG values interpolated to $z/h = 0.4$.

Figure 2.9 shows horizontal profiles of U/U_{clr} from the two RBG cutblocks and our two cutblocks. The similarity in wind statistics between the two so-different sized RBG cutblocks echoed the similarity we observed between our two cutblocks. However, RBG reported much higher values of U/U_{clr} than we observed. In the upwind forest they found a U/U_{clr} that was three times what we observed. These differences continued into the cutblock. We expected some differences in U/U_{clr}, given that important forest details almost certainly differed. The RBG model forest had an equivalent plant area index (PAI) of 0.5, calculated as the frontal area of the model canopy elements per unit floor area. This represents a low density forest, although RBG argued that their effective PAI was higher, because the drag of their canopy elements was higher than those of a real forest (see Finnigan and Mulhearn, 1978). The aerodynamic "density" of our forest is unknown. Sakai et al. (1997) estimated that $PAI \approx 1$ in a leafless mixed deciduous forest. Given the substantial spruce understory at Hotchkiss, we believe our forest had a PAI of between 1 and 2, and was therefore more dense than the RBG forest. This may account in part for the lower normalised wind velocity seen in our cutblocks.

Some differences in U/U_{clr} may also be explained by errors in the RBG measurements. The hot-film anemometers used by RBG could not differentiate reversed flow, but reversal was observed visually, so that errors in their U measurements certainly occurred. We simulated a perfect hot-film sensor that measures only $|u|$, and found that this sensor would overestimate U at Hotchkiss by up

to 16% in the wide cutblock and 25% in the narrow cutblock, and underestimate σ_u by up to 19%. Errors of similar magnitude may have occurred in the RBG experiment.

While there were large differences in the average wind velocity between our cutblocks and the RBG clearings, the turbulence observations were surprisingly similar (Figure 2.9). Although σ_u/U_{clr} and σ_w/U_{clr} in the RBG forest were higher than we observed (perhaps the result of differences in forest structure), the in-cutblock values were in good agreement[3]. RBG observed a maximum σ_u/U_{clr} of approximately 0.3 (at x/h = 4.2) compared with our maximum of 0.29 (at x/h = 5.4), and a maximum σ_w/U_{clr} of 0.19 compared with our 0.17. RBG observed that both σ_u and σ_w fell slowly after this peak in their wide clearing.

4.3. Experiment of Liu et al. (1996)

The wind tunnel observations described by Liu et al. (1996), referred to as LCBN, were also directly comparable with our observations. LCBN looked at a forest-clearing interface, with forest upwind of a large clearing (x/h > 22). Velocity measurements were made in the clearing at x/h = 22, providing a "clearing" velocity scale (U_{clr}) nearly matching our reference scale. We compared our wind measurements (at z/h = 0.4) with the closest measurement height of LCBN.

Figure 2.9 shows horizontal profiles of U/U_{clr} from the LCBN study. The U/U_{clr} = 0.09 observed by LCBN at the upwind forest edge was similar to our forest observations. However, the increase in U/U_{clr} with x in the LCBN clearing was steeper than we found, so that U/U_{clr} was double our observations by x/h ≈ 3. Again, we expected some differences in U/U_{clr} due to differences in forest structure, and the potential for hot-film errors. The LCBN forest had an equivalent PAI of 6.3, and represented a much more dense forest than ours. It is interesting that in both the RBG clearings (where we believe the forest was less dense than ours) and in the LCBN clearing (where we believe the forest was more dense than ours) the values of U/U_{clr} were larger than we observed. This suggests that differences in forest density do not explain the differences in U/U_{clr}.

Individual turbulent velocity components were not reported by LCBN, although they reported TKE, and this is shown in Figure 2.9. Compared with our measurements, LCBN observed lower levels of TKE at the forest edge. Some underestimation of TKE was likely due to hot-film errors near the forest edge (where at Hotchkiss we observed frequent flow reversal). However, we believe that most of the difference relative to our data was due to the very dense LCBN forest, which results in low U and TKE in the subcanopy of the upwind forest, and in the clearing immediately downwind of the forest. At locations x/h > 1, TKE/S^2_{clr} in our cutblocks was statistically indistinguishable from LCBN's observations.

---

[3] We scaled σ_u, σ_w, and TKE at Hotchkiss by S_{clr}, and the RGB observations were scaled by U_{clr} (as were the LCBN observations). Since we looked at periods when V was small, the difference between the two normalisations was slight.

4.4. Similarity in wind "recovery"

We looked at a dimensionless shape factor for relative wind "recovery" across a forest clearing[4], to focus on the spatial pattern of wind statistics across different experiments. This wind recovery factor for U was defined as,

$$R_u(x) = \frac{U(x) - U_{for}}{U_{clr} - U_{for}} ,$$

where U_{for} was the velocity at (or near) the upwind forest edge, while U_{clr} was the reference clearing velocity (in our case measured at x/h = 20). We similarly defined a shape factor for TKE (R_{TKE}). For the wide cutblock we assumed that U_{for} and TKE_{for} were given by their values at x/h = -0.8. For the narrow cutblock we assumed that U_{for} and TKE_{for} were given by their values at x/h = 0.2.

Figure 2.10 shows R_U for the different experiments. While the RBG and LCBN data were in good agreement, we observed a much lower U recovery ($\partial R/\partial x$) in our cutblocks, particularly for the narrow cutblock (where there was U deceleration with x). The scatter in R_U suggests there is no "universal" recovery curve for average winds across a forest clearing. We speculate that the differences in R_U were due to large differences in the pressure fields, presumably induced by differences in forest/clearing geometry (although this apparently had little influence on the TKE, as described below). In the third phase of this study (Chapter 4) for example, we show model results predicting strong "adverse" pressure gradients across cutblocks ($\partial P/\partial x > 0$), which are sensitive to changes in the forest-clearing geometry.

In contrast to U, the different TKE observations collapsed about a "universal" R_{TKE} curve as shown in Figure 2.10 (we assumed $TKE = (2\sigma_u^2 + \sigma_w^2)/2$ in the RBG case). These experiments showed an initially rapid rise in TKE with x at the upwind edge of the clearing, with TKE reaching the clearing level at $x/h \approx 3$. From Figure 2.10 it appears that TKE peaked between x/h = 4 and 6, then fell slowly with increasing x. The fact that R_{TKE} was similar across experiments having different clearing dimensions (X_c/h = 1.7, 4.3, 6.1, 21.3, and > 22), and different upstream forest "entry-region" borders (2h, 6h, 15h, 53h), points to a limited influence of both upwind and downwind features on the *pattern* of TKE within a cutblock. We are hesitant to conclude this is universally true however, as the wind flow model described in the third phase of this series (Chapter 4) predicts otherwise.

5. Conclusions

We believe the "quiet" zone/"wake" zone picture provides a good description of the wind pattern in a forest cutblock. When the winds were oriented across the cutblock width, the quiet zone, where U and TKE were reduced from values in a large clearing, extended from $0 < x/h \leq 3$ (at our

---

[4]As mentioned by McNaughton (1989), it is ambiguous to speak of a wind recovery downwind of a forest -- what is the wind recovering to? For our purposes, we will speak of a wind "recovery" to conditions at our clearing location at x/h = 20.

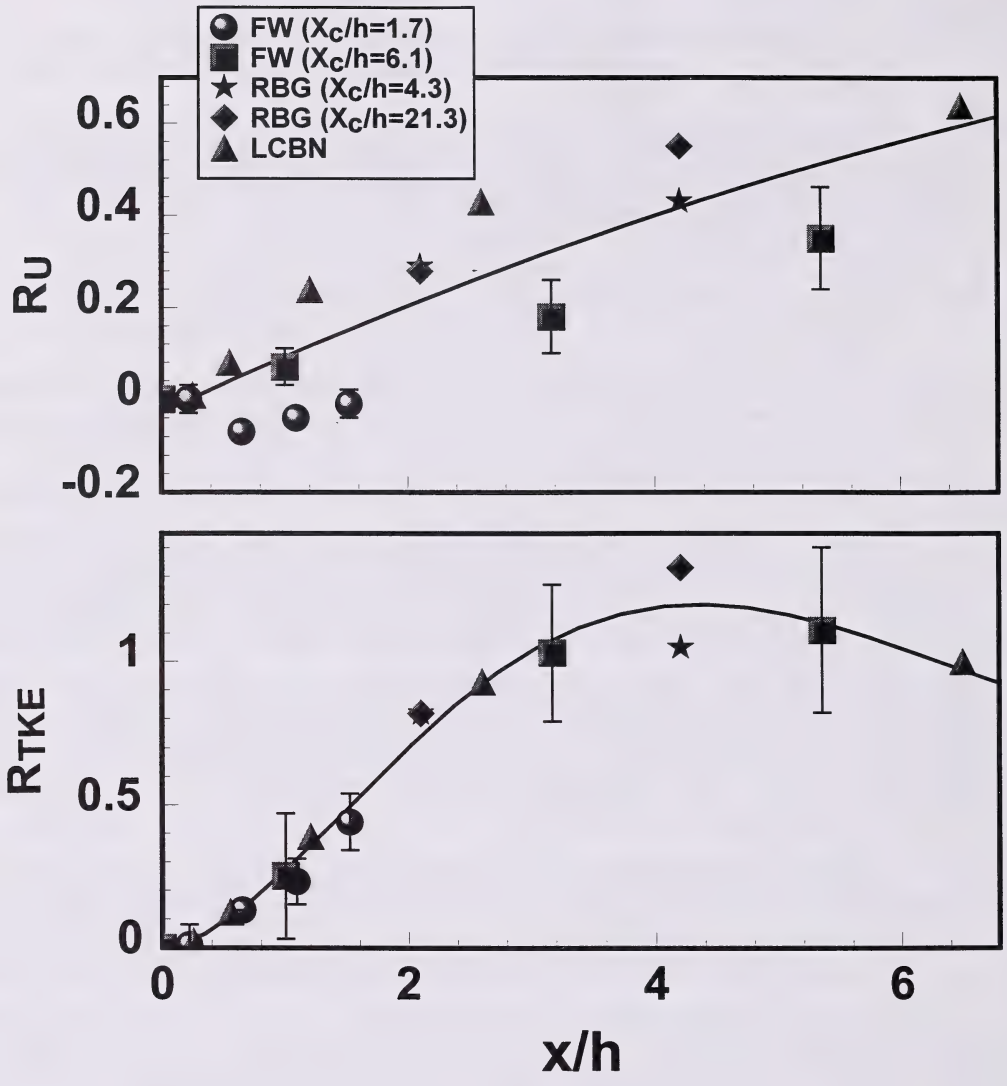

Figure 2.10. Relative recovery of U (R_U) and TKE (R_{TKE}) with distance from the upwind forest edge (x/h) for several experiments. FW denotes our observations, RBG denotes Raupach et al. (1987), and LCBN denotes Liu et al. (1996).

measurement height of z/h = 0.4). Downwind of this was a wake zone, where the TKE was above clearing values. Based on comparisons with other studies, we believe that this quiet/wake zone pattern exists across a wind range of cutblocks (with different dimensions, different upstream features, and different forest architectures).

The natural question asked by forest managers when considering shelterwood harvest designs, is how do cutblock dimensions affect wind shelter, and ultimately the windthrow of remnant spruce? Here we have considered only the case of winds oriented across the cutblock/forest strips, the expected circumstance during high wind events. We believe that the pattern of average wind velocity in a cutblock will vary according to the dimensions of the cutblock (and the upwind landscape). However, beyond the complicated region near the forest edge, it appears that U increases across the cutblock monotonically. Our observations do not point to an obvious optimum cutblock width that would balance economic efficiency (i.e., larger cutblocks) and good average wind reduction (smaller cutblocks).

This is not so in terms of the turbulence. The evidence suggests that once a cutblock width exceeds 3h, remnant trees beyond x/h = 3 will be subject to turbulence as energetic as observed in a large clearing (for trees of height $z \approx 0.5h$). This presupposes a significant border of upwind forest (at least 2h) -- the situation for all of the cutblocks/clearings studied here.

Our observations show that the extent of protection afforded by a sheltered cutblock depends on whether the focus is on the average wind velocity or turbulence. The relative importance of each in causing windthrow will depend on the frequency characteristics of the turbulence and the dynamical characteristics of the tree. This was the focus of the next phase of our work (Chapter 3). However, we can conclude that effective shelter for both U and TKE seems guaranteed within three tree heights of the upwind forest edge (for trees of height $z \approx 0.5h$).

6. References

Amiro, B.D., 1990. Comparison of turbulence statistics within three boreal forest canopies. Boundary-Layer Meteorol. 51: 99-121.

Baldocchi, D.D., and Meyers, T.P., 1988. A spectral and lag-correlation analysis of turbulence in a deciduous forest canopy. Boundary-Layer Meteorol. 45: 31-58.

Baldocchi, D.D., and Meyers, T.P., 1989. The effects of extreme turbulent events on the estimation of aerodynamic variables in a deciduous forest canopy. Agric. For. Meteorol. 48:117-134.

Bergen, J.D., 1975. Air movement in a forest clearing as indicated by smoke drift. Agric. Meteorol. 15: 165-179.

Finnigan, J.J., and Mulhearn, P.J., 1978. Modelling waving crops in a wind tunnel. Boundary-Layer Meteorol. 14: 253-277.

Finnigan, J.J., and Raupach, M.R., 1987. Transfer processes in plant canopies in relation to stomatal characteristics. In Stomatal Function, eds. Zeiger, Farquhar, and Cowan. Standford University Press.

Gash, J.H.C., 1986. Observations of turbulence downwind of a forest-heath interface. Boundary-Layer Meteorol. 36: 227-237.

Horst, T.W., 1972. A computer algorithm for correcting non-cosine response in the Gill anemometer. Pacific Northwest Laboratory Annual Report for 1971 to the USAEC Division of Biology and Medicine, Vol. II: Physical Sciences, Part 1: Atmospheric Sciences, BNWL-1651-1. Battelle, Pacific Northwest Laboratories, Richland, Wash.

Horst, T.W., 1973. Corrections for response errors in a three-component propeller anemometer. J. Appl. Meteorol. 12: 716-725.

Kaganov, E.I., and Yaglom, A.M., 1976. Errors in wind-speed measurements by rotation anemometers. Boundary-Layer Meteorol. 10: 15-34.

Liu, J., Chen, J.M., Black, T.A., and Novak, M.D., 1996. E-ε modelling of turbulent air flow downwind of a model forest edge. Boundary-Layer Meteorol. 77: 21-44.

McNaughton, K.G., 1989. Micrometeorology of shelter belts and forest edges. Phil. Trans. R. Soc. Lond. B 324: 351-368.

Navratil, S., Brace, L.G., Sauder, E.A., and Lux, S., 1994. Silvicultural and harvesting options to favor immature white spruce and aspen regeneration in boreal mixedwoods. Nat. Resour. Can., Can. For. Serv., Northwest Reg., Edmonton, Alberta. Inf. Rep. NOR-X-337.

Raine, J.K., and Stevenson, D.C., 1977. Wind protection by model fences in a simulated atmospheric boundary layer. Jour. Industrial Aerodynamics. 2, 159-180.

Raupach, M.R., Bradley, E.F., and Ghadiri, H., 1987. Wind tunnel investigation into the aerodynamic effect of forest clearing of the nesting of Abbott's Booby on Christmas Island. Progress Report, CSIRO Division of Environmental Mechanics, GPO Box 821, Canberra, ACT 2601, Australia.

Sakai, R.K., Fitzjarrald, D.R., and Moore, K.E., 1997. Detecting leaf area and surface resistance during transition seasons. Agric. For. Meteorol. 84:273-284.

Stull, R.B., 1988. An Introduction to Boundary Layer Meteorology. Kluwer Academic Publishers, Dordrecht, 666 pp.

Weiss, A., and Allen, L.H., 1976. Air-flow patterns in Vineyard Rows. Agric. Meteorol. 16, 329-342.

Wyngaard, J.C., 1981. Cup, propeller, vane, and sonic anemometers in turbulence research. Ann. Rev. Fluid Mech. 13: 399-423.

Appendix: Anemometer Errors

A.1. Cup anemometer errors

Comparing average cup windspeed (S) measured concurrently from cup anemometers and 3-D propeller anemometers showed cup overspeeding of up to 35% (we expected only small overspeeding from the propellers: Wyngaard, 1981). We observed increased overspeeding with increased turbulence intensity (e.g., σ_u/U), roughly as described by Kaganov and Yaglom (1976). A simple correction was used to account for overspeeding, by recalculating S as:

$$S = 0.93\, S_{unc} - 0.21 \qquad (m s^{-1}) \quad ,$$

where S_{unc} is the uncorrected cup anemometer windspeed. This formula was given by regression of S from the propellers and cup anemometers, and implicitly accounts for the effect of turbulent intensity -- the greatest turbulent intensities occurred where windspeed was low. A better correction factor would use turbulence intensity directly, but for most S observations we did not have turbulence measurements.

A.2. Propeller anemometer errors

Propeller anemometers have two deficiencies that lead to errors in turbulence statistics: propeller stalling and poor high frequency response. Stalling was obvious at three of our locations (at x/h = -0.8, 1.0, 7.2 at the wide-cutblock), as showed by spikes in the velocity probability density functions (PDFs). We believe that the resulting errors were not significant: our correction schemes (e.g., "redistributing" the spike in PDF at u = 0) did not significantly change the resulting statistics. This echos Horst (1973), who found stalling errors did not seriously affect commonly computed wind statistics. The poor high frequency response of the propellers was a more significant problem. Two approaches were used to estimate the frequency response errors: 1) a comparison between the propellers and a sonic anemometer, and 2) a spectral correction to the propeller velocity power spectra.

A 3-D sonic anemometer (CSAT-3, Campbell Sci. Inc.) was temporarily co-located with a 3-D propeller anemometer at x/h = 0.6 in the narrow cutblock (z/h = 0.4), and the u and w velocity statistics compared. We focused on two 30-minute periods (where $U > |V|$ and $\sigma_u > 0.5$ m s^{-1}). We found:

- the average U_{prop}/U_{sonic} was 1.04; the average $\sigma_{u\_prop}/\sigma_{u\_sonic}$ was 0.99;
- the average of $|W_{prop} - W_{sonic}|$ was 0.015 m s^{-1}; the average $\sigma_{w\_prop}/\sigma_{w\_sonic}$ was 0.88;
- the average of $|Sk_{u\_prop} - Sk_{u\_sonic}|$ was 0.17; the average Kt_{u_prop}/Kt_{u_sonic} was 1.14;
- the average of $|Sk_{w\_prop} - Sk_{w\_sonic}|$ was 0.35; the average Kt_{w_prop}/Kt_{w_sonic} was 1.69.

The agreement between the two anemometers was excellent for u statistics. As expected, the agreement in w statistics was worse. We also found disappointing agreement in v (e.g., $\sigma_{v\_prop}/\sigma_{v\_sonic}$ = 0.86), which we partially blame on flow interference caused by our anemometer setup.

We also considered a "spectral" correction to the propeller σ_u, σ_v, and σ_w values. The power spectra of velocity (S_u, S_v, S_w) were expected to show the theoretical -5/3 "fall-off" with frequency (ω) in the inertial subrange: e.g., $S_u(\omega) \propto \omega^{-5/3}$ (see Stull, 1988)[5]. We observed that at frequencies above 0.1 to 0.3 Hz, the propeller spectra departed from a -5/3 fall-off (Figure A2.1). The propeller power spectra were extended along a -5/3 fall-off (for $\omega > 0.1$ Hz), and "corrected" velocity variances were recalculated at all cutblock locations. This indicated that the propellers underestimated σ_u and σ_v by 1.5 to 4%, and underestimated σ_w by 6 to 10%.

We believe that the propellers gave reasonably accurate measurements of the turbulent statistics within the forest cutblocks, particularly for u and v. On this basis we decided not to correct the velocity statistics, recognizing that w turbulence statistics are in error, and that TKE was likely underestimated by between 5 and 10%.

[5] Although this seems reasonable within the cutblock, it is questionable within the forest, where vegetation may "short-circuit" the normal energy cascade (Baldocchi and Meyers, 1988).

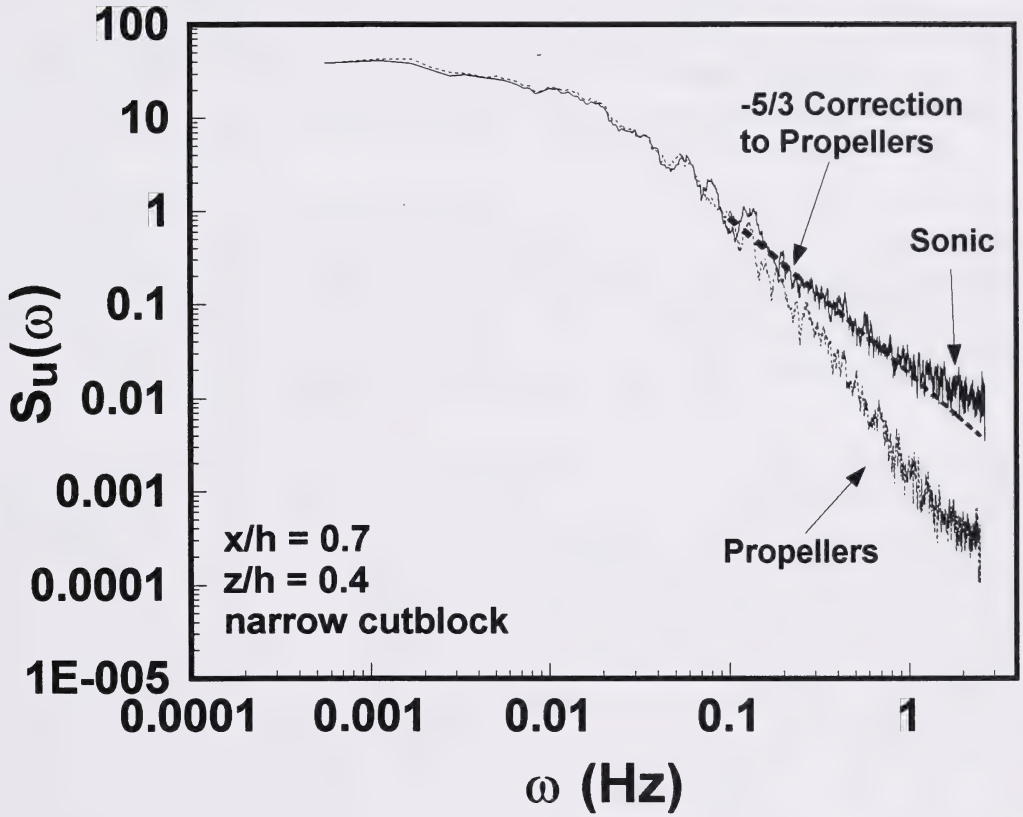

Figure A2.1. Power spectrum of u (S_u) versus frequency (ω) for a single 30-min period, during which there were simultaneous observations from a 3-D propeller and sonic anemometer. Also show is a -5/3 correction for the propeller spectrum.

CHAPTER 3

RELATING MEASURED TREE SWAY TO WIND STATISTICS

Thomas K. Flesch and John D. Wilson

1. Introduction

In the aspen (Populus tremuloides) and white spruce (Picea glauca) mixedwoods of Canada, foresters are investigating aspen harvest techniques that preserve the commercially and ecologically valuable spruce understory. An obstacle to this "two-stage" harvest is the susceptibility of the remnant spruce to windthrow (uprooting) after aspen removal. One approach to this problem, discussed in Chapter 2, is a shelterwood harvest system. In a shelterwood design (Figure 3.1) the aspen is harvested in a series of narrow cutblocks that are separated by unharvested forest strips (shelterwood). The forest strips provide a degree of wind shelter for the remnant spruce.

In Chapter 2 we described the wind statistics in two shelterwood cutblocks when the wind was oriented across the cutblock width. In the cutblock immediately downwind of the forest edge was a quiet zone, where the average across-cutblock wind velocity (U) and the turbulent kinetic energy (TKE) were reduced relative to the levels found in a nearby large reference clearing. This "quiet" zone was concentrated within three forest canopy heights (h) of the upwind forest edge (at the measurement height of $z = 0.4h$). Further downwind was a "wake" zone, where the TKE was at, or slightly above, the level in the reference clearing.

Although these observations confirm the existence of wind shelter within cutblocks, the extent and effectiveness of this shelter in terms of windthrow reduction are indefinite without consideration of the nature of the vulnerable trees themselves. Because the strain on the tree/soil complex results from the interaction of wind forces and tree mechanical properties (as well as soil properties), we cannot assume that wind statistics alone fully determine tree behaviour, and therefore windthrow occurrence. The work of Holbo et al. (1980), Mayer (1987), Gardiner (1994), and others have shown that trees behave as vibrating systems. In the terminology of systems theory, trees can act as amplifiers, with wind energy near their natural frequency(s) (ω_n) preferentially transferred into tree sway and strain on the tree/soil complex, and as low-pass filters, with high frequency wind energy adding little to the strain. If the turbulent wind force fluctuates at frequencies near ω_n, windthrow may occur at wind forces below the critical static load required to uproot a tree (Oliver and Mayhead, 1974; Blackburn et al., 1988). Understanding tree response therefore requires consideration of not only simple wind statistics, such as the average and standard deviation of the wind, but also of the frequency characteristics of the turbulence and the dynamical characteristics of the tree.

In this study we attempt to quantify cutblock wind shelter in terms of the magnitude of tree sway. Our assumption is that greater sway means greater strain on the tree/soil complex, and a greater likelihood of windthrow. Our analysis is based on a set of tree sway measurements, from which we formulated a simple mathematical model of tree displacement for a "characteristic" remnant spruce. This model is combined with observations of wind velocity in harvest cutblocks to diagnose the spatial variation in tree sway. Our analysis relies on spectral methods, similar to those employed by Holbo et al. (1980) and Mayer (1987). We consider only the case where the ambient wind direction was across the width of the cutblocks.

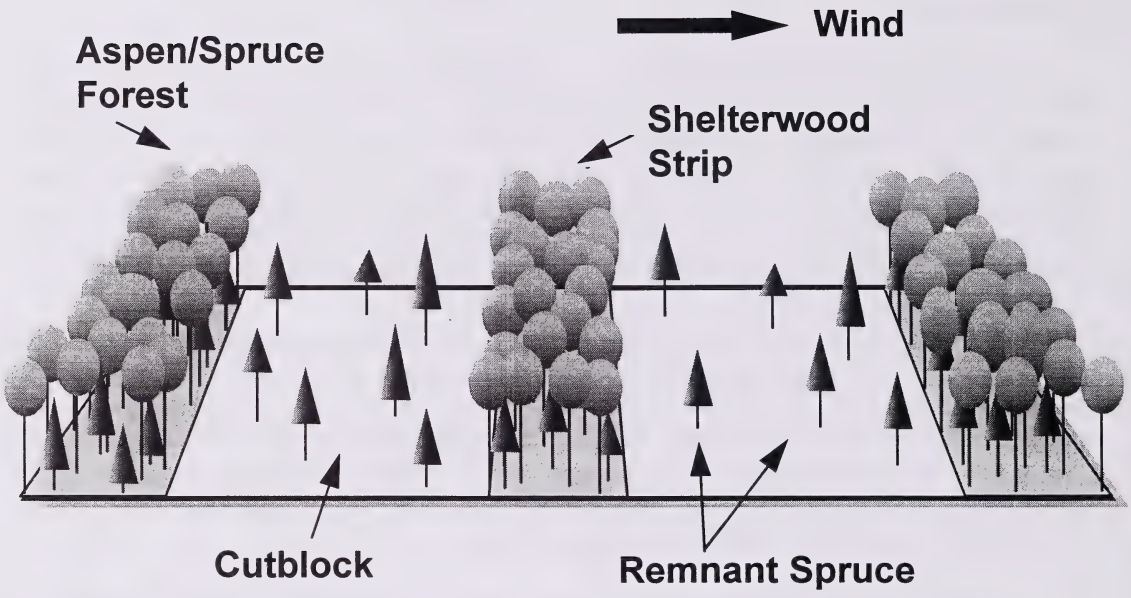

Figure 3.1. Idealised view of shelterwood harvest system. Cutblocks are created by selectively harvesting the mature aspen overstory, leaving the spruce understory intact. Forest strips (shelterwood) separate the cutblocks, providing wind shelter.

2. Field Measurements

2.1. Study site

Field measurements were made at the site of silvicultural trials at Hotchkiss River, near Manning, Alberta, Canada. The area is classified as boreal mixedwoods, having a predominately aspen overstory of 20 to 25 m in height, with a significant white spruce understory averaging 10 m in height. The site is on a gently rolling landscape. During the initial harvest, aspen and mature spruce were removed from long rectangular cutblocks. These varied in length from approximately 500 to 1000 m, and ranged in width from approximately 40 to 150 m. The cutblocks were oriented perpendicular to the direction of the expected maximum winds (westerly). Remnant spruce density in the cutblocks varied according to the density of the original understory. The forest canopy height (h) was 23 m.

Two cutblocks were studied: a wide cutblock with width X_c = 140 m (X_c/h = 6.1) and a length of 500 m, and a narrow cutblock with X_c = 40 m (X_c/h = 1.7) and length of 700 m. These cutblocks were each one of a periodic series, separated by forest strips of roughly the same width as the cutblock (the layout of these cutblocks are illustrated in Figure 2.2a and 2.2b in Chapter 2). We defined x as the across-cutblock coordinate (very nearly east-west), y as the along-cutblock coordinate (we expect flow properties to be roughly independent of y when winds were westerly), and z as the vertical coordinate. The coordinate x was set to zero at the upwind (west) edge of the instrumented cutblocks.

2.2. Wind measurements

Wind velocity time series were measured using three-dimensional propeller anemometers (R.M. Young Co., Gill UVW anemometer). Anemometers were placed at a height z = 9 m (z/h = 0.4) in transects across the two study cutblocks (the wide cutblock in 1994 and 1995, and the wide cutblock in 1996 and 1997). Measurements were made at five locations across the wide cutblock (at x/h = -0.8, 1.0, 3.2, 5.4, and 7.2), and five locations across the narrow cutblock (at x/h = -1.2, 0.2, 0.7, 1.1, and 1.5). We selected sites where the residual spruce density was low, and cut down the few trees that might have created wind anomalies along the transect. Measurements were made during periods of strong winds oriented directly across the cutblock (along the x direction, ± 30 deg). The sampling periods lasted either 15 minutes (wide cutblock) or 30 minutes (narrow cutblock), with a sampling frequency of 5 Hz. At each location there were either five or six observation periods (excepting observations at x/h = -1.2 and 0.7 in the narrow cutblock, where only two periods were used). The measurement periods are listed in Table 3.1. We used u, v, w to denote the instantaneous across-cutblock velocity (x direction), along-cutblock velocity (y direction), and the vertical velocity, respectively.

During our experiment, average wind speed (S_{clr}) and direction were measured in a large "reference" clearing 5 km from the study cutblocks. A cup anemometer (Met-One, model 013A) and wind vane were placed at z = 9 m approximately 20h downwind from the forest edge (for the wind direction studied here). The clearing extended a further 20 h downwind of the tower. Throughout this work we will use S_{clr} as a velocity scale to normalise our in-cutblock data, to permit

Table 3.1. Measurement periods used in the study.

No.	Cutblock Width	Date	Time	S_{clr} (ms^{-1})	Wind direction (0 is across the cutblock)	Gill UVW locations	Tree sway measurement locations
W-1	6.1h	27 Oct. 1994	1345-1400	6.41	3 deg	x/h = 1.0, 3.2, 5.4	x/h = 3.1, 3.3
W-2	6.1h	28 Oct. 1994	1015-1030	4.85	4 deg	x/h = 1.0, 3.2, 5.4	x/h = 3.1, 3.3
W-3	6.1h	28 Oct. 1994	1145-1200	4.97	16 deg	x/h = 1.0, 3.2, 5.4	x/h = 3.1, 3.3
W-4	6.1h	28 Oct. 1994	1200-1215	5.86	25 deg	x/h = 1.0, 3.2, 5.4	x/h = 3.1, 3.3
W-5	6.1h	4 Nov. 1994	1100-1115	6.21	3 deg	x/h = 1.0, 3.2, 5.4	x/h = 3.1, 3.3
W-6	6.1h	18 Nov. 1994	1615-1630	5.21	-16 deg	x/h = 1.0, 3.2, 5.4	x/h = 3.1, 3.3
W-7	6.1h	26 Oct. 1995	1145-1200	3.69	10 deg	x/h = -0.8, 3.2, 7.2	x/h = 3.0, 3.2
W-8	6.1h	26 Oct. 1995	1200-1215	3.70	24 deg	x/h = -0.8, 3.2, 7.2	x/h = 3.0, 3.2
W-9	6.1h	26 Oct. 1995	1545-1600	4.21	-7 deg	x/h = -0.8, 3.2, 7.2	x/h = 3.0, 3.2
W-10	6.1h	26 Oct. 1995	1615-1630	3.47	-14 deg	x/h = -0.8, 3.2, 7.2	x/h = 3.0, 3.2
W12	6.1h	26 Oct. 1995	1730-1745	4.39	-15 deg	x/h = -0.8, 3.2, 7.2	x/h = 3.0, 3.2
N-1	1.7h	7 Oct. 1996	1100-1130	4.71	4 deg	x/h = 0.2, 1.1, 1.5	x/h = 0.2, 1.5
N-2	1.7h	11 Oct. 1996	900-930	7.50	-13 deg	x/h = 0.2, 1.1, 1.5	x/h = 0.2, 1.5
N-3	1.7h	11 Oct. 1996	1000-1030	7.06	-10 deg	x/h = 0.2, 1.1, 1.5	x/h = 0.2, 1.5
N-4	1.7h	11 Oct. 1996	1200-1230	6.89	-3 deg	x/h = 0.2, 1.1, 1.5	x/h = 0.2, 1.5
N-5	1.7h	11 Oct. 1996	1400-1430	7.82	0 deg	x/h = 0.2, 1.1, 1.5	x/h = 0.2, 1.5
N-6	1.7h	26 Sep. 1997	1300-1330	4.94	-26 deg	x/h = -1.2, 0.7	No measurement
N-7	1.7h	26 Sep. 1997	1330-1400	4.94	-26 deg	x/h = -1.2, 0.7	No measurement

an assessment of the windiness of the cutblock *relative to* an essentially open region. We will also use S_{clr} and the wind direction to derive a reference velocity in the across-cutblock direction (U_{clr}). In November of 1995 we placed a 3-D propeller anemometer in the reference clearing to record the turbulence characteristics.

2.3. Tree sway measurements

The sway of selected remnant white spruce trees was measured concurrently with 16 wind measurement periods (Table 3.1). Bi-axial tilt sensors (Mountain Watch Inc., Calgary, AB), mounted on the stems at $z \approx 3$ m, gave angular displacements in the x and y directions (θ_x, θ_y). These were sampled at a frequency of 5 Hz, for durations of either 15 or 30 minutes. Two trees were measured during each observation period, with six trees measured in total: four near the centre of the wide cutblock, and one each at the upwind and downwind edge of the narrow cutblock (at x/h = 0.2 and 1.5). These trees were selected because they: 1) had a height near 15 m; 2) were isolated from other trees; and 3) were co-located (x-wise) with an anemometer. Selected trees were 30 to 60 m away from the anemometer transect lines. The height and diameter at breast height of the six measured trees are given in Table 3.2.

3. Modelling Tree Motion

We adopted a mechanical model of tree motion to relate winds to tree sway, but this was not absolutely necessary. A spectral approach can be used without employing a mechanical model, as discussed by Mayer (1987), by relying on a measured spectral transfer function to relate sway to the wind force spectrum[1]. This has the advantage of simplicity, and avoids characterising a tree mechanically. However, we believe that a mechanical model of tree sway provides a useful framework for analysis, allowing for more confident extrapolation of our results, and giving greater insight into tree behaviour. We modelled tree sway in the x and y direction separately, using the x- and y-components of the wind force. In the following discussion, we demonstrate our analysis for the x direction only, although there was a completely analogous treatment of y motion.

3.1. Mass-spring-damper tree model

Trees respond to variable forcing with an oscillating motion. A mass-spring-damper model was taken as the simplest means of describing this behaviour. In our conceptual model (Figure 3.2), the tree stem is a rigid rod which responds to the wind with an angular displacement of the stem. Flexibility occurs via a rotary spring attachment to the soil, which is damped by a rotary dashpot. The tree has a mass m which is uniformly distributed over a height z_t. Displacement in the x direction (θ_x), due to a distributed wind moment (W_x), is described by the following equation of motion:

---

[1] The wind "force" may be defined in different ways: as u at some point in the canopy (e.g. Gardiner, 1994); as the product of u and w above the canopy (e.g. Holbo et al., 1980); or as the height integral of the product of u|u|, foliage area, and a drag coefficient (Flesch and Grant, 1991).

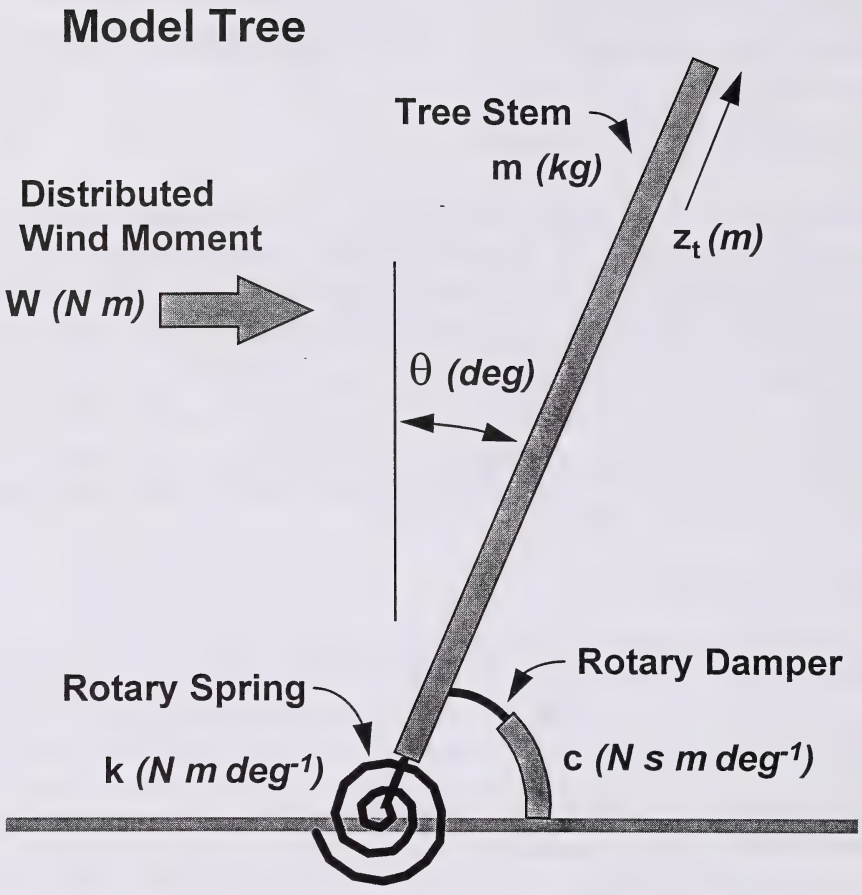

Figure 3.2. Conceptual model of tree. Stem is a rigid rod with mass m, attached to the ground via a rotary spring having a spring constant k. Angular displacement (θ) is damped with a rotary damper having a damping constant c.

$$\underbrace{(\frac{1}{3} m z_t^2) \frac{d^2\theta_x}{dt^2}}_{a1} + \underbrace{c \frac{d\theta_x}{dt}}_{a2} + \underbrace{k\theta_x}_{a3} - \underbrace{(\frac{m g z_t}{2}) \sin\theta_x}_{a4} = W_x(t) \quad , \tag{1}$$

where k is a spring constant (N m deg^{-1}), c is a damping constant (N s m deg^{-1}), and g is the gravitational acceleration. Terms a1, a2, a3, and a4 are the moments of inertia, damping, spring, and displaced mass, respectively. The wind moment W_x (N m) should properly be specified as the height integral of height multiplied by the wind-force (see Eq. (6) below). Assuming small displacements ($\sin\theta \cong \theta$), we defined $M = mz_t^2/3$ and $K = k - mgz_t/2$, so that Eq. (1) becomes:

$$M \frac{d^2\theta_x}{dt^2} + c \frac{d\theta_x}{dt} + K\theta_x = W_x(t) \quad . \tag{2}$$

If we specify $W_x = Kf_x$ (where f_x is a non-dimensional wind force), and divide Eq. (2) by M, we get the classic equation of motion for a mass-spring-damper system:

$$\frac{d^2\theta_x}{dt^2} + 2\zeta\omega_n \frac{d\theta_x}{dt} + \omega_n^2 \theta_x = \omega_n^2 f_x(t) \quad , \tag{3}$$

where ζ is a non-dimensional damping coefficient ($\zeta = c/2M\omega_n$), and ω_n is the natural frequency of the tree ($\omega_n^2 = K/M$). If the model tree is displaced and released, it oscillates at a frequency near ω_n, while ζ determines how quickly (in terms of a timescale c/M) the oscillations decay.

If the non-dimensional wind force is a simple cosine wave of frequency ω, where $f_x = (\beta/K) \cos \omega t$, the solution to Eq. (3) is (see Meirovitch, 1986)

$$\theta_x(t) = \frac{\beta}{K} |G(\omega)| \cos\big(\omega t - \Omega(\omega)\big) \quad , \tag{4}$$

with

$$|G(\omega)| = \sqrt{\frac{1}{\Big(1 - (\omega/\omega_n)^2\Big)^2 + \Big(2\zeta\omega/\omega_n\Big)^2}} \quad ,$$

$$\Omega(\omega) = \tan^{-1}\left(\frac{2\zeta\omega/\omega_n}{1 - (\omega/\omega_n)^2}\right) \quad . \tag{5}$$

The tree response is therefore a cosine wave with the same frequency as the wind force: the displacement amplitude is given by the transfer function |G|; and the displacement lags the input force by a phase lag Ω. Examples of |G| and Ω are given in Figure 3.3.

While the actual wind force W_x acting on a tree will not be a simple cosine wave, the solution expressed as Eq. (4) generalises to more complex cases. Because the mass-spring-damper model

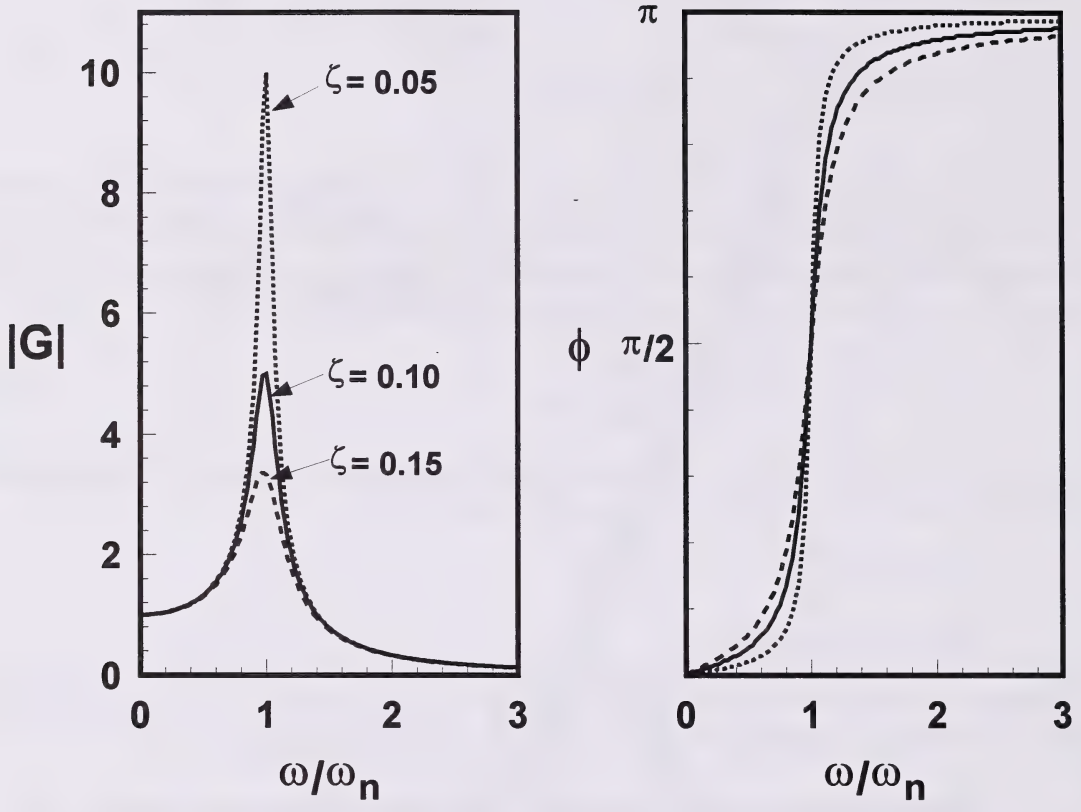

Figure 3.3. Transfer functions |G| and φ plotted versus normalised frequency (ω/ω_n). These are for an ideal mass-spring-damper system.

is linear, we can invoke superposition to determine the response to complicated forcing. If W_x is expressed as a Fourier series, then the total response of the tree is given by the sum of the individual responses to each frequency component of W_x. At each frequency, Eqs. (4) and (5) describe that mode of displacement.

3.2 Estimating the wind moment

The wind moment W_x acting a tree should be written as the height integral of the product of the drag coefficient (C_d), the tree frontal area density (A, m^2m^{-1}), and the relative wind velocity at the tree location (u - z dθ/dt):

$$W_x(t) = \frac{1}{2}\rho \int_0^{z_t} C_D(z)\, A(z) \left((u - z\frac{d\theta}{dt})\,|(u - z\frac{d\theta}{dt})| \right) z\, dz \quad , \tag{6}$$

where ρ is the air density. Application of this rigorous formulation requires height profiles of A, C_d, and U: comprehensive information that is rarely available, and was not for this study. Instead we assumed that W_x can be parameterised as proportional to u|u| at a single reference location, here chosen as a point at our wind measurement height z = 9 m, and at the same x location as the tree in question ($u|u|_{x,z=9m}$). We also assumed that u(z) >> z dθ/dt, thus

$$W_x(x,t) = C_0\,(u|u|)_{x,\,z=9m} \quad , \quad or \quad f_x(x,t) = \frac{C_0}{K}\,(u|u|)_{x,\,z=9m} \quad , \tag{7}$$

where C_0 (kg) is an aggregate drag constant,

$$C_0 = \frac{1}{2}\rho \left(\int_0^{z_t} C_d(z)\, A(z)\, u(x,z)|u(x,z)|\, z\, dz \right) / (u|u|)_{x,\,z=9m} \quad . \tag{8}$$

The value of C_0 will vary from tree to tree due to differences in z_t and A. It would also change if one were to choose an alternative reference height for the wind velocity input[2]. The ratio C_0/K, which we later define as the reciprocal of tree "stiffness", is in essence a proportionality constant which relates u|u| to tree displacement. Hereafter, u|u| will refer to velocity measurements taken at z = 9 m and at a specific x location, and we drop the subscript (x, z = 9 m).

Our analysis of tree motion relied on expressing the wind force as a Fourier series. A discrete time series of u|u|, providing N observations over time T (with a sampling interval Δt), was written as a finite Fourier series (Chatfield, 1984):

$$u|u|(t) = \langle u|u| \rangle + \left(\sum_{p=1}^{N/2-1} R_{u|u|}(p\omega_0) \cos\left(2\pi p \omega_0 t + \varphi_{u|u|}(p\omega_0)\right) \right) + a_{N/2} \cos(\pi t / \Delta t) \quad , \tag{9}$$

where $\omega_0 = 1/T$, $R_{u|u|}(p\omega_0)$ and $\varphi_{u|u|}(p\omega_0)$ are the amplitude and phase of the p^{th} harmonic, and $\langle u|u| \rangle$

[2] C_0 will also vary with time for a single tree: C_d and A are likely to be velocity dependent (Thom, 1971); and the shape of the instantaneous velocity profile may also exhibit variability.

is the time average of u|u|. The coefficient $a_N/2$, defined as $\sum(-1)^{t/\Delta t}\, u|u|(t) / N$, is usually small and was thus neglected. We defined the power spectrum $S_{u|u|}$ as

$$S_{u|u|}(p\omega_0) = R^2_{u|u|}(p\omega_0) / (2\omega_0) \quad , \tag{10}$$

so that

$$\sigma^2_{u|u|} = \sum_{p=1}^{N/2-1} S_{u|u|}(p\omega_0)\ \omega_0 \quad . \tag{11}$$

Power spectra were obtained by standard Fourier analysis, and smoothed using a simple moving average. At each location we created an ensemble-averaged spectrum from the five or six observed u|u| spectra, making the transform to wavenumber $\kappa = \omega / S_{clr}$. The basis for using this transform is the belief that turbulent eddies in the forest environment have invariant spatial dimensions (which scale on h). While increasing wind speeds advect these eddies more rapidly, therefore shifting $S_{u|u|}$ toward higher frequencies, a power spectral density defined in terms of wavenumber, $S_{u|u|}(\kappa)$, remains invariant[3].

3.3. Estimating ζ, ω_n, and K/C_0

A determination of ζ, ω_n, and an equivalent stiffness (K/C_0) is necessary to apply the mass-spring-damper model. This was done by reconciling the model transfer function |G| with the measured power spectra of tree displacement ($S_{\theta x}$) and wind force ($S_{u|u|}$). In our mass-spring-damper model, $S_{\theta x}$ and $S_{u|u|}$ are related by the simple algebraic expression,

$$S_{\theta x}(\omega) = \left(\frac{C_0}{K}\right)^2 |G(\omega)|^2\, S_{u|u|}(\omega) \quad , \tag{12}$$

where $|G(\omega)|$ is given by Eq. (5). We can then calculate a "measured" transfer function by rearranging Eq. (12),

$$|G(\omega)|_{meas.} = \frac{K}{C_0} \sqrt{S_{\theta x}(\omega) / S_{u|u|}(\omega)} \quad . \tag{13}$$

If the mass-spring-damper model was accurate, and u|u| was the exact wind force acting on the tree, then $|G(\omega)|_{meas}$ should exactly equal $|G(\omega)|$, so that

$$\frac{(C_0/K)^2}{\left(1 - (\omega/\omega_n)^2\right)^2 + \left(2\zeta\omega/\omega_n\right)^2} = S_{\theta x}(\omega) / S_{u|u|}(\omega) \quad . \tag{14}$$

---

[3] In fact it was not clear whether $S_{u|u|}$ showed smaller sampling variation when plotted versus κ or ω. The range of S_{clr} in our experiment was relatively small, so the superiority of scaling with respect to κ may not have been apparent.

One could then solve for K/C_0, ζ and ω_n. Because our observations of tree sway were made at a different y location than were our observations of the wind, and because $S_{\theta x}$ and $S_{u|u|}$ were "noisy", the function $S_{\theta x}/S_{u|u|}$ was not smooth. Values of K/C_0, ζ, and ω_n were found by iteration, minimizing the error between the (modelled) left-hand side of Eq. (14), and the (measured) right-hand side. This fitting exercise was confined to $\omega < 0.6$ Hz, due to the inaccuracy of the mass-spring-damper model at higher frequencies (as discussed below).

3.4. Predicting tree sway

With values of ζ, ω_n, and K/C_0 established, the mass-spring-damper model allows predictions of θ_x from a time series of u|u|. Our approach was to predict the variance of sway angle, and the maximum sway angle, for our characteristic tree during a "characteristic" 15 minute time period (defined by the ensemble average $S_{u|u|}/\sigma^2_{u|u|}$). The variance of θ_x (with N observations over time T), is given by:

$$\frac{\sigma^2_{\theta_x}}{(C_0/K)^2} = \sum_{p=1}^{N/2-1} |G(p\omega_0)|^2 S_{u|u|}(p\omega_0)\ \omega_0 \ , \qquad \textbf{(15)}$$

where $\omega_0 = 1/T$. A discrete θ_x time series is implied by the $S_{u|u|}$ and $\varphi_{u|u|}$ spectra:

$$\frac{\theta_x(t)}{C_0/K} = \langle u|u| \rangle + \sum_{p=1}^{N/2-1} |G(p\omega_0)| \sqrt{2\omega_0 S_{u|u|}(p\omega_0)}\ \cos\left(2\pi p\omega_0 t + \varphi_{u|u|}(p\omega_0) - \Omega(p\omega_0)\right) \ . \qquad \textbf{(16)}$$

Equation (16) allows us to predict a maximum displacement (θ_{xmax}) from a u|u| time series. Equations (15) and (16), and their equivalents in the y direction, were employed at three locations in the narrow cutblock, five locations across the wide cutblock, and in the reference clearing. The steps used to make sway predictions were as follows:

1. Select an average wind velocity U_{clr} in the reference clearing ($S_{clr} \approx U_{clr}$). We considered the case of winds oriented directly across the cutblock ($V = 0$, $\langle v|v| \rangle = 0$).

2. Assign $\langle u|u| \rangle$, $\sigma_{u|u|}$, and $\sigma_{v|v|}$ values at each location based on our observations of the value of $\langle u|u| \rangle / U^2_{clr}$, $\sigma_{u|u|}/U^2 clr$, and $\sigma_{v|v|}/U^2_{clr}$.

3. Convert the ensemble-average wavenumber-based $S_{u|u|}(\kappa)/\sigma^2_{u|u|}$ and $S_{v|v|}(\kappa)/\sigma^2_{v|v|}$ at each location to the frequency-based $S_{u|u|}(\omega)$ and $S_{v|v|}(\omega)$.

4. Calculate $\sigma_{\theta x}$ using Eq. (15), then create $\sigma_{\theta y}$. The total displacement variance is defined as:
$$\sigma^2_\theta = \sigma^2_{\theta_x} + \sigma^2_{\theta_y} \ . \qquad \textbf{(17)}$$

5. Calculate 15 minute time-series of θ_x using Eq. (16), from which θ_{xmax} is determined (five or six time-series of θ_x were created for each location, using the ensemble-average $S_{u|u|}$ combined with the five or six observed $\varphi_{u|u|}$ spectra, from which an average θ_{xmax} was

calculated). A simultaneous θ_y time series was created from the v|v| spectra. The maximum displacement is calculated as:

$$\theta_{max} = maximum \sqrt{\theta_x^2(t) + \theta_y^2(t)} \quad . \qquad \textbf{(18)}$$

3.5. Accuracy of the tree model

How well does a simple mass-spring-damper model describe tree sway? Reasonably well, based on the agreement between the model transfer function |G| (Eq. 5) and the measured transfer function $|G|_{meas}$ (Eq. 13). Figure 3.4a illustrates this agreement for one tree during one of our 15-minute measurement periods. The result was typical, with $|G|_{meas}$ closely resembling |G| for $\omega \lesssim 0.6$ Hz. The sharp peak in $|G|_{meas}$ near $\omega = 0.5$ Hz corresponds to the natural frequency of the tree (ω_n). A more stringent test of model fidelity is the comparison of modelled sway angle $\theta_x(t)$ (from Eq. 16) with an actual displacement time series. Figures 4c and 4d show such a comparison. The two series should not be identical. The wind observations were made more than 30 m from the actual tree, so that u|u| should correspond to the actual forcing on the tree only in a statistical sense (rather than a deterministic sense). We considered that there was tolerable agreement between the actual and reconstructed sway, as reflected in agreement between the actual and modelled probability density function (PDF) for θ_x (Figure 3.4b).

While the tree illustrated in Figure 3.4 exhibited mass-spring-damper behaviour at low frequencies, this was not the case for $\omega \gtrsim 0.6$ Hz. The poor fidelity of our model at high frequencies was partially the result of the tree being a continuous system (as opposed to our single degree-of-freedom model), possessing many vibrating modes and a corresponding number of natural frequencies above the fundamental natural frequency. Vibrations at these higher natural frequencies would appear as secondary peaks in |G|. Our observations showed a consistent secondary peak in |G| at two to three times the fundamental peak Another contribution to the poor high frequency performance of our too-simple model may be the shaking branches of the trees, which transmit high frequency motion to the stem.

Given our focus on windthrow, we believe that a mass-spring-damper model is a good choice to describe tree sway, despite its inaccuracy at high frequencies. The model gives an accurate description of stem motion (at a single point) for frequencies up to, and including the fundamental natural frequency. All indications are that tree sway in the fundamental mode is the predominate form of motion, and is responsible for windthrow. For instance, Wood (1995) analysed a composite Sitka spruce tree and found that vibration in the fundamental mode resulted in a maximum stress at the ground (consistent with uprooting), while second mode vibration resulted in a maximum stress at 80% of the tree height, and is therefore unlikely to explain uprooting.

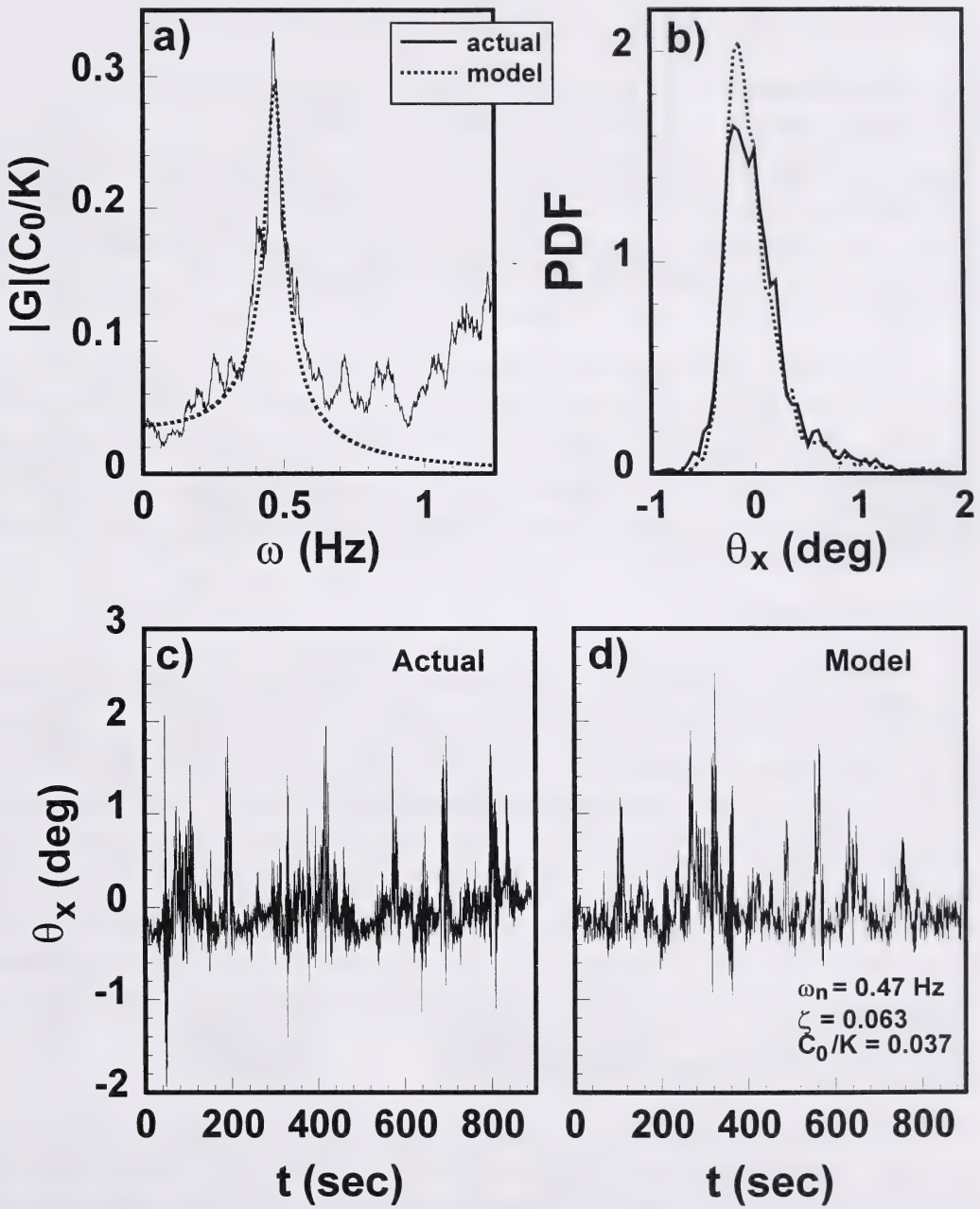

Figure 3.4. Comparison of actual and modelled tree displacement (x direction) during a 15-min observation period: a) the normalised transfer function $|G|(K/C_0)$ plotted versus frequency ω; b) the probability density function (PDF) of the fluctuating displacement ($\theta_x - \langle\theta_x\rangle$); c) the actual displacement time series; and d) the displacement time series from mass-spring-damper model in response to the measured u|u| forcing.

4. Wind Forces in the Cutblocks[4]

4.1. Average wind force

The average alongwind wind "force" ($\langle u|u| \rangle$) in the cutblocks was significantly reduced relative to concomitant values in the nearby large reference clearing (Figure 3.5). In the cutblocks, $\langle u|u| \rangle$ was never greater than 25% of the corresponding value in the reference clearing (for winds oriented across the cutblock). The average displacement of our characteristic remnant spruce in the cutblocks would therefore be less than 25% of that in the clearing (since $\langle \theta_x \rangle \propto \langle u|u| \rangle$). In terms of average tree displacement, the cutblocks provided very effective shelter.

The pattern of $\langle u|u| \rangle$ across the cutblocks was as expected, given the velocity statistics described in Chapter 2, noting that $\langle u|u| \rangle \approx \langle u^2 \rangle \equiv U^2 + \sigma_u^2$. Upwind of the wide cutblock (x/h = -0.8), $\langle u|u| \rangle$ was only 2% of that in the reference clearing. Its value increased steadily with x across the cutblock, reaching 25% of the clearing value at x/h = 5.4, before rapidly decreasing into the downwind forest. In the narrow cutblock, $\langle u|u| \rangle$ remained at only 3-5% of the clearing values. Interestingly, we observed an initial decrease in $\langle u|u| \rangle$ with x in the narrow cutblock, so that the minimum $\langle u|u| \rangle$ lay at x/h = 1.1.

4.2. Turbulent wind force

Figure 3.5 also shows the (normalised) standard deviation $\sigma_{u|u|}$ of the wind force across the cutblocks. An increase in $\sigma_{u|u|}$ would indicate an increase in the peak wind force, and correlate with increased tree sway. Compared with the reference clearing, $\sigma_{u|u|}$ in the cutblocks was reduced, but not by so large a factor as was $\langle u|u| \rangle$. In the forest upwind of our wide cutblock (x/h = -0.8), $\sigma_{u|u|}$ was only 4% of the clearing value. Its value increased to 50% at x/h = 5.4 in the wide cutblock, before falling rapidly in the downwind forest. In the narrow cutblock $\sigma_{u|u|}$ remained at low levels, ranging from 8-16% of the clearing values. The pattern of $\sigma_{u|u|}$ differed from that of σ_u, which was described in Chapter 2. While σ_u in the cutblock reached or exceeded its value in the reference clearing, $\sigma_{u|u|}$ remained well below its clearing value (because the average velocity U, a component of $\sigma_{u|u|}$, remained well below its clearing value). The across-wind force fluctuations ($\sigma_{v|v|}$) exhibited a pattern similar to $\sigma_{u|u|}$. In the wide cutblock $\sigma_{v|v|}$ was approximately 60% of $\sigma_{u|u|}$. In the narrow cutblock, the magnitudes of $\sigma_{u|u|}$ and $\sigma_{v|v|}$ were nearly equal.

4.3. Power spectra

Our observations showed that the sheltered cutblocks provided an environment where wind forces were reduced compared with large clearings. However, the frequency characteristics of the turbulent wind force are also important in determining the effectiveness of wind shelter at reducing tree sway. Figure 3.6 shows ensemble-averaged power spectra of the wind force ($S_{u|u|}/\sigma^2_{u|u|}$) at different cutblock locations. These normalised spectra do not reflect differences in the magnitude

---

[4] Our measurements of u|u| were subject to errors due to the poor high frequency response of the propeller anemometers. These errors, and our correction to the u|u| time series, are discussed in the Appendix.

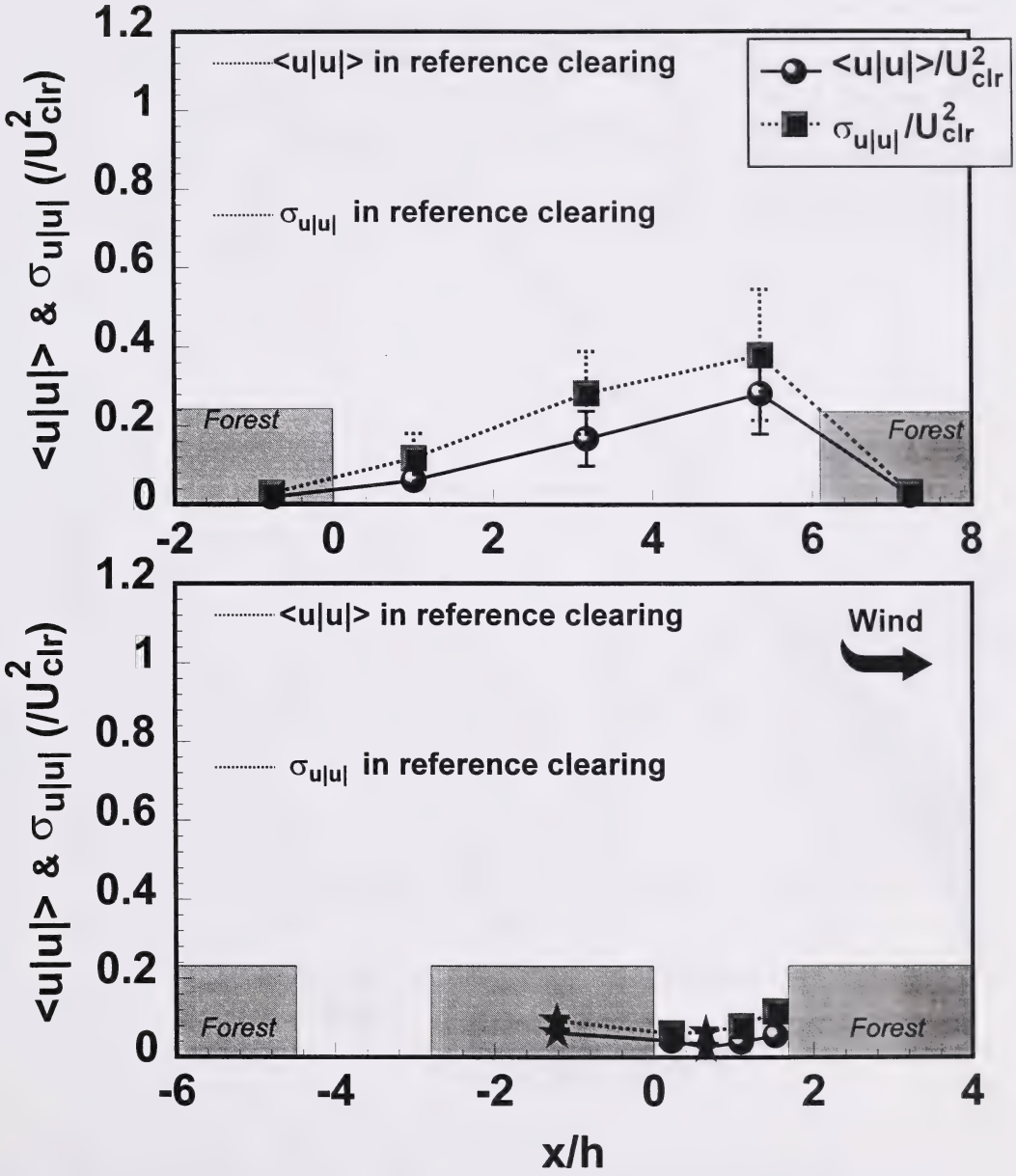

Figure 3.5. The average across-cutblock wind force <u|u|> and standard deviation $\sigma_{u|u|}$, scaled on the average velocity in the reference clearing (U_{clr}), plotted versus x across the wide cutblock (top) and the narrow cutblock (bottom). The average wind direction was across the cutblock (along x direction, ± 30 deg). The "error bars" surrounding each observation are ± one standard deviation. Values of normalised <u|u|> and $\sigma_{u|u|}$ in the reference clearing are shown by the level dashed line.

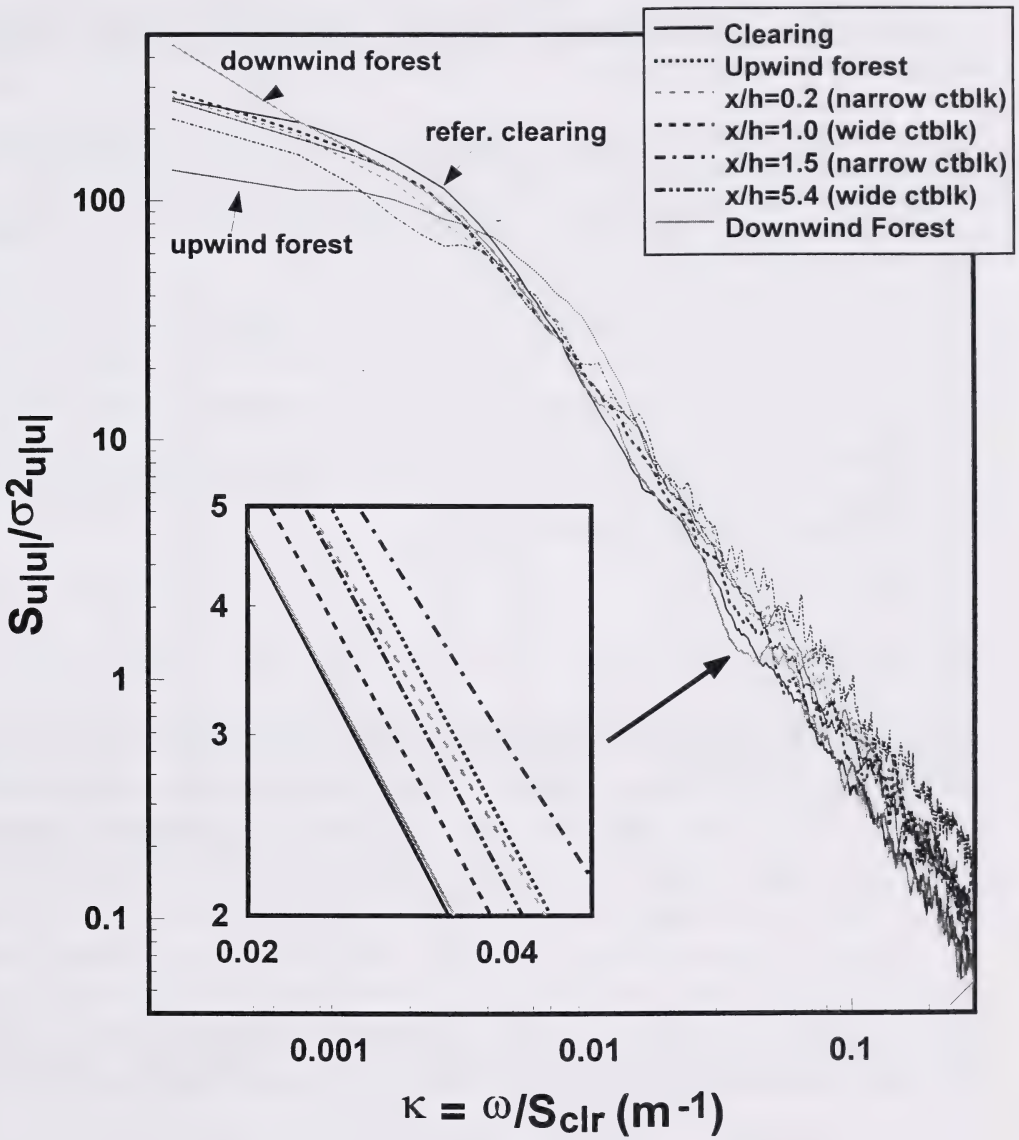

Figure 3.6. Ensemble-averaged power spectra of the across-cutblock wind force ($S_{u|u|}$), scaled on the variance of u|u| ($\sigma^2_{u|u|}$), and plotted versus wavenumber κ ($= \omega/S_{clr}$). Different lines represent spectra at different locations in the wide and narrow cutblock. Inset is geometric fit to spectra in the κ range corresponding to the tree natural frequency.

of u|u| fluctuations between locations, only differences in the relative wavenumber contributions (e.g., because $\sigma^2_{u|u|}$ in the clearing was 600 times greater that in the forest, $S_{u|u|}$ in the clearing greatly exceeded that in forest at all wavenumbers). The $S_{u|u|}/\sigma^2_{u|u|}$ had a shape as expected, with the greatest "power" at the lowest wavenumbers.

The higher frequency range is of most interest when considering tree sway. Trees will respond preferentially to u|u| in the frequency range near ω_n, and literature values of ω_n generally exceed 0.1 Hz. The inset of Figure 3.6 focuses on $S_{u|u|}/\sigma^2_{u|u|}$ from $\kappa = 0.02$ to 0.05 m^{-1} (this corresponds to $\omega = 0.2$ to 0.5 Hz when $S_{clr} = 10$ m s^{-1}). Two trends were evident in this wavenumber region. First, the high wavenumber contributions to u|u| were larger in the narrow cutblock than in the wide cutblock, which were in turn larger than in the clearing. Second, within each cutblock there was an increase in the high wavenumber contribution with increasing downwind distance x. We can therefore speculate that the "effectiveness" of the wind in generating tree sway varies with cutblock location. The wind effectiveness would be lowest in the clearing, and highest in the narrow cutblock. So while the sheltered cutblocks provided an environment of reduced $<u|u|>$ and $\sigma_{u|u|}$, this was accompanied by an increase in the effectiveness of the wind at creating tree sway (we show later, however, that differences in wind "effectiveness" did not significantly change the fact that sway at all locations was well correlated with $\sigma_{u|u|}$).

5. Modelled Tree Sway

5.1. "Characteristic" remnant spruce

The effective stiffness (K/C_0), natural frequency (ω_n), and damping coefficient (ζ) of the six remnant spruce examined in our study are shown in Table 3.2. The average K/C_0 was 63 $m^2s^{-2}deg^{-1}$, with a standard deviation of almost the same magnitude. This high variability was expected, given the variability in tree features which effect K and C_0: differences in tree height, stem diameter, soil strength, and root patterns all affect the stiffness K; and differences in tree height and foliage amount and distribution affect the effective drag coefficient (C_0). There was considerably less variation in ζ and ω_n. Among the six trees, ζ averaged 0.11, with a standard deviation of 0.04. The average ω_n was 0.41 Hz, with a standard deviation of 0.06 Hz. While we observed directional differences in these characteristics for each tree, they were not consistent (e.g., some trees were stiffer in the x direction, others in the y direction). When we compare these values of ζ and ω_n with values found in other studies of similar trees (Table 3.3), we conclude that our "characteristic" remnant spruce had a ω_n within the expected range, although it was more heavily damped than expected.

5.2. Sway characteristics

Using the mass-spring-damper model, we predicted remnant tree sway over a "characteristic" 15 minute period (defined by the ensemble average $S_{u|u|}/\sigma^2_{u|u}$ and $S_{v|v|}/\sigma^2_{v|v|}$) for the case of winds oriented across the cutblock. Our characteristic tree was defined to have $\zeta = 0.11$ and $\omega_n = 0.4$ in both the x and y directions. Since our interest was in the spatial variation of the sway of a single reference tree, not absolute displacements, we did not define a characteristic stiffness K/C_0. Hereafter, we report displacements scaled on C_0/K (the units of the scaled θ are m^2s^{-2}). We emphasise that the following results are predictions (not measurements) of tree sway, founded on

Table 3.2. Properties of the six white spruce trees examined during this study. Displacement properties are presented in both x and y directions. The y motion of tree 6 was not properly recorded.

Tree no.	tree height: z_t (m)	stem diameter: dbh* (m)	effective stiffness: K/C_0 ($m^2\ s^{-2}\ deg^{-1}$)	damping coeff.: ζ	natural freq.: ω_n (Hz)
1	12.1	0.19	x: 28.5 (2.8) y: 25.7 (3.2)	x: 0.083 (0.015) y: 0.089 (0.021)	x: 0.49 (0.03) y: 0.48 (0.01)
2	12.8	0.19	x: 106.6 (13.4) y: 63.6 (9.9)	x: 0.095 (0.019) y: 0.095 (0.018)	x: 0.49 (0.02) y: 0.45 (0.04)
3	13.1	0.22	x: 7.9 (1.3) y: 14.0 (3.4)	x: 0.165 (0.032) y: 0.159 (0.020)	x: 0.30 (0.01) y: 0.33 (0.02)
4	14.6	0.30	x: 162.1 (26.0) y: 169.5 (43.9)	x: 0.108 (0.042) y: 0.140 (0.026)	x: 0.37 (0.01) y: 0.38 (0.01)
5	12.7	0.17	x: 24.5 (5.1) y: 13.5 (1.9)	x: 0.092 (0.012) y: 0.052 (0.004)	x: 0.43 (0.01) y: 0.44 (0.00)
6	17.2	0.19	x: 76.7 (6.1) y: ---- ----	x: 0.153 (0.020) y: ---- ----	x: 0.34 (0.01) y: ---- ----
Ave			63.0 (56.6)	0.112 (0.035)	0.41 (0.06)

* Diameter at Breast Height

Table 3.3. The natural frequency (ω_n) and damping coefficient (ζ) of trees reported in the literature. These trees had a similar height (z_t) and stem diameter (dbh: diameter at breast height) as our study trees.

Tree Type	z_t (m)	dbh (m)	ω_n (Hz)	ζ	Reference
White Spruce	12 - 17	0.17 - 0.30	0.30 - 0.49	0.05 - 0.17	This study
Sitka Spruce	13 - 14	0.14 - 0.21		0.01 - 0.05	Blackburn et al. (1988)
Sitka Spruce	13 - 15	0.11 - 0.18	0.26 - 0.40	0.06 - 0.07	Milne (1991)
Sitka Spruce	10 - 14	0.10 - 0.18	0.39 - 0.47	0.04 - 0.08	Gardiner (1995)

the measured wind plus the (now calibrated) tree model. Actual tree displacements were used only in the development of the tree model. Although we have shown model skill at replicating actual tree displacements, an uncertainty follows from the use of a model.

Figure 3.7 shows our predictions of tree sway, in the form of the normalised standard deviation of displacement σ_θ/U^2_{clr}, and normalised maximum displacement θ_{max}/U^2_{clr} (recall the factor C_0/K has been absorbed in θ). Two features are evident: the effect of increasing ambient wind velocity on sway, and the change in sway magnitude with location. Our predictions show that increasing the ambient wind velocity increases the sway more than the corresponding increase in wind forces. On average σ_θ/U^2_{clr} was about 10% higher when U_{clr} was 15 m s^{-1} compared with 5 m s^{-1}, and θ_{max}/U^2_{clr} was about 15% higher (these ratios would remain unchanged if sway were purely proportional to wind force). This sway "amplification" is attributed to an increase in wind "power" at frequencies near ω_n -- an increase in U_{clr} shifts $S_{u|u|}$ toward higher frequencies. This was a consequence of our assumption that $S_{u|u|}/\sigma^2_{u|u|}$ and $S_{v|v|}/\sigma^2_{v|v|}$ were invariant when plotted with wavenumber κ, and therefore this result should not be taken as an independent observation. Because the sensitivity of tree sway to U_{clr} was predicted to be roughly the same at all locations, the relative sway in the cutblocks (i.e., sway relative to an identical tree in the clearing) was insensitive to U_{clr}. We therefore predict that the shelter effectiveness (given by the relative sway) will not change with changing ambient windspeed.

The most distinctive feature in Figure 3.7 is the increase in both σ_θ and θ_{max} with increasing x across the cutblocks. In the forest immediately upwind of our wide cutblock, we calculated that σ_θ would be 6% of the corresponding value for that tree if located in the clearing (with no inter-tree contact), implying excellent wind shelter. By x/h = 5.4, σ_θ had reached approximately 60% of its value in the reference clearing. The value of σ_θ then fell rapidly in the downwind forest. The pattern of maximum displacement was slightly different. The θ_{max} varied from 10% of its clearing value in the upwind forest, to 57% at x/h = 3.2; however there appeared to be a plateau between x/h = 3.2 and 5.4. As expected, both σ_θ and θ_{max} in the narrow cutblock were low, ranging from 10 to 30% of their clearing values. Other features of predicted sway in the cutblocks included:

1. The average displacement $<\theta_x>$ was small compared with the maximum displacement, with $\theta_{xmax}/<\theta_x> \approx 20$. This was larger than the value of 10 measured by Stacey et al. (1994) in a wind tunnel model forest. At our reference clearing $\theta_{xmax}/<\theta_x> \approx 5$.

2. Relative to the clearing, θ_{max} was never reduced by as much as was σ_θ. This reflects the intermittent nature of the cutblock winds, where the maximum gust velocities are not reduced to the same fractional extent as the reduction in U of σ_u.

3. The ratio $\theta_{max}/\sigma_\theta$ ranged from 5 to 10. It was highest in the forest, lowest in the reference clearing, and ranged from 6 to 8.5 in the cutblocks. This ratio was predicted to increase slightly with increasing U_{clr}.

We can infer from the tree model that a significant amount of tree motion can be labelled as "resonant sway". In a "static" system the displacement is proportional to the driving force, so that $\sigma_{\theta x}/\sigma_{u|u|} = \theta_{xmax}/u|u|_{max} = 1$ (recall the stiffness K/C_0 has been absorbed in θ). But as u|u| fluctuates,

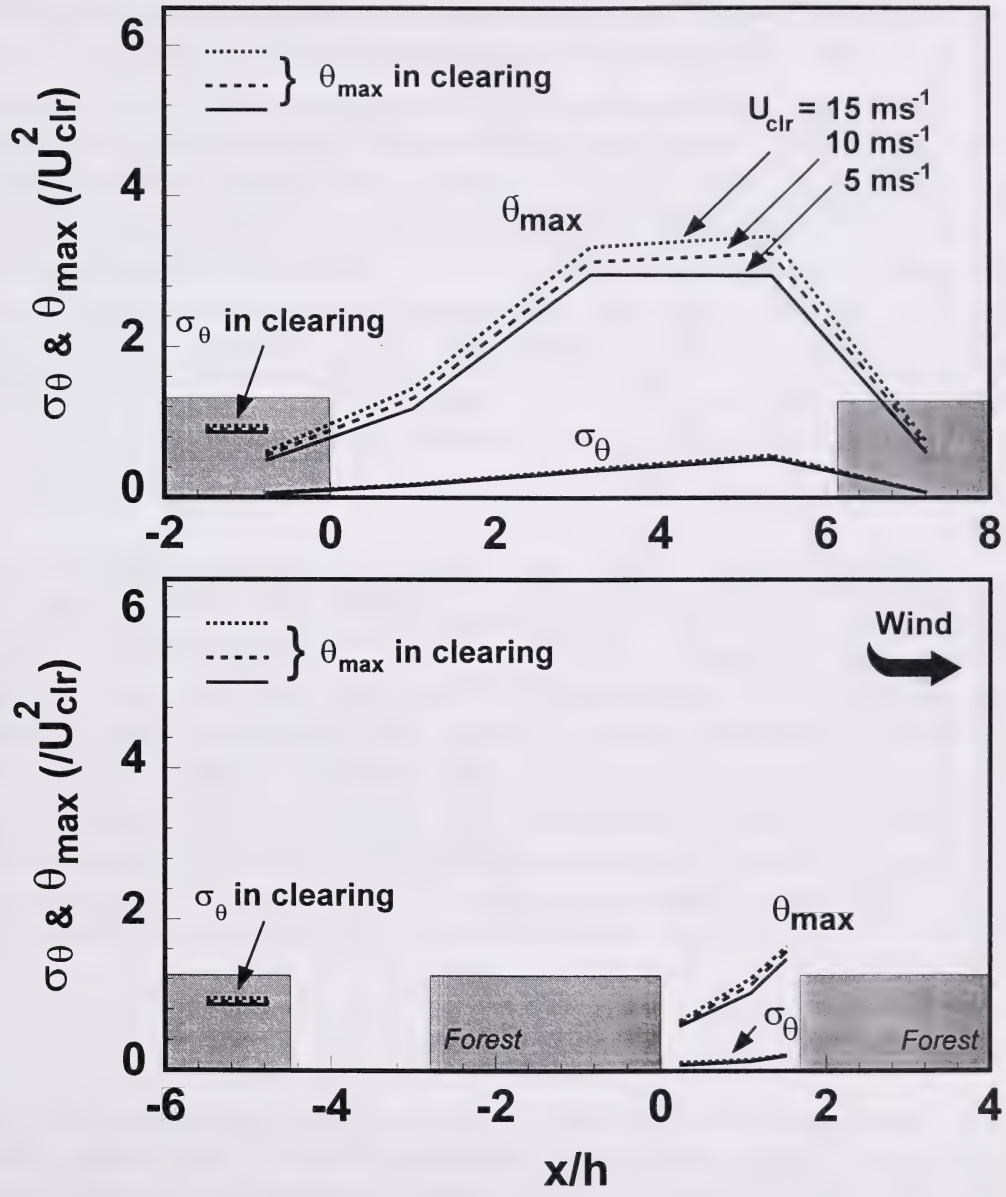

Figure 3.7. Predictions of the standard deviation of tree sway (σ_θ) and maximum displacement (θ_{max}) of our characteristic tree at three different reference clearing velocities (U_{clr}), plotted versus x across the wide cutblock (top) and the narrow cutblock (bottom). Displacements are scaled on U^2_{clr} (the stiffness K/C_0 has been absorbed in θ). Also shown (in level lines) are σ_θ/U^2_{clr} and θ_{max}/U^2_{clr} for that tree when located in the reference clearing.

these ratios can exceed one due to u|u| forcing near ω_n. We define this additional motion as "resonant sway". Our characteristic tree exhibited resonant sway in the cutblocks, as $\sigma_{\theta x}/\sigma_{u|u|}$ and $\theta_{xmax}/u|u|_{max}$ ranged from 1.10 to 1.35. In other words, the interaction of the turbulence with tree dynamics increased displacements 10 to 35% over that expected from a static analysis of the wind.

Our predictions of resonant sway support the conclusions of Stacey et al. (1994), that the dynamic nature of tree response results in greater maximum displacements than if the response were static. However, the increased sway that we diagnosed was less than that calculated by Stacey et al. for model trees. They calculated a doubling of the standard deviation of tree displacement due to resonant sway, compared with our increase of 10 to 35%. This was not unexpected given that there were differences between our tree heights ($z_t = h$ vs. $z_t = 0.5h$), and tree locations (full canopy vs. cutblock). Our predictions of the magnitude of resonant sway were also at odds with the suggestion made by Blackburn et al. (1988). They suggested a "dynamic load factor" (roughly equivalent to $\sigma_{\theta x}/\sigma_{u|u|}$ and $\theta_{xmax}/u|u|_{max}$) of half the "resonant load factor" (the maximum value of |G|) be used to estimate tree response to the wind. In our case (where the maximum |G| was approximately 5), this would have resulted in an overprediction of tree sway by roughly a factor of two.

5.3. *Sensitivity to ζ and ω_n*

Given the "dynamic" response of trees to the turbulent wind force, one expects and ζ and ω_n to strongly influence sway characteristics. This was certainly true in terms of "absolute" sway predictions (Figure 3.8). When ζ was reduced 50%, σ_θ in the cutblocks increased by 17 to 23%, and θ_{max} increased by 5 to 16%. When ω_n was reduced 50%, σ_θ increased by 3 to 9%, although θ_{max} decreased by 8 to 24%[5]. Nonetheless, the relative sway (sway relative to that of that of an identical tree sited in the clearing) was insensitive to ζ and ω_n. This is illustrated in Figure 3.9, which shows the ratios of σ_θ and θ_{max} to their values in the reference clearing. The insensitivity of these ratios to ζ and ω_n can be traced to the similarity in the shape of $S_{u|u|}$ and $S_{v|v|}$ at the different locations (e.g., if ω_n is decreased, the increase in wind "power" at frequencies near ω_n is proportionally the same at all locations). While earlier we documented differences in $S_{u|u|}$ with location, these differences were clearly not significant in terms of sway response. From these predictions we conclude that the effectiveness of a cutblock shelter in reducing tree sway will not depend on the dynamical properties of the remnant spruce.

5.4. Relationship of tree sway to simple wind statistics

Our diagnoses of tree sway required a spectral analysis of u and v time series, and a model of tree motion. Is there a simpler means of determining tree sway? The insensitivity of relative sway (sway relative to an identical tree in the reference clearing) to tree dynamics suggest that wind statistics alone may provide a way of discriminating regions of high and low tree sway. We believe $\sigma_{u|u|}$ to be a good index of relative sway, as we found it to be highly correlated with predictions of both σ_θ and θ_{max}. For example, the ratio $\sigma_\theta/\sigma_{u|u|}$ was relatively constant in the cutblocks (1.56 ± 0.22).

---

[5] This was contrary to expectations that greater θ_{max} accompanies greater σ_θ. Apparently a lower ω_n results in a more "sluggish" tree, less responsive to maximum u|u| events.

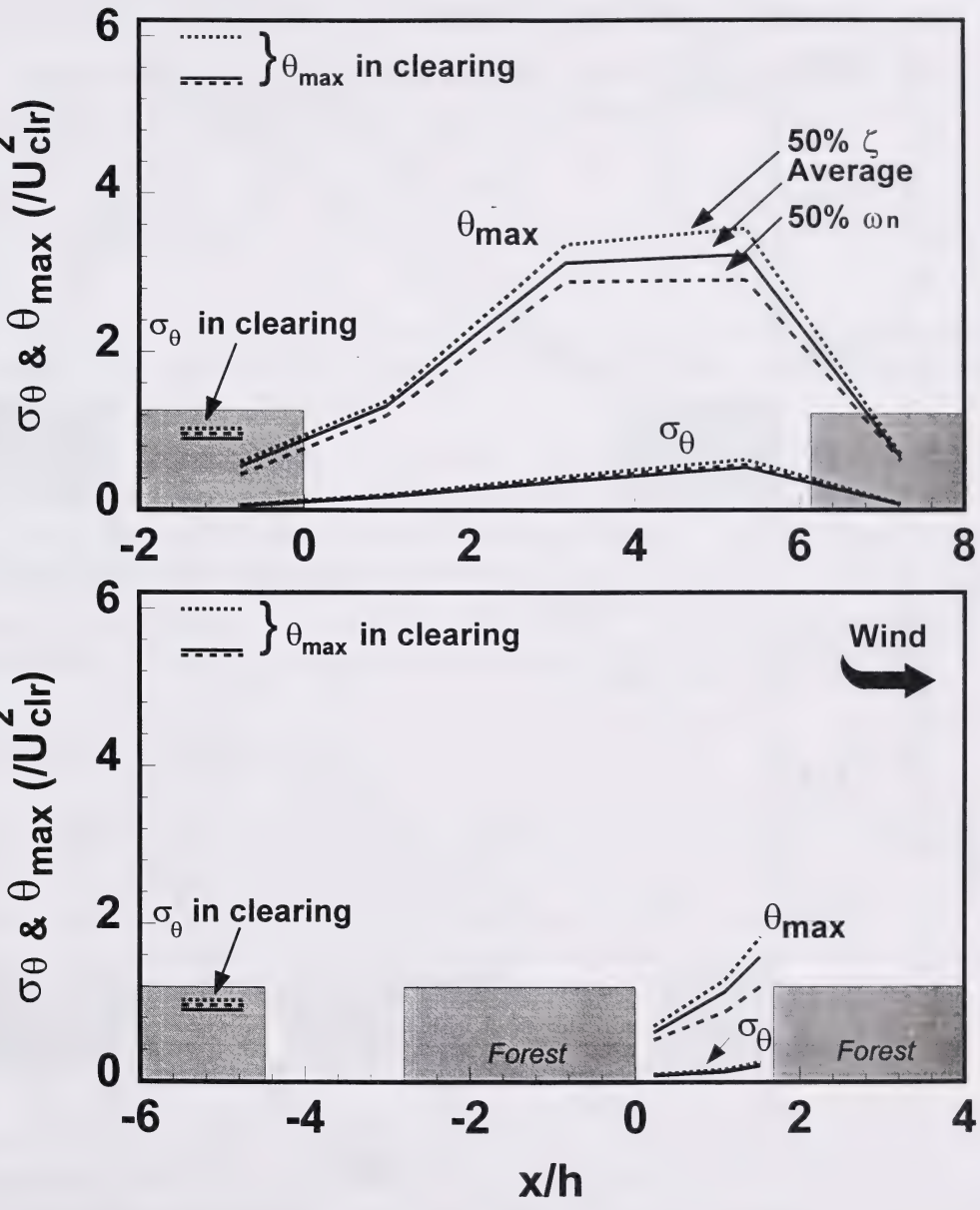

Figure 3.8. Predictions of the standard deviation of tree sway (σ_θ) and the maximum displacement (θ_{max}), plotted versus x across the wide cutblock (top) and the narrow cutblock (bottom). Different lines are for: a tree having the average damping coefficient (ζ) and natural frequency (ω_n) we observed (denoted "Average"); a tree having ζ reduced to 50% of the observed average (denoted "50% ζ"); and a tree having ω_n reduced to 50% of the observed average (denoted "50% ω_n"). Displacement are scaled on U^2_{clr}, where θ has been scaled on C_0/K. Also shown (in level lines) are σ_θ/U^2_{clr} and θ_{max}/U^2_{clr} for these trees when located in the reference clearing.

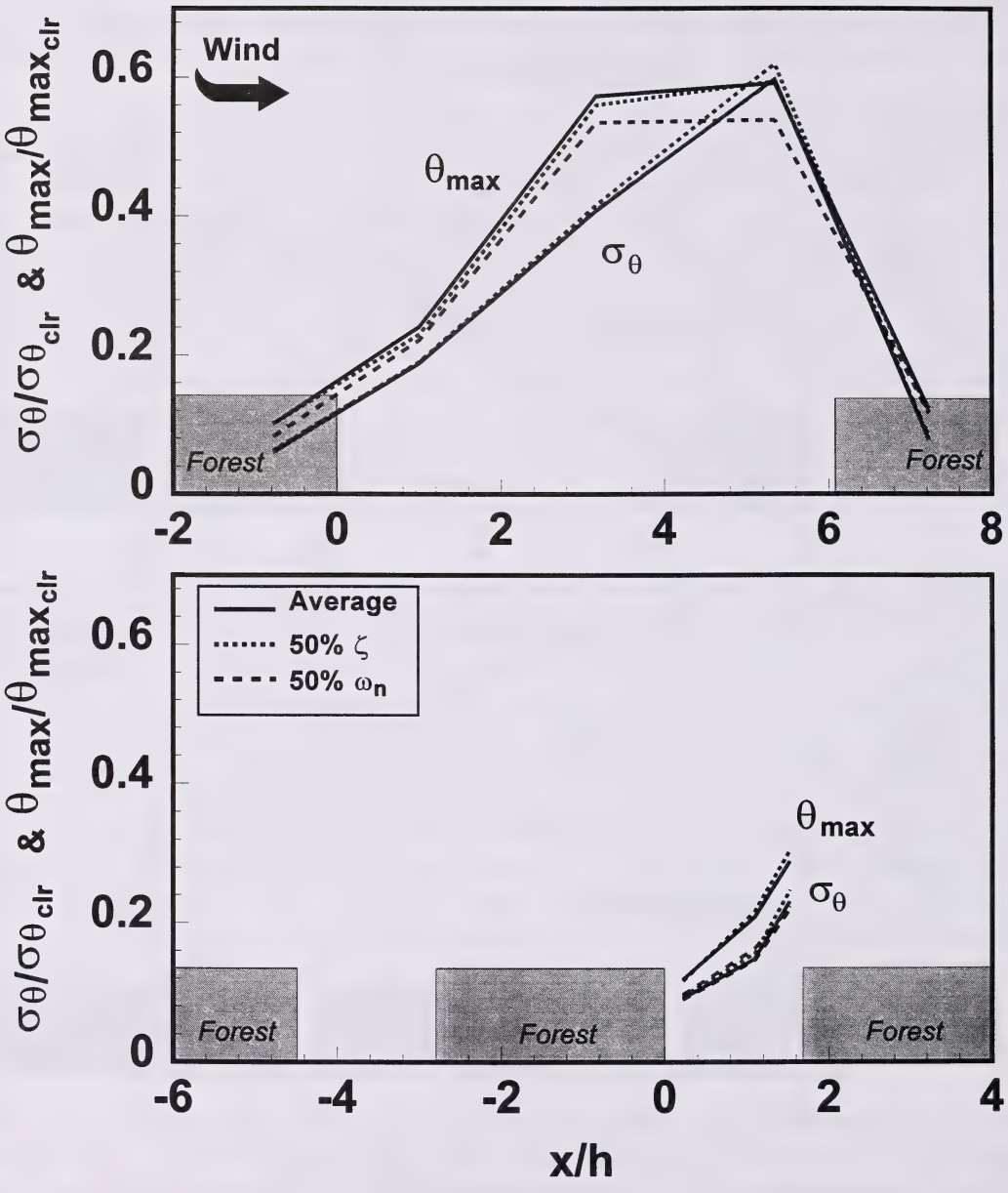

Figure 3.9. Ratio of tree sway in cutblocks to the corresponding sway in the reference clearing (for σ_θ and θ_{max}). Different lines are for: a tree having the average damping coefficient (ζ) and natural frequency (ω_n) we observed (denoted "Average"); a tree having ζ reduced to 50% of the observed average (denoted "50% ζ"); and a tree having ω_n reduced to 50% of the observed average (denoted "50% ω_n").

The ratio $\theta_{max}/\sigma_{u|u|}$ was only slightly more variable (11.4 ± 2.8). If we were to change ζ and ω_n, these ratios would change, but their values would remain relatively constant with location.

Because statistics of u|u| have not been reported in the literature, it is useful to relate $\sigma_{u|u|}$ to ordinary wind velocity statistics of which we are more knowledgeable. We found that $\sigma_{u|u|}$ can be approximated by σ_u^2 (to within 4% at all locations), so that

$$\frac{\sigma_{u|u|}^2}{\sigma_u^4} \approx \frac{\sigma_{u^2}^2}{\sigma_u^4} = Kt_u - 1 + 4\left(\frac{U}{\sigma_u}\right)^2 + 4\left(\frac{U}{\sigma_u}\right) Sk_u \ , \qquad \textbf{(19)}$$

where Kt_u and Sk_u are the skewness and kurtosis of u. If U, σ_u, Sk_u, and Kt_u can be accurately estimated, either by an educated guess, measurements, or by a wind flow model, then $\sigma_{u|u|}$ can be estimated (and thus by implication σ_θ and θ_{max}).

With the expectation that Sk and Kt would be more difficult to predict than U and σ_u, we calculated $\sigma_{u|u|}$ from just our observations of U and σ_u, assuming Gaussian values of $Sk_u = 0$ and $Kt_u = 3$. The result was a 18-29 % underestimation of $\sigma_{u|u|}$ in the cutblocks. Using more realistic values of $Sk_u = 1$ and $Kt_u = 4$ (i.e., values around the average of those we observed), the estimates of $\sigma_{u|u|}$ improved to within 6% of the actual $\sigma_{u|u|}$. This leads us to conclude that accurate estimates of the variation in Sk_u and Kt_u are not very important in estimating $\sigma_{u|u|}$. We believe that constant, non-Gaussian, values of Sk_u and Kt_u can be used with good accuracy to determine $\sigma_{u|u|}$ via Eq. (19).

6. Estimating Shelter Effectiveness

If windthrow is the result of tree sway exceeding a critical value, then our sway predictions can be used to quantify the effectiveness of sheltered cutblocks at reducing windthrow of remnant spruce. Our approach was to predict a threshold average wind velocity (U_w, measured in our large reference clearing; essentially a weather station windspeed) which correlates with occurrence of windthrow in the cutblocks. Our *assumption* was that an average velocity of 10 m s^{-1} causes windthrow of unprotected trees in our large reference clearing (Dr. S. Navratil, 1994, Canadian Forest Service, personal communication). Larger windspeeds (U_w) ought to be needed to cause windthrow in the cutblocks.

The pattern of U_w in the cutblocks is illustrated in Figure 3.10. In the wide cutblock U_w ranged from 25 m s^{-1} in the upwind portion of the cutblock, to 13 m s^{-1} at the downwind edge. This means windthrow at the upwind edge of the cutblock would require a weather station windspeed of 25 m s^{-1}, compared with the much lower 10 m s^{-1} needed in our large clearing. Even the least protected zone of the wide cutblock would require a 30% higher wind velocity to cause windthrow than is needed in the large clearing. The difference in U_w between x/h = 3.2 and 5.4 was slight, indicating the most effective windthrow protection occurs in the region x/h < 3. The wind shelter in the narrow cutblock was impressive, with U_w ranging from 30 m s^{-1} (upwind) to 19 m s^{-1} (downwind).

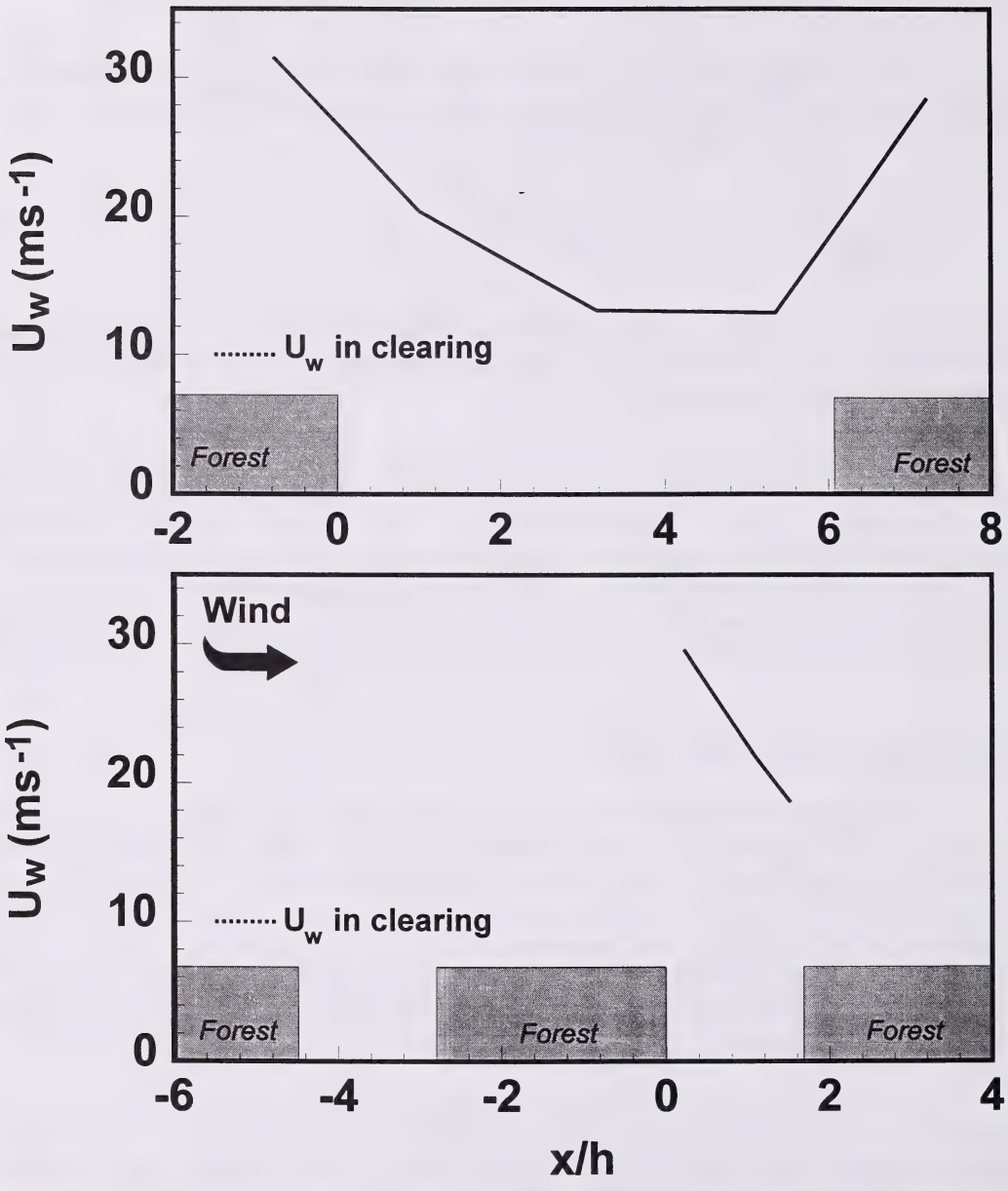

Figure 3.10. Predictions of the threshold average wind velocity measured in the open (U_w, essentially a weather station windspeed), which correlates with the occurrence of windthrow of remnant spruce in the cutblocks. Our *assumption* is that a U_w of 10 m s^{-1} causes windthrow of unprotected trees in the open. Larger wind velocities (U_w) are needed to cause windthrow in the cutblocks.

How significant is the level of wind shelter in the cutblocks? From an extreme value analysis of wind gusts, we estimate that an average windspeed of 11 m s^{-1} is expected every 2 years at the Hotchkiss site[6], a 13 m s^{-1} windspeed would occur every 5 years, while a windspeed of 15 m s^{-1} is expected only every 20 years. This suggests that windthrow in the narrow cutblock, or in the upwind portion of the wide cutblock (where the critical $U_w > 15$ m s^{-1}), would rarely occur.

Our map of windthrow velocity thresholds across the cutblocks was based on the assumption that our characteristic tree is mechanically identical at all locations. However, we expect ζ to be higher in the clearing because of increased aerodynamic damping due to the higher winds it would experience, and C_0 might differ because of differences in the shape of the vertical wind profile at each location. Furthermore, trees adapt to higher wind exposure, the remnant spruce in a large clearing would eventually differ from those in a cutblock. Therefore our assignment of a U_w would at best be valid only for a short time after harvest -- however, it is this post-harvest period that is critical for windthrow.

Given the uncertainty in our assumptions, and bearing in mind the wide range of remnant tree types (with properties varying substantially from our "characteristic" tree), the actual magnitude of our U_w values must be viewed skeptically. However, we feel confident that the pattern exhibited in Figure 3.10 exists, with the most effective shelter occurring within three tree heights of upwind forest.

7. Conclusions

Our diagnoses of tree sway confirm what we speculated in the first paper of this series: that the most effective windthrow shelter for remnant spruce in harvest cutblocks is within three tree heights of the upwind forest -- corresponding to the "quiet zone". This result holds irrespective of the dynamic parameters (ω_n and ζ) of our characteristic model tree, or strength of the ambient wind velocity. We believe it has generality to other cutblock dimensions and forest types, since the wind regime in our cutblocks was generally consistent with observations taken in a wide range of cutblocks/clearings (see Chapter 2). In designing shelterwood harvest systems to reduce windthrow of remnant understory spruce, we therefore suggest cutblocks should not exceed three tree heights in width (at least when cutblocks have an upwind forest border greater than 2h). While wind shelter should exist beyond this distance, remnant trees so far from the upwind shelter would not be dramatically more protected than if they were exposed in a large clearing.

Our results cannot be used to predict the shelter effectiveness of *any* possible shelterwood harvest design. For example, our results tell us little about the sensitivity of windthrow protection to the width of the upwind forest border; and we cannot be sure that a dramatically different forest structure, or different topography, would uphold the features we observed. We believe that a wind flow model is the best avenue for investigating the range of possible harvest designs. We have shown that the wind statistics generated by a typical flow model (e.g., U and σ_u) can be used to

---

[6] This was based on maximum wind gust statistics at nearby High Level, Alberta (Flesch and Wilson, 1993).

estimate $\sigma_{u|u|}$, which is a good predictor of tree sway and therefore windthrow potential. The formulation of a wind flow model appropriate to forest cutblocks is reported in Chapter 4.

8. References

Blackburn, P., Petty, J.A., and Miller, K.F., 1988. An assessment of the static and dynamic factors involved in windthrow. Forestry. 61:29-43.

Chatfield, C., 1984. The Analysis of Time Series. Chapman and Hall Ltd., London. 286 pp.

Flesch, T.K., and Grant, R.H., 1991. The translation of turbulent wind energy to individual corn plant motion during senescence. Boundary-Layer Meteor. 55: 161-176.

Flesch, T.K., and Wilson, J.D., 1993. Extreme value analysis of wind gusts in Alberta. Partnership Agreement in Forestry (PAR) Report 107. Nat. Resour. Can., Can. For. Serv., Northwest Reg., Edmonton, Alberta.

Gardiner, B.A., 1994. Wind and wind forces in a plantation spruce forest. Boundary-Layer Meteorol. 67:161-186.

Gardiner, B.A., 1995. The interactions of wind and tree movement in forest canopies. In Wind and Trees, eds. Coutts and Grace. Cambridge University Press. Cambridge, 485 pp.

Holbo, H.R., Corbett, T.C., and Horton, P.J., 1980. Aerodynamic behavior of selected Douglas-fir. Agric. Meteorol. 21: 81-91.

Horst, T.W., 1972. A computer algorithm for correcting non-cosine response in the Gill anemometer. Pacific Northwest Laboratory Annual Report for 1971 to the USAEC Division of Biology and Medicine, Vol. II: Physical Sciences, Part 1: Atmospheric Sciences, BNWL-1651-1. Battelle, Pacific Northwest Laboratories, Richland, Wash.

Meirovitch, L., 1986. Elements of Vibration Analysis. McGraw-Hill Book Co., New York.

Mayer, H., 1987. Wind-induced tree sways. Trees. 1:195-206.

Milne, R., 1991. Dynamics of swaying Picea sitchensis. Tree-Physiol. 9:383-399.

Oliver, H.R., and Mayhead, G.J., 1974. Wind measurements in a pine forest during a destructive gale. Forestry. 47:185-195.

Stacey, G.R., Belcher, R.E., Wood, C.J., and Gardiner, B.A., 1994. Wind flows and forces in a model spruce forest. Boundary-Layer Meteorol. 69: 311-334.

Thom, A.S., 1971. Momentum absorption by vegetation. Quart. J. Roy. Meteorol. Soc., 94:414-428.

Wood, C.J., 1995. Understanding wind forces on trees. In Wind and Trees, eds. Coutts and Grace. Cambridge University Press. Cambridge, 485 pp.

Appendix: Propeller Anemometers Errors

Propeller anemometers have poor high frequency response to wind fluctuations, and this results in errors in velocity statistics. A 3-D sonic anemometer (CSAT-3, Campbell Sci. Inc.) was temporarily co-located with a Gill UVW propeller anemometer at x/h = 0.6 in the narrow cutblock (z/h = 0.4), and the velocity statistics of u|u| were compared (there was v interference with the propellers in these cases, and we did not compare v|v| statistics). The propeller observations were corrected for cosine response using the algorithm of Horst (1972). We focussed on two 30-minute periods where $U > |V|$, and $\sigma_u > 0.5$ m. For simple wind force statistics, the agreement between the two anemometers was excellent. The magnitude of $\langle u|u| \rangle$ from the propeller exceeded that from the sonic by only 3%, while $\sigma_{u|u|}$ from the propeller exceeded that from the sonic by 5%. We therefore concluded that the propellers gave accurate estimates of $\langle u|u| \rangle$ and $\sigma_{u|u|}$ (and we believe accurate v|v| statistics).

Though we were satisfied that the simple statistics of u|u| and v|v| from the propellers were accurate, we worried about errors in the power spectra $S_{u|u|}$. We were particularly concerned about underestimating $S_{u|u|}$ near the ω_n of our characteristic remnant spruce (0.4 Hz). A plot of $S_{u|u|}/\sigma^2_{u|u|}$ for one 30-minute period, when both the sonic and propeller anemometers were operated simultaneously, shows that this underprediction did occur (Figure A3.1). At $\omega \geq 0.2$ Hz the propellers underestimated $S_{u|u|}$. At $\omega = 1$ Hz, $S_{u|u|}$ from the propellers was about one tenth of the sonic value. We attempted to correct $S_{u|u|}$ (and $S_{v|v|}$) to give more accurate estimates of the tree sway properties.

We began by correcting the velocity power spectra (S_u), extending the spectrum along the expected -5/3 "fall-off" at frequencies above 0.1 Hz (see Appendix in Chapter 2). This correction is questionable within the forest, where vegetation elements may cause a "short-circuit" of the normal energy cascade. We used the corrected S_u spectra and recreated the u time series for each measurement period (assuming the phase lag φ_u was without error -- we had no theoretical basis to judge φ_u accuracy). From this "corrected" time series of u, we recalculated the u|u| series, and a "corrected" $S_{u|u|}$. How well does this correction work? Figure A3.1 shows that for one 30-minute period, the corrected propeller $S_{u|u|}$ was in good agreement with that from the sonic. The other periods showed similar results. All the u|u| and v|v| series were corrected in this manner.

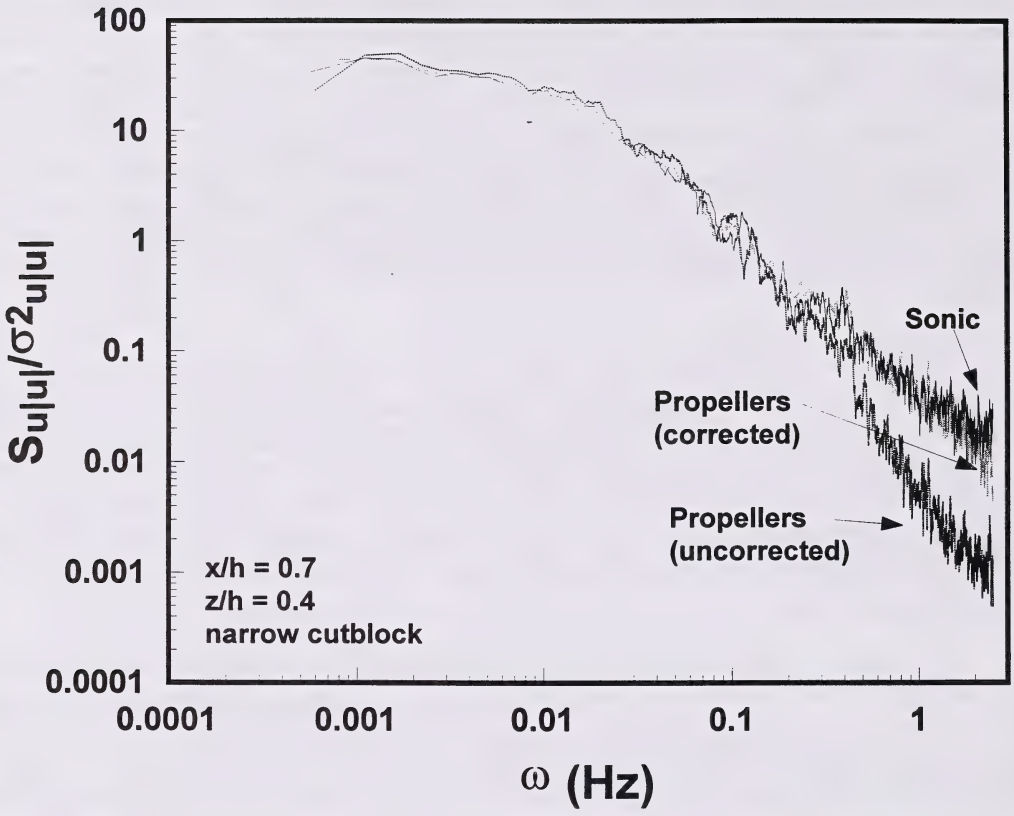

Figure A3.1. Normalised power spectra of u|u| ($S_{u|u|}$) versus frequency (ω) for a 30-min period during which there was simultaneous observations from a 3-D propeller and sonic anemometer. Also show is the "corrected" propeller spectrum, where the u|u| time series was corrected by applying a "-5/3 fall-off" to the propeller spectrum of u.

CHAPTER 4

A WIND FLOW MODEL TO DIAGNOSE SPATIAL VARIATION IN CUTBLOCK WINDS

John D. Wilson and Thomas K. Flesch

1. Introduction

Management trials in the boreal mixedwood forest of Northern Canada are evaluating felling practises that, at the time of aspen harvest, preserve the spruce understory ("released spruce") for later cutting. It is considered necessary to leave uncut or partially-cut forest strips to shelter the selectively-cut zones, because the previously-sheltered remnant spruce are very vulnerable to windthrow. An overall description of this long-term, practically-oriented project, which is being carried out at Hotchkiss (near Manning, Alberta) is given by Navratil et al (1994). The work we report here was initiated in the hope of interpreting the observed *spatial variation* of tree windthrow across such arrays of cutblocks, so as to permit generalisation. It involves our own measurements of turbulence and tree sway in two cutblocks, each the leeward member of a periodic series; an analysis of the response of instrumented trees to the wind forcing; and, in this paper, an attempt to establish a framework for generalisation of our findings by numerically modelling the winds.

The link between tree sway statistics and wind statistics is discussed at length in Chapter 3. Briefly, we treated the tree as a rigid rod, free to swing about a ground-level pivot in response to the wind force, but under the moderation of an angular spring and damper. We derived a transfer function relating the short-term power spectrum S_θ of tree angular displacement (θ) to the concurrent power spectrum $S_{u|u|}$ of the wind force $u|u|$, where u is the instantaneous alongwind velocity component, measured nearby. By "short-term" statistics, we mean statistical properties (standard deviations of tree sway angle σ_θ and of wind force $\sigma_{u|u|}$, variance spectra S_θ, $S_{u|u|}$, etc.) defined by a sample taken over about 15 to 60 minutes, such intervals being sufficiently short that "external" or large-scale conditions are roughly constant, but sufficiently long that many "cycles" of the rapid turbulent variations are captured. Thus the "view" of our windthrow analysis consists of (say) 30 min snapshots, from which a longer-term view may be constructed by integration; and the fluctuating (turbulent) variables, eg. the alongwind velocity u, are decomposed

$$u(x,y,z,t) = U(x,y,z) + u'(x,y,z,t) \qquad (1)$$

into sums of the average (in this case, the mean alongwind velocity U, a function of position only) and the instantaneous deviation (or fluctuation, here u') from it. This terminology (upper-case for mean values; prime for fluctuation from average) will apply throughout our paper.

Returning to our tree sway model, the wind-force spectrum $S_{u|u|}$ was observed not ***at*** the "subject" remnant tree, but merely, at the same *alongwind* location relative to the upwind edge of the cutblock, and at a convenient, arbitrary height (9m). We found that *normalized* wind force spectra $S_{u|u|}/\sigma_{u|u|}^2$ were similar at all points across the cutblocks (ie. practically invariant), so that the sway (σ_θ) of a tree, no matter where located, could be definitively related to $\sigma_{u|u|}^2$ at that point. But in turn, the force-variance $\sigma_{u|u|}^2$ can be determined from the lowest order statistics of the wind

$$\sigma_{u|u|}^2 \approx \sigma_{uu}^2 \equiv \sigma_u^4 \left(Kt_u - 1 + 4\left(\frac{U}{\sigma_u}\right)^2 + 4\left(\frac{U}{\sigma_u}\right) Sk_u \right) \qquad (2)$$

where the right-hand equality is exact. Within our framework then, the wind statistics governing root-mean-square (r.m.s.) tree sway are: mean U, variance σ_u^2, skewness Sk_u, and kurtosis Kt_u. A

sensitivity analysis (see Appendix 1) indicates that under conditions typical of the flow in our Hotchkiss cutblocks ($Sk_u \approx 1$, $Kt_u \approx 4$), spatial modulation of the wind-force variance (and thus of σ_θ^2) is controlled, in order of importance, by spatial variation in the velocity variance σ_u^2 (one component of the turbulent kinetic energy[1]), and in the mean velocity U. Thus for the remainder of this paper, our focus is on modelling the spatial variation, around and about forest edges, of these principal wind and turbulence statistics, U and k. As regards the connexion of our method to the practical issue of tree windthrow, by hypothesizing that the *spatial pattern* of wind statistics implies the corresponding *spatial pattern* of windthrow, we obviously are assuming that the key factor in the cross-landscape *variation* of treefall susceptibility is the wind forcing, rather than any systematic variation in soil conditions, rooting depth, tree health, etc. It is also implicit that we presume *extreme* tree displacements (or wind forces) scale with the standard deviation σ_θ (or with $\sigma_{u|u|}$).

Having motivated our focus on mean wind (U) and turbulence (k) in forest clearings, we now review previous efforts to model forest edge flows; describe a numerical wind flow model, developed by Wilson et al (1998) specifically for the description of disturbed canopy winds; compare simulations using that model against others' observations of forest-edge flows; and finally simulate the spatial pattern of the wind and turbulence in our cutblocks at Hotchkiss for comparison with our observations.

2. Wind Flow Across Forest Boundaries, and Models Thereof

We have elsewhere (Chapter 2) discussed the experiments to date on forest edge flows, in comparison with our own. Here we consider only the issue of whether or not one might expect to see universal patterns across such experiments.

Shinn (1971) analysed his own and others' experiments on forest edge flow. His observations of wind in *uniform* canopies are also important: he showed that due to the Coriolis force there occurs a large swing (about 80°) in mean wind direction between tree-top level and the base of the canopy (see Appendix 2 for a discussion), and for this reason we anticipate that the Coriolis force ought to be included in any complete analysis or model of forest edge flow.

Shinn demonstrated that mean windspeed profiles in the forest entry region from a number of field experiments on forest-wall flow formed a fairly consistent pattern, a pattern which, not withstanding the above caution with respect to Coriolis effects, resembled the corresponding pattern from a wind tunnel experiment: at low levels a jet penetrates the canopy, decaying by about x/h = 10. Shinn normalised the observations using lengthscale h and velocity scale $U_0(h)$, the windspeed at canopy height some distance upwind from the forest wall. Differences not erased by the normalisation are of course expected, for in general, even in neutrally-stratified flow at a forest edge having along-edge (y) symmetry, one expects on the basis of dimensional analysis a similarity relationship at least as complex as:

---

[1] Turbulent kinetic energy (TKE, k) is defined as $k = \frac{1}{2} (\sigma_u^2 + \sigma_v^2 + \sigma_w^2)$. The flow model we shall describe does not partition k into its components, so we have assumed that *equilibrium* partitioning prevails everywhere throughout disturbed flows: ie. that everywhere $\sigma_u^2 = \alpha_u k$, where α_u is a constant, given in Appendix 3.

$$\frac{U}{U_{ref}} = F\left(\frac{x}{h}, \frac{z}{h}, \frac{\delta}{h}, \frac{z_{oc}}{h}, c_d a h, \frac{f}{c_d a U_{ref}} \right) \qquad (3)$$

where F is an unknown function of its bracketed (and dimensionless) arguments; U_{ref} is the normalising velocity scale; δ is boundary layer depth; z_{oc} is the effective surface roughness length in the clearing; $c_d a\, h$ is a bulk (constant) drag coefficient characterising the forest block(s), $a = a(x,z)$ being the forest drag area density, [m^{-1}]; and f is the Coriolis parameter. In general, atmospheric stratification and the *vertical distributions* of drag coefficient and foliage area density probably play a role, implying we could add, as further dimensionless arguments of the unknown function F, the factors h/L_{MO} (where L_{MO} is the Monin-Obukhov length), $c_d(z/h)$, and $ah(z/h)$. And because the drag coefficient may be Reynolds-number dependent, we might also add a Reynolds number $U_{ref}\, h/\nu$, ν being the kinematic viscosity of the air. Our point here is that by no means ought one to *expect* there exists a universal pattern (of the normalised flow variables) across differing forest edge flows.

2.1. Background on Numerical Simulation of Turbulent Flows

Simulations of disturbed micrometeorological flows are most often based on numerical integration of the Reynolds equations, which are obtained by averaging the Navier-Stokes equations so as to obtain governing equations for the flow *statistics* (see Hinze, 1975, or almost any text on turbulence or micrometeorology). If the flow has (statistical) symmetry along one spatial axis (say, y-axis), the Reynolds equation expressing conservation of mean alongwind (x-axis) momentum can be written as:

$$\frac{\partial}{\partial x}\left(U^2 + \sigma_u^2\right) + \frac{\partial}{\partial z}\left(UW + \tau\right) = -\frac{1}{\rho}\frac{\partial P}{\partial x} + \Phi_u \qquad (4)$$

where U and W are the mean alongwind and vertical (z-axis) velocities; P is the mean pressure; ρ is the mean air density; Φ_u represents the Coriolis force and drag of vegetation on the flow; and $\tau = \langle u'w' \rangle$ is the statistical covariance between u-fluctuations and w-fluctuations, which in physical terms is the turbulent shearing stress, known as the Reynolds stress. We need not elaborate on Eq. (4) at this point (it reappears later in approximate form as Eq. 7), except to mention that whereas this is an equation "for" the *mean* x-wise momentum, ie. for velocity U, its derivation has introduced spatial derivatives of higher (and unknown) statistics of the velocity field, namely of the variance σ_u^2 and of the covariance $\tau = \langle u'w' \rangle$. These "stress-gradients," physically, are *forces*, "felt by" the mean flow: and in particular the term $\partial\tau/\partial z$ in Eq. (4) is crucial in most turbulent flows. In order to progress, one has necessarily to introduce a hypothesis with respect to the Reynolds stresses (a "closure hypothesis"). The oldest and simplest such hypothesis is the eddy-viscosity closure, often called "K-theory," or "first-order closure",

$$\tau = -K\left(\frac{\partial U}{\partial x} + \frac{\partial W}{\partial z}\right) \qquad (5)$$

to note that simulations under the two alternatives, ie. explicit imposition (or otherwise) of the clearing roughness length, did not differ sufficiently to warrant giving the matter further attention.

As the lower boundary condition on TKE in conjunction with Eq. (19), we adopted the equilibrium relationship $k_{gnd} = u_*^2/c_e$. The alternative prescription $(\partial k/\partial z)_0 = 0$ performed neither better nor worse.

3.3.3. Convergence criterion

SIMPLE ensures that the governing equations, in their integral forms which express the balance of sources within each control volume against the net flux across the control-volume surface, are satisfied to within machine precision (in each such volume). Iterative refinement of all fields was continued until the integral form of the U-momentum equation (7), covering the entire flow domain, was satisfied to within 1% of the total forest drag.

3.4 Role of the "velocity scale"

A feature of small scale wind models that may be unfamiliar to some readers, and is crucial for the interpretation of results given in this paper, is that such models diagnose not the actual mean winds at some point(s), but rather, *ratios* of the mean velocities to some reference value U_{REF}, a reference windspeed at some point *within, or at the boundary of, the model domain.* U_{REF} is chosen as the reference (or "scale") on grounds of convenience, and might for example be the wind aloft at the top of the boundary layer, or possibly for models resolving only a shallower layer of the PBL, the "friction velocity" implied by the shear stress along the top of the model domain. And if *on external grounds* (ie. from a measurement, or as provided by some model of wider cognizance) we know or postulate a numerical value for U_{REF}, we can infer a definite value for the velocity at any other point within the model domain. A direct implication of all this for the present study, is that local wind flow models can at best predict not the absolute variance of tree sway angle, but rather, how much greater is that variance at one point in the flow domain than at another.

4. Simulation of Raynor's Forest-edge flow

Raynor (1971) reported mean profiles of horizontal windspeed at various distances from the upwind edge of a pine forest, during periods of flow at near-normal incidence to the forest edge. We simulated Raynor's experiment with the full model (ie. including a full PBL, with Coriolis forces and the transverse component V) described in Section (3). Our motivation in doing so was to determine whether the excellent simulations of Raynor's experiment given by Li et al. (1990) rested in any essential way on the closure they used, that of Li et al. (1985), described earlier - or whether the present closure would perform as well. In particular, LLM did not state whether their successful simulation of the jet observed near the base of the canopy depended on their having included their parametrization of the sweep-ejection mechanism (the term $c(U_h-U)$ in Eq. 6), or whether the jet was an edge effect associated with low area density deep in the canopy.

4.1. Numerical details

Our computational domain for simulating Raynor's experiment extended alongwind from x/h = -20 to x/h = 30, with the forest edge at x = 0. The height of the domain was 40h. Resolution was uniform at $(\Delta x/h, \Delta z/h) = (0.1, 0.1)$ over the region $x/h \leq 15$, $z/h \leq 2$; outside that region, the grid was gently stretched. Inflow profiles were obtained by solving the governing (U, V, k) equations with $\partial/\partial x = 0$, and with $c_d ah = 0$. The lengthscale was treated as adjusting instantly at the forest edge, from the open-plain profile to the forest profile ($\gamma = \infty$).

LLM adopted an approximately triangular area-density profile for Raynor's forest (their Figure 2), but did not report the value used for their drag coefficient. Adopting essentially the same area-density profile, and treating the drag coefficient as free to be optimised, we set:

$$c_d ah = \begin{cases} \left(c_d ah\right)_0 \dfrac{z/h}{0.75} & , \quad \dfrac{z}{h} \leq 0.75 \\ \left(c_d ah\right)_0 \dfrac{1 - z/h}{1 - 0.75} & , \quad \dfrac{z}{h} > 0.75 \end{cases} \qquad \textbf{(20)}$$

4.2. Results

A simulation using this area density profile, with $(c_d ah)_0 = 2.0$, is given on Figure 4.1. The observed windspeeds, which we extracted from Raynor's Figure 3, have been normalised on windspeed at z = 108 m on his "Ace tower." Similarly, model windspeeds were re-normalised on the inflow windspeed at that height. Agreement of our simulation with Raynor's data is good, comparable in quality with the LLM simulation. We find the occurrence of the "jet" in the base of the canopy is dependent on specifying the reduced area-density near ground; it vanished when we set $c_d ah$ = const. It follows that the heuristic source c(U(h)-U) introduced by LLM in their U-momentum equation did not play a vital role in their simulation: the (simulated) jet is an edge effect in the open region at the bottom of the pine canopy.

We did not add the simple lengthscale-interpolation used by LLM near the forest edge, nor try to equal in detail their results. In our view Figure 4.1 establishes that our closure and our formulation of the lengthscale provide a simulation of Raynor's experiment that is as good as that of Li et al. (1990), while being more general in scope (eg. use of TKE to derive velocity scale; canopy lengthscale linked to inflexion-point shear rather than leaf area density) and carrying a reduced burden of closure constants.

5. Simulation of Wind-Tunnel Clearing-Edge Flow ("Abbott's Booby Study")

In a study concerned with nesting habits of birds near forest clearings, Raupach et al. (1987; hereafter RBG) measured mean windspeed and turbulence statistics across clearings of widths 4.3h and 21.3h in a model canopy, within a wind tunnel. The same canopy was later used in the "Furry Hill" experiments (Finnigan and Brunet, 1995), but some unexplained and possibly important differences are evident between the respective *equilibrium* flows (ie. between dimensionless flow

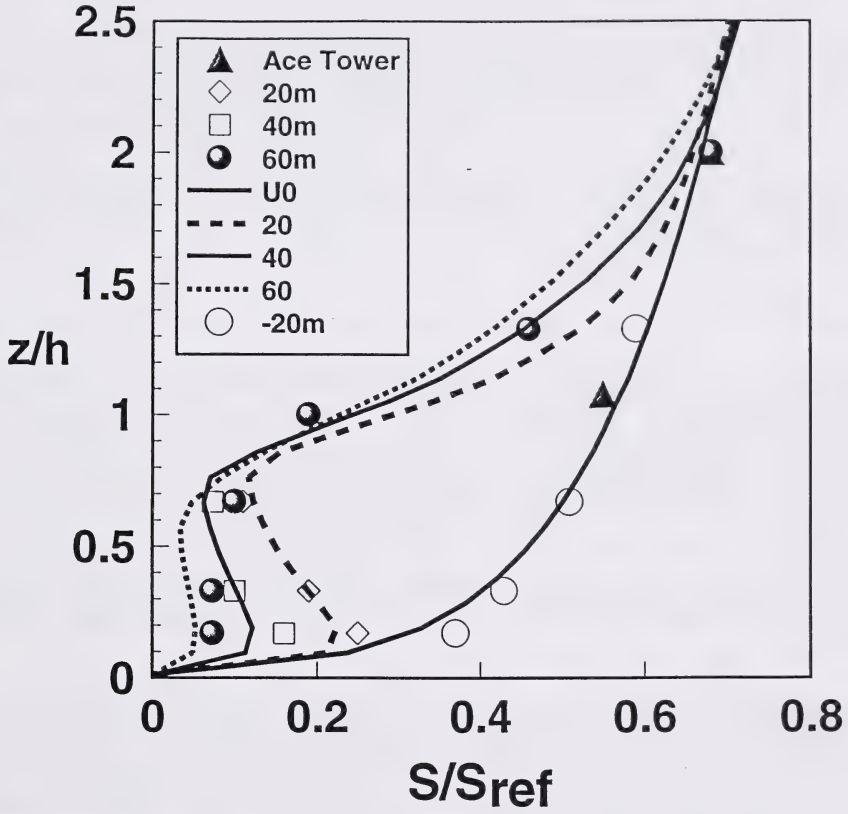

Figure 4.1. Vertical profiles of mean horizontal windspeed observed by Raynor (1971) at various locations near the edge of a pine forest, in comparison with a simulation using the present model. Profile locations are given in [m] relative to the forest edge, with positive values lying *within* the forest. Note the jet deep in the canopy, simulated quite well by the model.

properties upstream from the clearing and from the hill). In simulating the Abbott's Booby flow we adopted the same canopy and flow parameters as did WFR for simulating Furry Hill, namely $c_d ah = 0.32$, $d/h = 0.71$.

Experimental data cited below were extracted for heights $z/h = 0.25, 0.5, 0.75, 1, 1.5$ from graphs in the RBG report. A sizeable uncertainty surrounds some of the data, where several profiles merged on the original graphs. The floor of the wind tunnel was roughened with gravel (nominal diameter, $d_g = 7$ mm) within the clearing. A rough estimate of the effective roughness length is $z_{0c} \approx d_g/10$, giving $z_{0c}/h \approx 0.015$; while at mid-clearing ($x/h = 12.8$) the mean windspeeds at $z/h = (¼, ½)$, if plotted against $\ln_e z$, imply $z_{0c}/h = 0.001$. Simulations were not very sensitive to this parameter (clearing roughness length).

5.1. Numerical details

We dropped the V-momentum equation and the Coriolis term in the U-momentum equation, the model reducing essentially to that given by WFR, but differing in that the disturbance is here driven, not by a hill-induced pressure-gradient (WFR), but by the irregular distribution of canopy drag. Like WFR, we simulated the entire wind tunnel boundary layer, incorporating the vertical gradient in shear stress above the canopy by the imposition of an effective streamwise pressure gradient, in the present case estimated (from the observed stress gradient) as $\partial(P/\rho u_*^2)/\partial(x/h) \approx -0.23$. This step results in reproduction of the above canopy stress and TKE gradients by the model, but as WFR also found, it is not crucial for a good simulation of the streamwise changes near and within the canopy.

We simulated the flow through the wide (21.3h) clearing, because RGB provided more complete documentation of that case, giving profiles both within and downwind of the clearing. Our computational domain extended alongwind from $x/h = -10$ to $x/h = 40$, with the upwind edge of the clearing at $x = 0$. The domain height was 40h. Resolution was uniform at $(\Delta x/h, \Delta z/h) = (0.2, 0.1)$ over the region $x/h \leq 21.3$, $z/h \leq 2$; outside that region, the grid was gently stretched.

As mentioned above, the Abbott's Booby profiles reported at $x/h = -2$ are somewhat unusual. Largest shear stress occurred not at $z = h$ (where normally expected in a wind tunnel boundary layer), but at $z \approx 1.5h$. Relationships between velocity statistics at that height appear normal: the maximum shear stress implied a friction velocity $u_* \approx 1.08$ [m s^{-1}]; the corresponding maximum TKE[2] was approximately $k_{mx} = 6.11$ [m^{2}s^{-2}], implying $k_{mx}/u_*^2 = 5.24$ ($\sigma_u/u_* = 2.11$, $\sigma_w/u_* = 1.25$), which is close to the value observed upstream from Furry Hill, $k(h)/u_*^2 = 5.6$. However at $z = h$, TKE appears to be anomalously small, with $k(h)/U^2(h) = 0.25$, whereas the corresponding value for the equilibrium flow upwind from Furry Hill was $k(h)/U^2(h) = 0.37$.

5.2. Results

For the comparisons to follow we renormalised observed and modelled (U,k) on a velocity scale (U_{ref}) chosen as the velocity (observed/modelled) at (x/h,z/h) = (-2.1, 1): ie. $U_{ref} = U(-2.1,1)$.

---

[2] (σ_v was not measured: we assumed $\sigma_v = \sigma_w$)

The lengthscale adjustment parameter $\gamma = 0.05$ for the results shown. Figure 4.2a compares the observed and modelled mean winds across the clearing in the form of a set of horizontal profiles, while Figure 4.2b gives vertical profiles. The normalised profile of mean windspeed observed by RBG upwind from their clearing closely matches that observed by Finnigan and Brunet upwind from Furry Hill (first panel of Figure 4.2b), and as we use the same canopy parameters as did WFR, we obtain the same (excellent) model equilibrium profile, characterised by $U(h)/u_{*0} = 3.76$, where u_{*0} is the friction velocity based on shear stress at $z = h$.

At the highest level ($z/h = 1.5$) the simulation overestimates velocity at all stations, including the "inflow" station at $x/h = -2.13$. This may indicate an inconsistency between the model assumption of an infinite upwind extent of uniform canopy, and the actuality of the experiment. Otherwise the general response of the windspeeds across the clearing and back into the canopy is modelled quite well, except that in the middle of the clearing ($x/h = 12.8$) speeds have been overestimated. The observed data at that station are not subject to doubt, as least as regards their extraction by us off the RBG report, and we have no explanation as to why the adjustment of the clearing flow is modelled well everywhere but in this neighbourhood. Incidentally, the simulations were for all practical purposes insensitive to the manner of lengthscale blending near the forest wall, so that there is no justification (in this case) for anything more complex than immediate adjustment from the forest- to open-plain forms for the lengthscale.

Figure 4.2c compares simulated and observed vertical profiles of TKE from the Abbott's Booby experiment. Regarding the upwind profile, we have already mentioned that observed TKE at $z = h$ is surprisingly small, $k(h)/U^2(h) = 0.25$ (cf. 0.37 for the Furry experiments with the same canopy in the same tunnel). This could be regarded as consistent with the reported shear stress profile for that location (not shown here), which places the most-negative shear stress not at $z/h = 1$, but at about $z/h = 1.5$. Just as a *positive* stress gradient (ie. magnitude of the shear stress decaying with increasing height) above $z = h$ implies $\partial k/\partial z<0$ in that region (eg., as seen far upwind from Furry Hill), the *negative* stress gradient above $z = h$ seen here can be taken as implying increasing shear-production of TKE - raising the height at which peak TKE occurs. These aspects of the observations could easily be reproduced in simulations, by incorporating a shallow region of *adverse* background pressure gradient below $z/h = 1.5$, and resulted in essentially perfect simulation of the TKE profile at $x/h = -2$. However that modification of the background pressure did not substantially alter predicted TKE at downwind stations (other than near $z/h = 1.5$). Therefore because this interpretation of a "back pressure" layer is entirely speculative, and the cause for it (if true) unknown, we have presented simulations without it.

Variation of the TKE across the Abbott's Booby clearing resembled that observed in a wider wind tunnel clearing by Chen et al. (1995; hereafter CBNA). Our simulation at least reproduces the dominant features, a transition near ground from low TKE deep in the canopy toward larger values characteristic of open ground, with concomitant decrease of TKE aloft (smoother surface), and rapid development of a strong vertical gradient near $z = h$, upon transition back into the canopy. Interestingly, the model equilibrium TKE-profile matches the observations farthest *downwind* (10.6h) from the clearing ($x/h = 31.9$) somewhat better than the observations upwind (we have already expressed some uncertainty about that upwind TKE profile). Nevertheless as the local

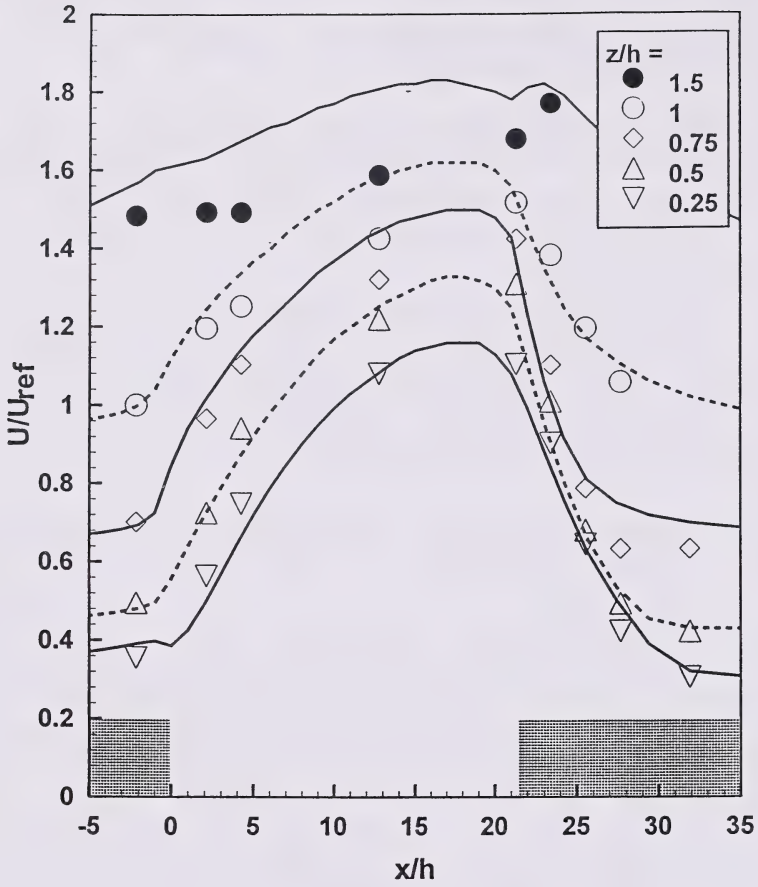

Figure 4.2a. Horizontal profiles of the normalised mean windspeed across a clearing in a model forest: comparison of observations (symbols) from the "Abbott's Booby" study with numerical simulation (lines). U_{ref} is the velocity at (x/h, z/h) = (-2.13, 1).

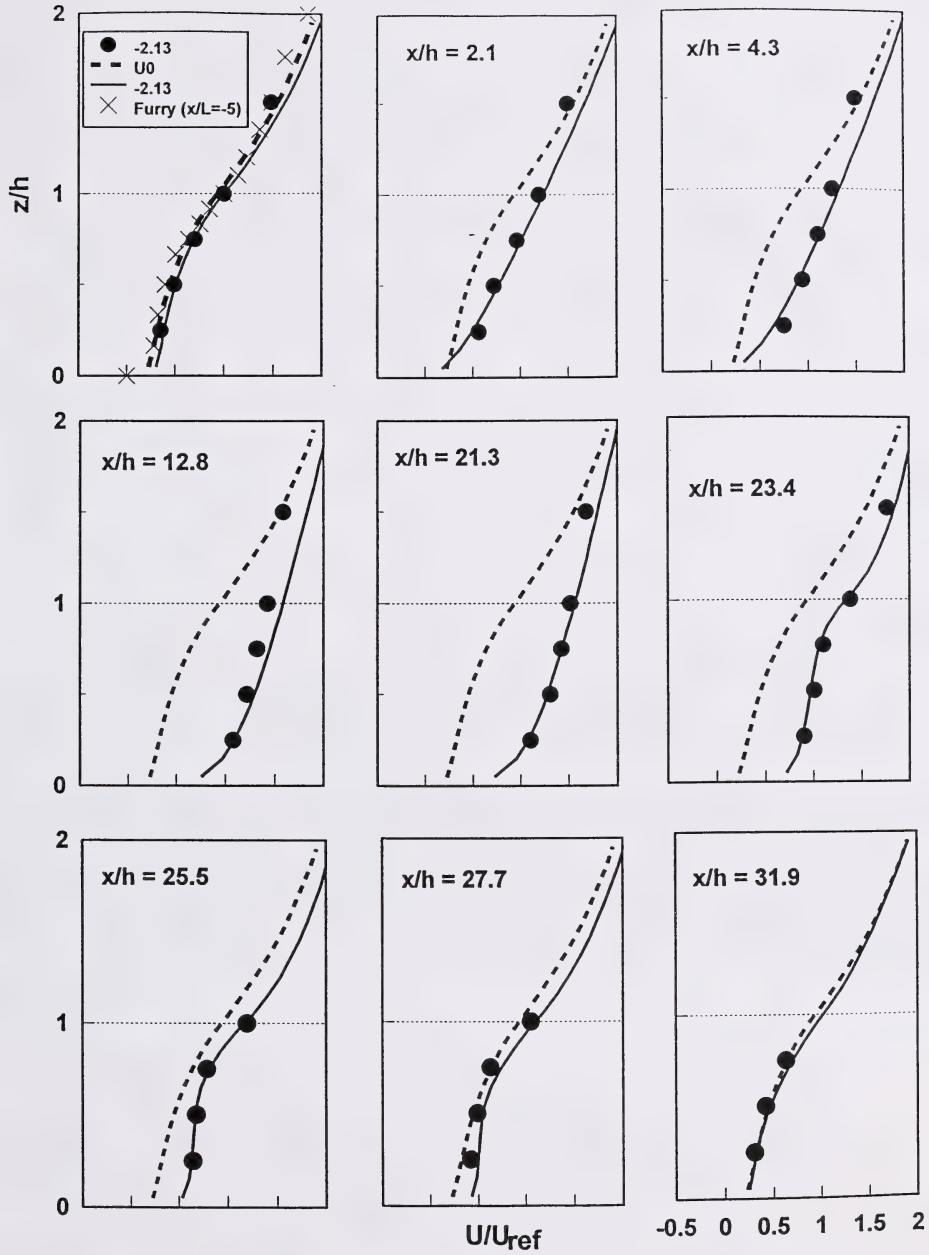

Figure 4.2b. Sequence of observed (●) and modelled (solid line) vertical profiles of the mean windspeed upstream across the Abbott's Booby clearing, which spanned $0 \leq x/h \leq 21.3$. The heavy dashed line on each panel gives the *equilibrium* model solution as a reference for the alongwind changes in windspeed. The first panel also shows the wind profile observed within the same canopy, in subsequent experiments by Finnigan and Brunet (1995), far upwind from Furry Hill.

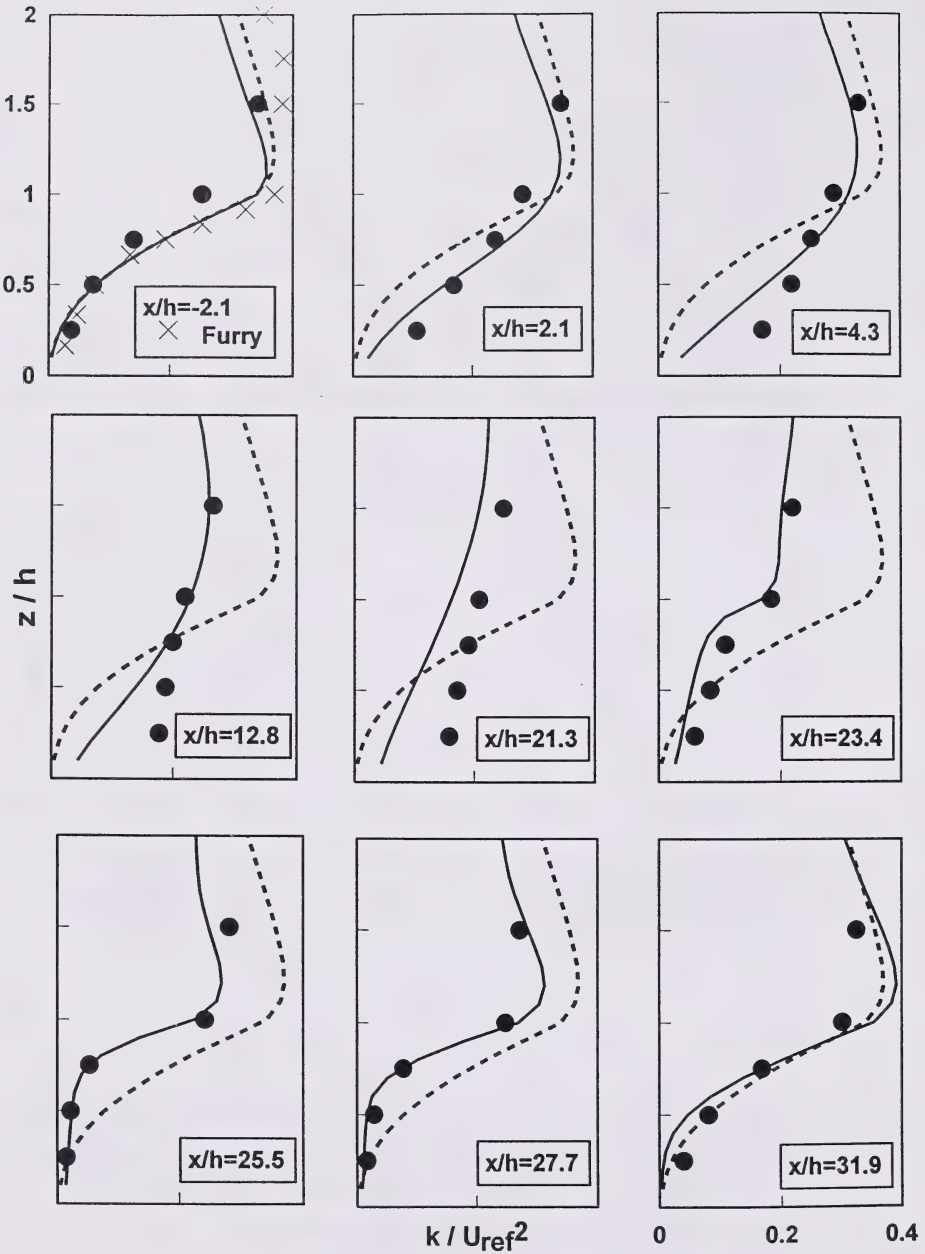

Figure 4.2c. Sequence of observed (●) and modelled (solid line) vertical profiles of normalised turbulent kinetic energy, k/U_{ref}^2, across the Abbott's Booby clearing. The heavy dashed line on each panel gives the *equilibrium* model solution as a reference for the alongwind changes. The reference windspeed $U_{ref} = U(-2.13, 1)$, and had observed value 4.22 [m s^{-1}]. Also shown (×) is the profile of k/U_{ref}^2 observed in the same canopy, far upwind from Furry Hill, where $U_{ref} = 3.60$ [m s^{-1}]. Observed values of k/U_{ref}^2 at $z = h$ were (0.25, 0.37) upwind of the clearing and upwind from Furry Hill, while $k/U_{ref}^2 = 0.32$ for the model equilibrium profile.

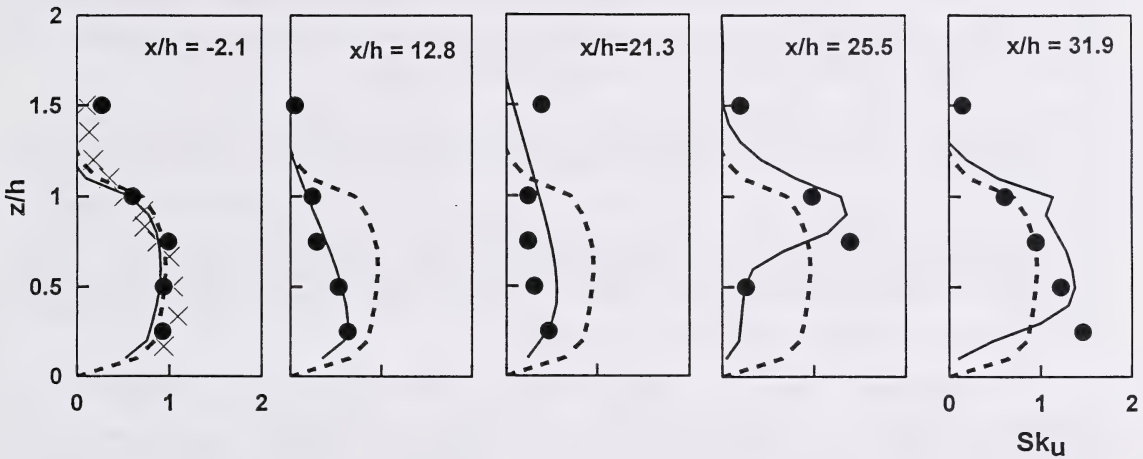

Figure 4.2d. Sequence of observed (●) and modelled (solid line) vertical profiles of the alongwind velocity skewness Sk_u across the Abbott's Booby clearing. The model skewness is the solution of Eq. (A2). The heavy dashed line, repeated on each panel, serves as a reference for the alongwind changes: it gives the *equilibrium* skewness for uniform flow in this canopy, and was calculated using Eq. (A3) with $\kappa = 1$ for the model's equilibrium profiles of shear stress, TKE, and TKE dissipation rate. Also shown (×) on the first panel is the profile of Sk_u observed in the same canopy, far upwind from Furry Hill.

solution at x/h = 31.9 differs from equilibrium, one cannot regard those observations as representing equilibrium.

Our modelled TKE was not appreciably improved by setting $\mu = 1$ within the clearing (as usually recommended for an equilibrium wall shear layer flow) to increase downward transport of TKE, nor by altering the surface boundary condition on TKE to increase k_{gnd} (by writing $k_{gnd} = \beta u_*^2/c_e$, with $\beta>1$). Liu et al. (1996) reported comparably successful simulation of the CBNA clearing flow, provided they re-tuned the standard k-ε model, without which step discrepancies of order 100% relative to the observations occurred (their Figure 9).

A very interesting aspect of the Abbott's Booby study was the identification of a region of very high velocity skewness just within the forest at the leeward edge of the clearing, believed to explain the birds' avoidance of such locations as nesting sites. Figure 4.2d compares modelled and observed skewness profiles. The equilibrium skewness profile is diagnosed rather well (except for the point at z/h = 1.5, which is remedied if one includes the adverse-pressure layer), as is the decrease in skewness within the clearing, and the prompt re-development of large skewness, building down from z/h, at the downwind edge of the clearing.

As mentioned earlier, simulations of the Abbot's Booby experiment with $\gamma = \infty$ (instantaneous adjustment of the lengthscale to the infinite-plain formulation upon passage into a clearing) were quite as satisfactory as any other choice. This insensitivity to the precise manner in which the lengthscale is adjusted at the forest boundaries suggests that, in the region of those boundaries, diffusion terms in the momentum and TKE budgets are of lesser importance than other terms, such as advection and the pressure-gradient force.

6. Simulation of Periodic Forest Cutblocks (Hotchkiss, Alberta)

We now arrive at the issue motivating this paper: can a flow model sufficiently well diagnose wind and turbulence within forest cutblocks as to provide (via the wind statistics/tree sway connection established in Chapter 3) a useful indication of implied (remnant) tree sway - an issue to be tested by comparison of our model, which we have argued is as well-tested and as successful as any earlier effort to describe flow in irregular forests, against observations in the Hotchkiss cutblocks.

As those data stem from very windy intervals, we shall not be concerned with any influence of thermal stratification upon the flow. We have no measurements whatsoever on the basis of which to diagnose the depth of mixing, and the winds aloft. Therefore although the simulations we present carry a full PBL, the aim was not to replicate the actual (unknown) details of the flow aloft, but merely to ensure that the modelling of the disturbed flow through the cutblocks was not compromised in its dynamics by an inherently unrealistic treatment.

6.1. Numerical details

One-dimensional solutions for U,V,k, representing an infinite forest block, were imposed at x/h = -80. A forest block covered $-80 \leq x/h < -60$; a large "reference clearing" spanned $-60 \leq x/h$

< -30, within which the model's "reference anemometer" lay at x/h = -40; and another forest block covered $-30 \leq x/h < 0$. At the model origin x = 0 lay the upstream edge of the first of a sequence of three (1.7h wide) or four (6.1h wide) cutblocks, labelled i = 1,2..., each of width X_c^i, and terminated by a forest strip of equal width $X_f^i \equiv X_c^i$. The leeward-most of these clearings represented our instrumented cutblock. At $x > \sum_i (X_c^i + X_F^i)$ a forest block extended downstream to the outflow boundary at x = +96h, where we imposed $\partial_x(U, V, k) = W = 0$.

Alongwind resolution was uniform ($\Delta x/h = 0.1$ for the 1.7h simulations; $\Delta x/h = 0.2$ for the 6.1h case) between x/h = -70 (which point lay upwind from the reference clearing) and a point lying well downstream of the final (ie. test) cutblock. Further towards either end of the domain, the grid was stretched. Below z = 2h, vertical resolution was 0.09h, while above, the grid was progressively stretched.

For simplicity, and as we lacked measurements to guide any more complex choice, we used constant values for a and c_d: we treated γ and the bulk dimensionless parameter $c_d a h$ as free to be optimised (see Section 6.3.3).

6.2. Rescaling model output to compare with observations

The field experiments at Hotchkiss mismatch the model in that slight irregularity in forest cover and topography occurred upstream from the windward (i = 1) cutblocks. Our choice of the (unknown) Geostrophic velocity component U_G as velocity scale for the model was simply a convenience. To compare model output with our data, we re-scaled observed and calculated velocity statistics. We shall show observations scaled on cup-windspeed ("S_{clr}") observed at z = 9 m in the large reference clearing, which lay some kilometers from our trial cutblocks. Model velocities were correspondingly re-scaled on the predicted (internal) value for the 9m windspeed in the (model's) reference clearing.

6.3. Results

In the figures to follow, the coordinate x^*/h represents alongwind location relative to the upstream edge ($x^* = 0$) of the instrumented cutblock. For all simulations to be shown, ie. both for the 1.7h and the 6.1h clearings, unless otherwise stated $c_d ah = \frac{3}{4}$, $\gamma = 0.05$. Better concordance of the model with the data could have been had by permitting these parameters to differ between the two geometries, with the justification that there may indeed have been differences. But we felt it a more convincing demonstration of model skill that we should change *nothing* across simulations for the cutblocks of differing X_C/h. We reason in Section (6.3.3) that the choice $c_d ah = \frac{3}{4}$ provides the best overall outcome, considering both mean wind speed (S) and, more importantly as regards tree motion, turbulent kinetic energy.

6.3.1 Inflow Profiles

Figure 4.3 gives equilibrium profiles, for the case ($U_G = 1$, $V_G = -1$), of wind velocities $U_0(z)$, $V_0(z)$, the cup windspeed $S_0(z) = [\, U_0^2 + V_0^2 \,]^{1/2}$, shear stress τ_0, turbulent kinetic energy k_0 and mean wind direction. We have (here only) re-normalised relative to the canopy-top friction velocity u_{*0}

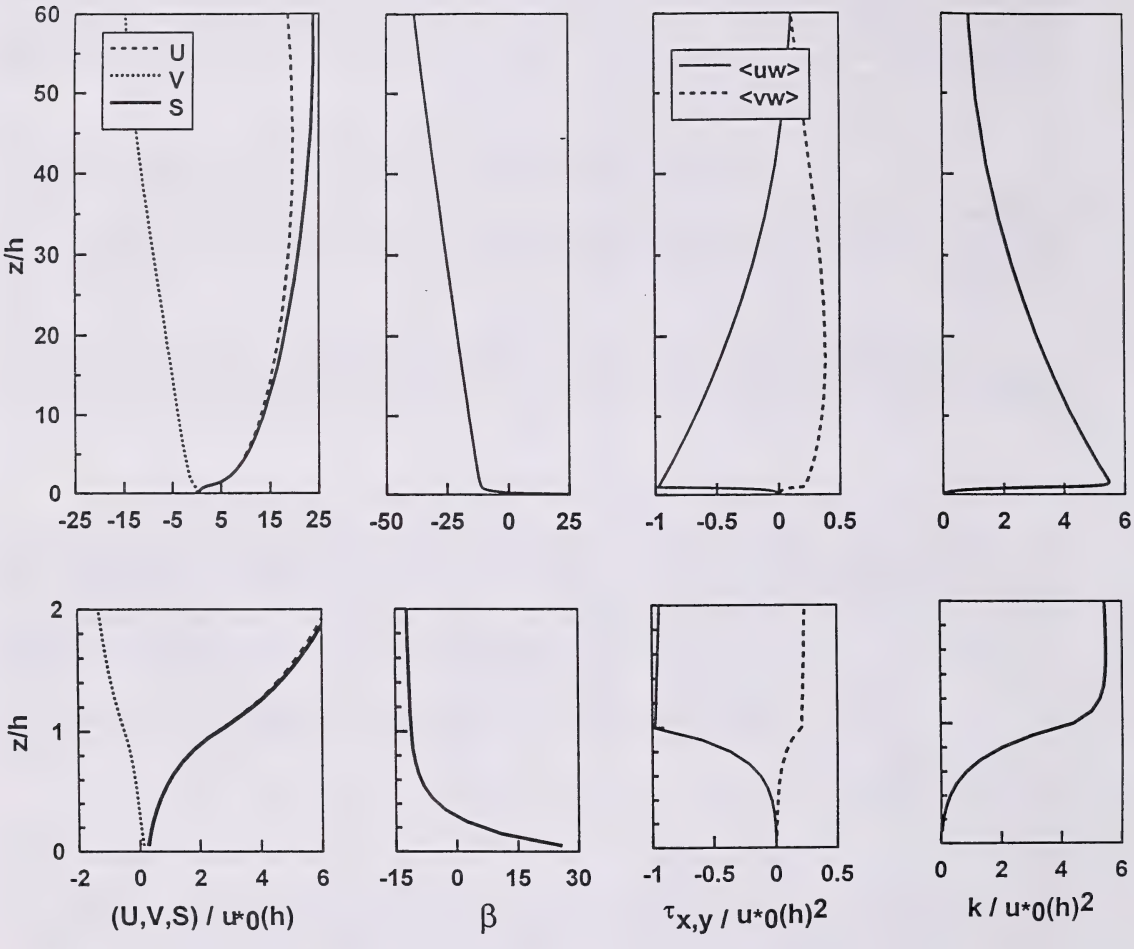

Figure 4.3. Equilibrium profiles of horizontal velocity components, cup windspeed (S) and mean wind direction (β), shear stress (τ) and turbulent kinetic energy (k), these being the inflow profiles for simulations of the Hotchkiss cutblock flows.

$= [\langle u'w' \rangle^2 + \langle v'w' \rangle^2]^{1/4}$, to permit easy comparison with other such forest profiles (u_{*0} being the velocity scale usually preferred); our ratio $S_0(h)/u_{*0} = 2.7$, a value which is fairly typical of a dense canopy. The profiles of Figure 4.3 constitute the inflow boundary condition, towards which the flow reverts on each re-entry into forest.

We were surprised by the large swing in wind direction across the canopy ($0 \le z/h \le 1$), which is as large as the swing across the entire upper domain $1 \le z/h \le 80$. An organised swing of mean wind direction within the canopy, induced by the rapidly-decreasing Coriolis force in a region of very low windspeed and resulting in alignment of the velocity with the pressure-gradient force, makes obvious sense. But it has not been widely apprehended in observational studies, perhaps because the database of wind observations within canopies is substantially derived from cup anemometers, and from wind tunnel studies. An implication is that, even in disturbed flows having two-dimensional symmetry, such as those of our cutblock records when the winds (at observation level) blew nearly perpendicularly across the forest borders, disturbances in wind direction may be anticipated. Of course, such Coriolis-force-related changes may well be masked by imperfections in the crosswind symmetry (gaps in the forest, or irregularities in the edge-line), and other departures of the flow from the ideal envisaged in the model. In any case, given this strong height-dependence of equilibrium wind direction, we are forced to accept that a full-scale forest-clearing flow which is at all heights perpendicular to the forest edges is unrealisable, ie. dynamically disallowed, except where it occurs in response to some fortuitous conspiracy of upwind topography, etc. The best we can hope for is a near-ground flow that is *roughly* perpendicular to the forest edges; our specification ($U_G = 1$, $V_G = -1$) results in the mean wind direction lying only 6° away from the x-axis, at (the model's equivalent of) the position of the anemometer in the "reference clearing."

6.3.2. Mean windspeed and pressure

Figure 4.4 compares the modelled and measured patterns of variation in the mean cup-windspeed $S(x, z_{instr})$ through the reference clearing and far downwind across the cutblock arrays. Similar patterns hold for the U component, because we assured $V \ll U$ at $z = 9$m by specification of V_G. Model and experimental data have been re-normalised on S_{clr}, which assures their agreement (that $S/S_{clr} = 1$) at instrument height ($z = z_{instr} = 9$m) at the distant reference point. So that anyone who wishes to may (again) re-normalise our model fields on u_{*0} (friction velocity based on the shear stress at $z = h$ of the equilibrium, ie. inflow, profiles) we note that in our simulations $S_{clr} / u_{*0} = 3.83$.

It is apparent from Figure 4.4 that the model calculates nicely the overall wind reduction in the cutblocks, relative to S_{clr}, which can be regarded essentially as a weather-station (open ground) reference. For the 6.1h cutblocks there is little variation from one cutblock to the next in the amplitude of the wind-modulation, and even the peaks differ only modestly from one cutblock to the next. This is consistent with findings of Raupach et al. (1987) for a clearing within a wind-tunnel model canopy. It follows that our instrumented cutblocks, at least in the 6.1h array, should have been "typical" of their neighbours, and that a periodic boundary-condition might be used to model the flow in a single representative cutblock. Simulations of the 6.1h experiment, using a three-dimensional generalisation of the present model that assumes periodicity on the x and y axes, agree closely with those presented here (A. Tuzet, pers. comm). Apparently however, windspeed may not have been periodic across the narrower, 1.7h cutblock array.

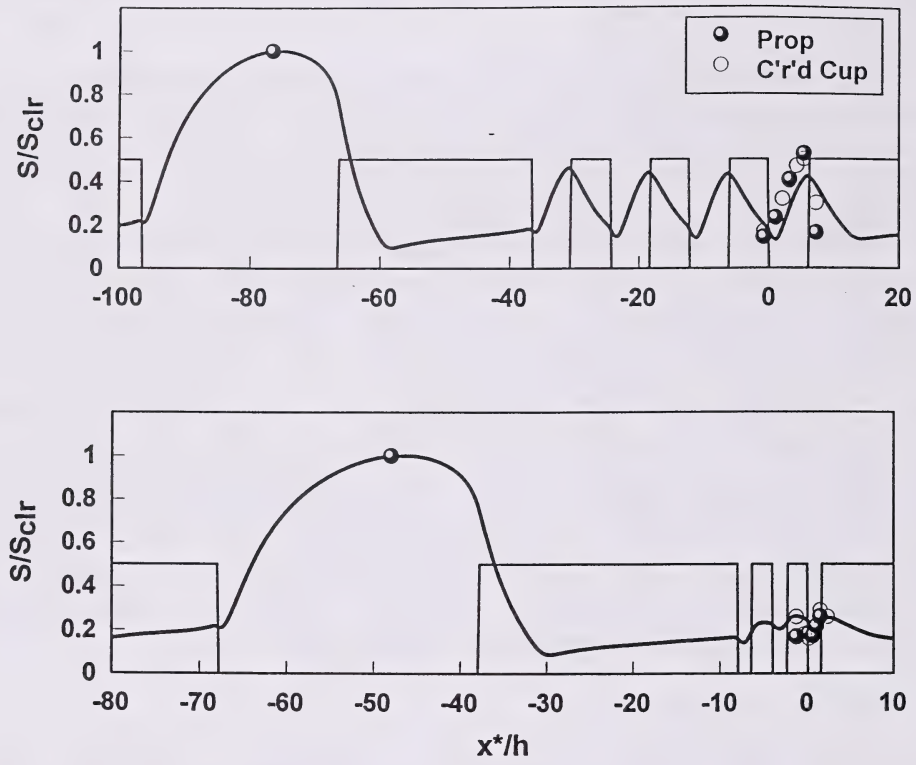

Figure 4.4. "Grand scale" comparison of measured and simulated spatial variation of the normalised mean cup windspeed S/S_{clr}, at z = 9m, across the reference clearing and through the periodic arrays into the instrumented cutblocks. Simulation assumes $c_d ah = ¾$, $\gamma = 0.05$. Range on the x* axis covers of order 5 km, and x* = 0 at the upwind edge of the instrumented cutblock. Observations consist of all propellor data for $|\beta| < 30°$, all cup data for $|\beta| < 10°$.

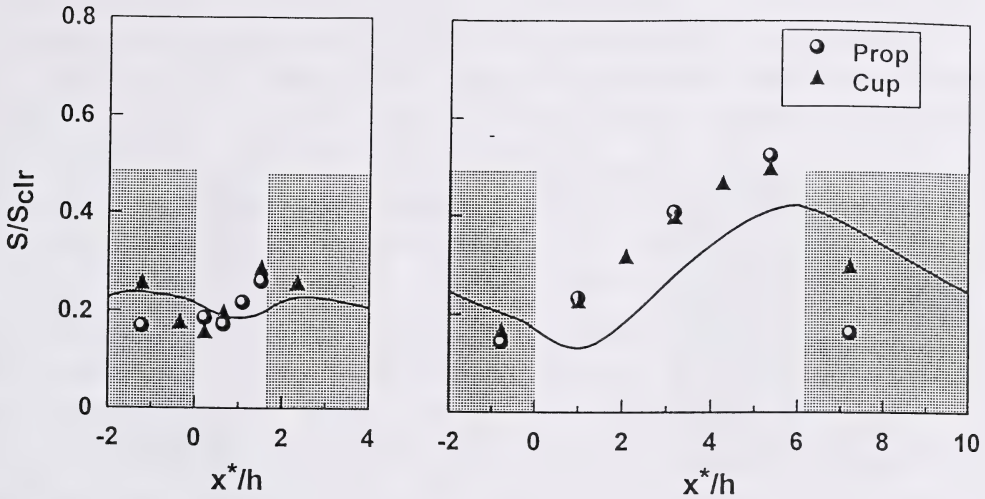

Figure 4.5. "Local view" of measured and simulated spatial variation of the normalised mean cup windspeed S/S_{clr}, at z = 9m, across the instrumented cutblocks. Simulation assumes $c_d ah = ¾$, $\gamma = 0.05$. Observations consist of all propellor data for $|\beta| < 30°$, all cup data for $|\beta| < 10°$.

Although good overall conformance of model and observation is apparent on Figure 4.4, on taking a close-up view (Figure 4.5) one observes that the amplitude of the variation of S/S_{clr} across the 1.7h cutblocks has been underestimated, and that in the 6.1h cutblock, the "wave" of S/S_{clr} seems slightly out of phase with the observations (the latter feature would vanish upon scaling on an in-cutblock reference windspeed S_{cb}, and so may be only a consequence of imperfect simulation of S_{clr}/S_{cb} by the model). In assessing Figure 4.5 one should bear in mind several mitigating points. Firstly, we have little confidence in our within-forest wind data. The forest blocks were quite inhomogeneous as regards tree height, spacing, and species-mix, and so a point measurement need not compare well with the model's implicitly spatially-averaged figure. Secondly, we have entirely neglected the topographic variations of the terrain, not to mention the drag of the remnant trees in the cutblocks. Thirdly, we have used the same, constant value for $c_d ah$ across the entire domain (except in clearings, where $c_d ah = 0$), whereas undoubtedly in-forest spatial variations in $c_d ah$ occurred. We did not feel it was warranted to "guess" our way about by adjusting a spatially-varying $c_d ah$, an approach which would amount to no more than an exercise in curve-fitting. Finally, perhaps most significantly of all as regards the apparently flawed model performance (Figure 4.5), the field reference windspeed S_{clr} was measured in a clearing about 5 km from our instrumented cutblocks, and separated from them by rather irregular terrain, whereas the model reference clearing lay immediately upwind of the cutblock array. Thus it would be naive to expect of the model a perfect profile of S/S_{clr}, and one might with some justification contend it would be fairer to assess model skill with respect to properties scaled on a *local* velocity scale (measured *in* the test cutblock); see Wilson and Flesch (1996), who gave model output in such form.

Our measurements provided no information on the vertical variation of the wind patterns throughout the cutblocks. Figure 4.6 gives an alongwind sequence of modelled vertical profiles of the U component, across the $X_C = 6.1h$ cutblock. An initially surprising feature is that, below about $z/h = ½$, the alongwind component U *accelerates* across the forest belts and *decelerates* in the clearing, to the degree of reversal ($U<0$) very near ground. The opposite behaviour is seen at larger heights. Unfortunately we do not have observations to confirm this complex pattern. But we feel it is plausible, in view of the reversing pressure gradients the flow encounters (more on this below).

Towards the middle of the wide clearing(s), a boundary-layer type profile is established, ie. there is not the inflexion point characteristic of a canopy wind profile. But upon passage back into a forest block, the characteristic canopy wind profile develops promptly, with acceleration of the flow very near ground, and deceleration higher up. At the downwind edge of the forest strip (see the profile at $x^*/h = -1$), the wind profile resembles the equilibrium profile, ie. the profile which would be observed within a forest of infinite extent (and which was used as the inflow boundary condition). More or less the same features are diagnosed by the simulations for the narrow cutblocks, with the exception that a boundary-layer type profile is not established.

In undisturbed micrometeorological flow the mean vertical velocity is of the order of a few cm/s. However sizeable vertical motion can be expected near forest edges. Figure 4.7 gives contours of the normalised mean vertical velocity W/S_{clr} in the wide cutblock.. Upward flow occurs within a distance of about 2h from the sheltering forest edge, beyond which there is descent over most of the cutblock, and even in the inflow region of the downstream forest block. Although these vertical velocities are small relative to the horizontal winds, peaking at about $0.06S_{clr}$, the implied

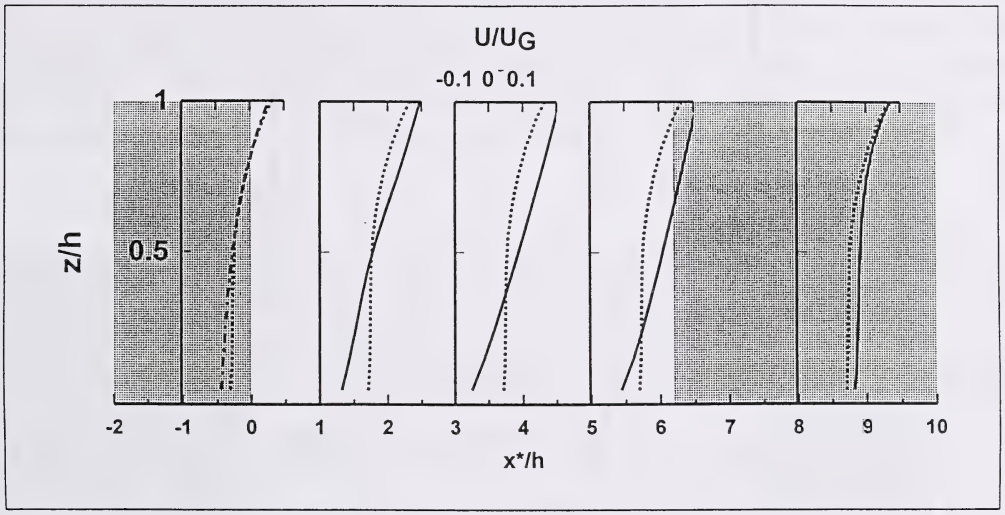

Figure 4.6. Vertical profiles of the alongwind velocity component U/U_G, at several locations across the $X_F = X_C = 6.1h$ cutblock. The span of the velocity axes is (-0.1, + 0.2) U_G , and the height-axes are placed so as to mark the locations (in x*/h) of the profiles. **(Chain line)**, the equilibrium solution (infinite fetch of forest); **(Dotted line)**, the solution at x*/h = -1, ie. just upwind of the forest->cutblock transition; and **(Solid line)**, the local solution.

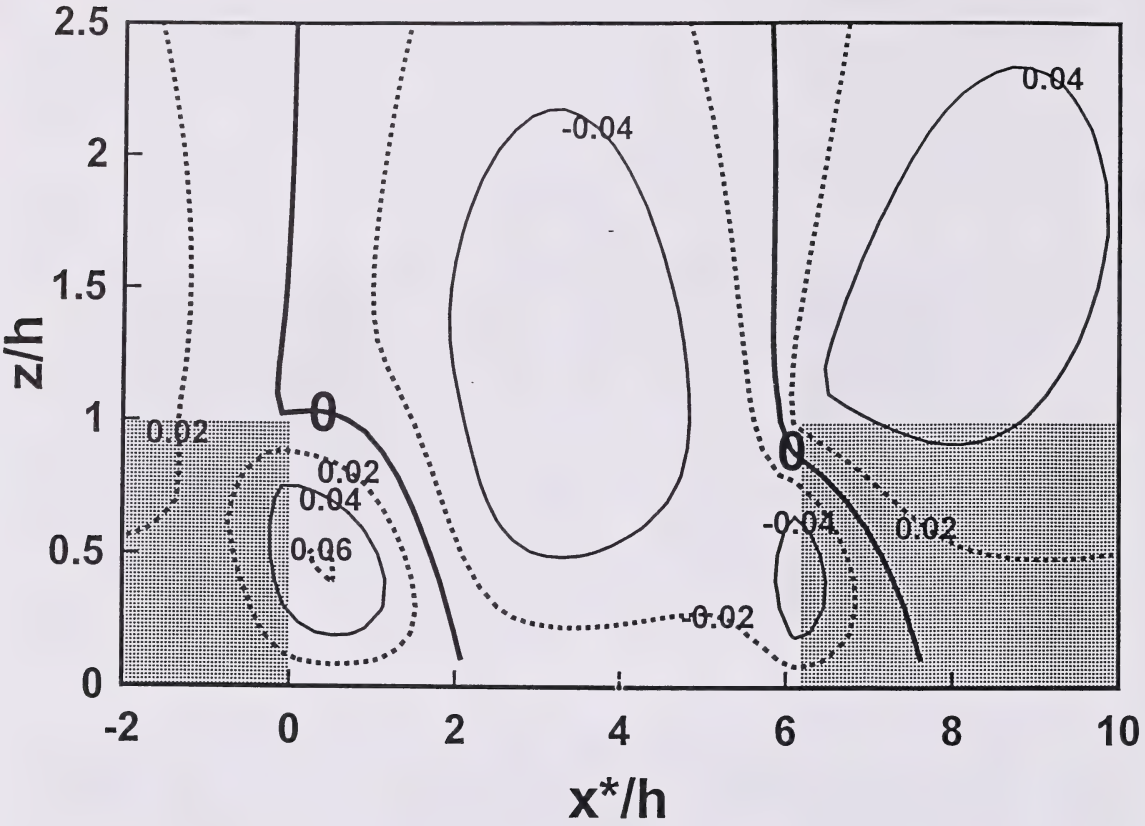

Figure 4.7. Contours of mean vertical velocity W/S_{clr} in the wide clearing.

dimensional mean velocity can be large, around ½ m/s when S_{clr} = 10 m/s, and is likely to have dynamical importance.

Figure 4.8 gives the local pressure field about the 6.1h clearings. A steeply adverse pressure gradient $\partial_x P$ upwind from the clearing→forest transition gives way within the forest block to a strongly favourable (accelerating) gradient. Deep within dense vegetation, the wind is only weakly coupled to the flow aloft, and thus essentially driven by a balance between form drag and the local pressure gradient. The favourable pressure gradient across the sheltering forest belts, clearly shown in Figure 4.8, presumably causes the accelerating windspeed seen near ground, while the adverse gradient in the clearing may explain the near-ground velocity-reversal.

6.3.3. Turbulent kinetic energy

Figure 4.9 gives a wide-area view of our simulation of the normalised turbulent kinetic energy k/S_{clr}^2, in comparison with the observations. The simulation captures nicely the overall patterns, and Figure 4.10 confirms that even the local detail is represented fairly well: the general *shape* of the modelled TKE profile matches that observed, with TKE increasing sharply over the upwind half of the 6.1h cutblock, and changing much less over the downwind half. In view of the provisos earlier expressed (instrument performance; neglect of terrain complexity; etc.), the modelled pattern of TKE is satisfactory, and we may infer from it the spatial variation of the velocity variance σ_u^2.

6.3.4. Weak sensitivity to lengthscale adjustment parameter γ

Figure 4.11 illustrates the rather modest sensitivity of these simulations to specification of the lengthscale adjustment parameter γ; entirely different formulations of the lengthscale transition (between equilibrium forest form λ_F and equilibrium open plain form λ_P as the asymptotic downwind limit in a large clearing) gave simulations which were equally acceptable. Variation of γ (or of the transition-formulation) has a greater impact on the TKE field than on the mean windspeed field. Although Figure 4.11 shows that the choice γ = 100 provides a much better simulation of the mean wind than the γ = 0.05 we settled on, the spatial modulation of the associated TKE field is seriously overestimated. Recall that the rms wind force $\sigma_{u|u|}$, whose specification is the goal of this investigation, is considerably more sensitive to TKE than to mean windspeed (Appendix 1).

There is one other "free" parameter, $c_d ah$: should we reduce this, we reduce the modulation of both S and k. However the consequence of that step is that the variation of S across the narrow cutblock, already underestimated (Figure 4.5) with $c_d ah$ = ¾, is further reduced. Our specification that $c_d ah$ = ¾, γ = 0.05 therefore represents a compromise, and as we shall later show, a good one as regards the resulting simulations of the rms wind force $\sigma_{u|u|}$. We do not hold that this choice is *uniquely* optimal, and the outcome is not very different for γ in the range $0.005 \le \gamma \le 0.5$.

6.3.5. Skewness Sk_u

Figure 4.12 compares the average pattern of skewness observed, with solutions of the simplified Sk_u budget equation given in Appendix (3). We observed large run to run variability in

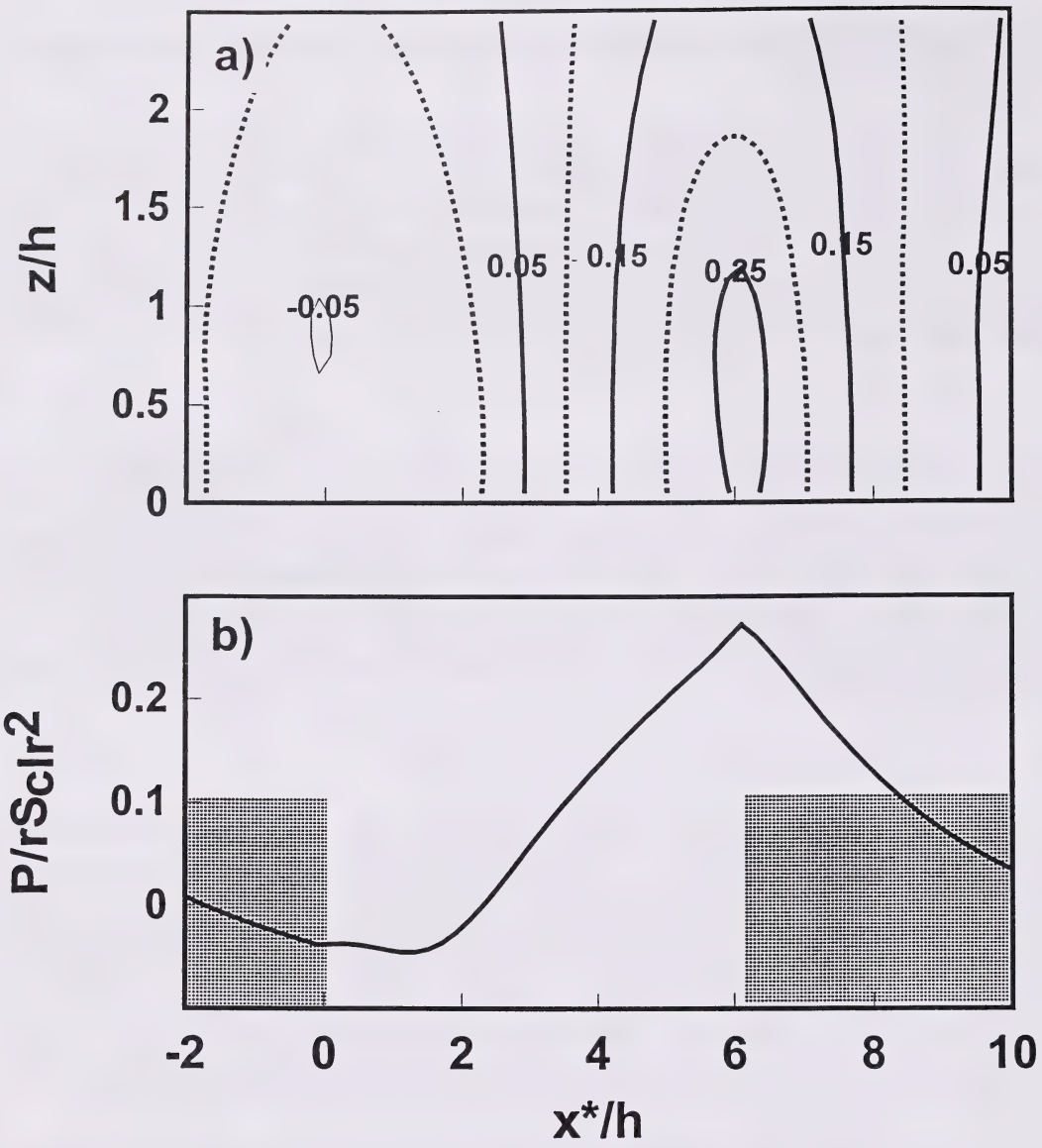

Figure 4.8. Normalised pressure field $P/\rho S_{clr}^2$ about the wide (6.1h) cutblock, according to the numerical model; (a) contours; and (b) horizontal profile at z/h = 0.4. Pressure is not necessarily positive, being *relative* to ground-level pressure at the outflow boundary.

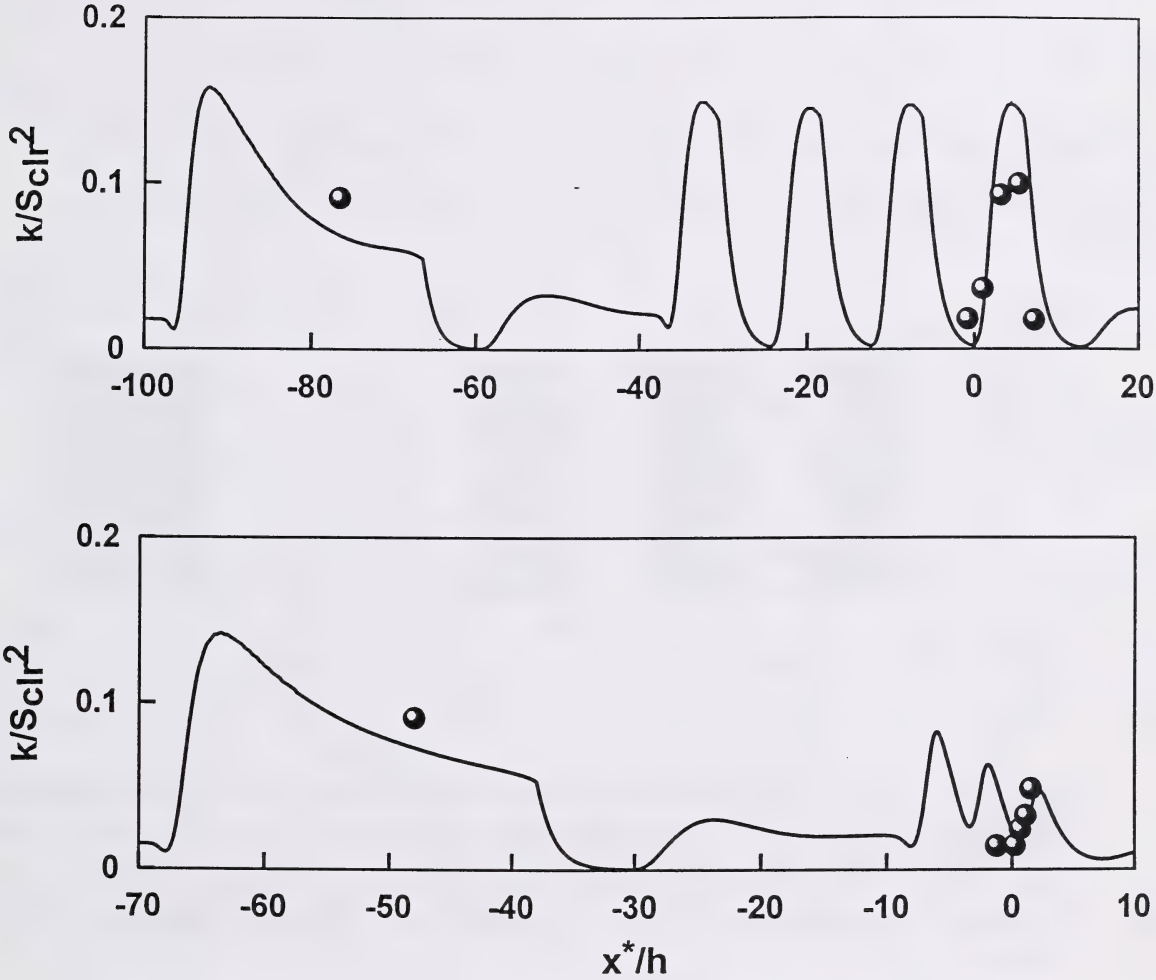

Figure 4.9. "Grand scale" comparison of measured and simulated spatial variation of the normalised turbulent kinetic energy k/S_{clr}^2, at z = 9m, across the reference clearing and through the periodic arrays into the instrumented cutblocks. Simulation assumes $c_d ah = ¾$, $\gamma = 0.05$. Range on the x* axis covers of order 5 km, and x* = 0 at the upwind edge of the instrumented cutblock.

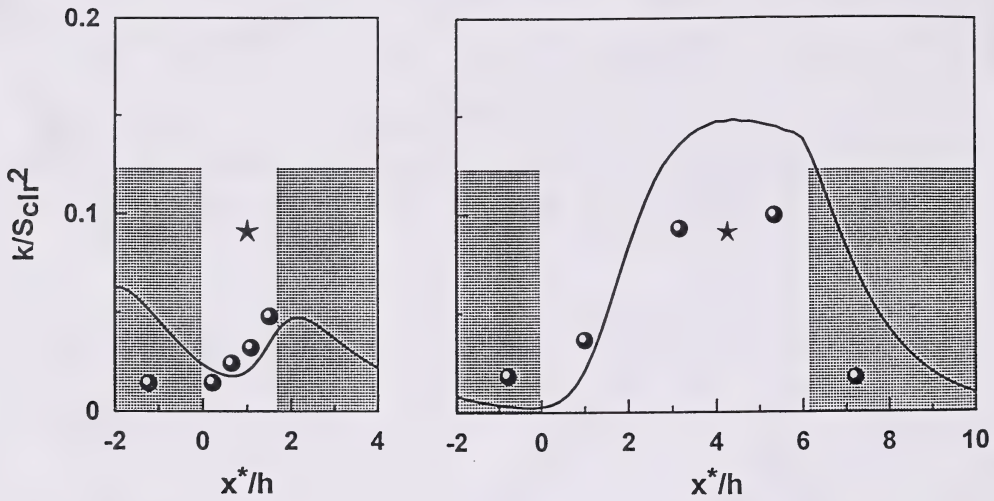

Figure 4.10. "Local view" of measured and simulated spatial variation of the normalised turbulent kinetic energy k/S_{clr}^2, at z = 9m, across the instrumented cutblocks. The simulation assumes $c_d ah = ¾$, $\gamma = 0.05$. Also plotted (★) on both graphs, though not at the proper point (which lies offscale) on the x*/h axis, is the measured value of k/S_{clr}^2 in the distant reference clearing. Thus, towards the leeward region of the wide cutblock, TKE exceeds somewhat its value in that much wider, reference clearing.

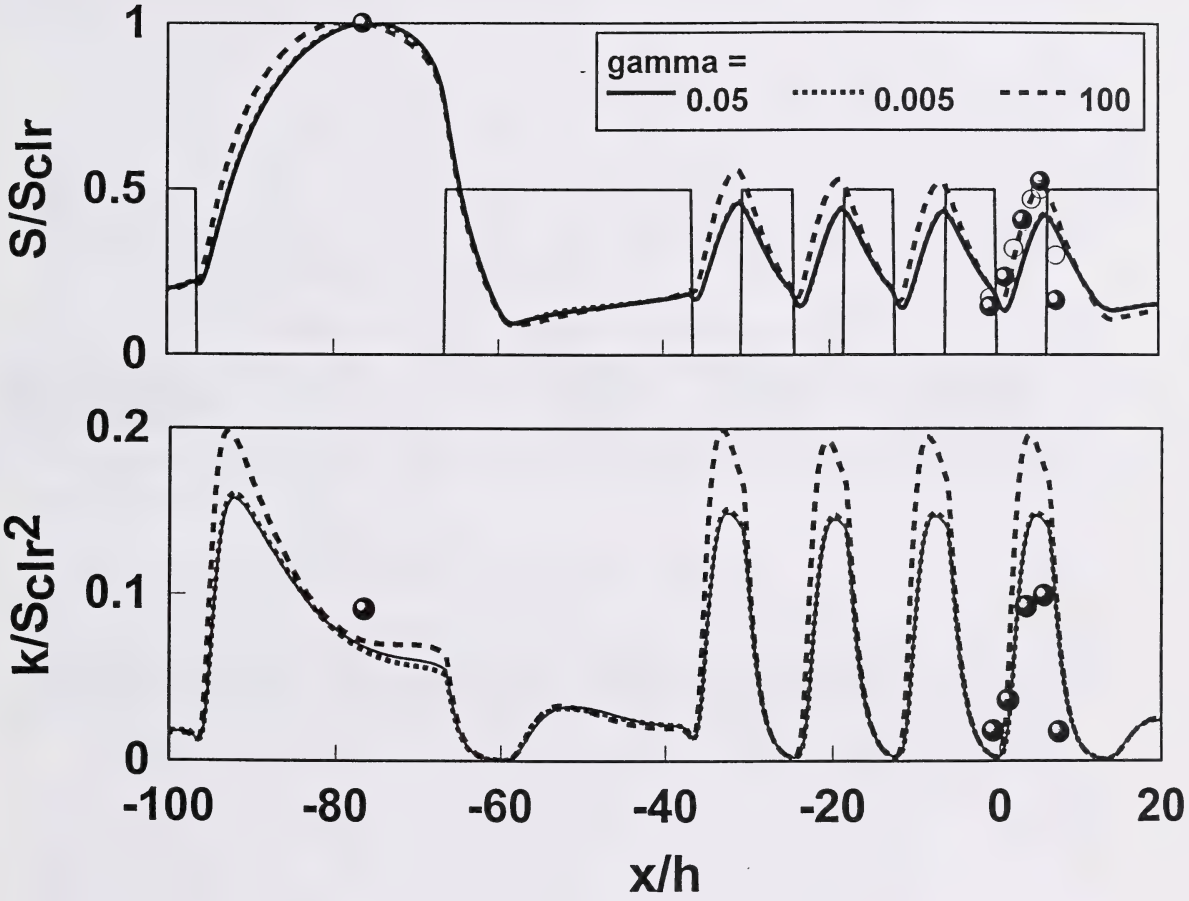

Figure 4.11. Sensitivity of simulations of cup windspeed (S) and turbulent kinetic energy (k) across the wide (6.1h) cutblocks, to specification of the lengthscale adjustment parameter γ. The bulk drag coefficient $c_d ah$ = ¾ for all curves. The observations (as on Figures 4.5, 4.9) are also shown for comparison.

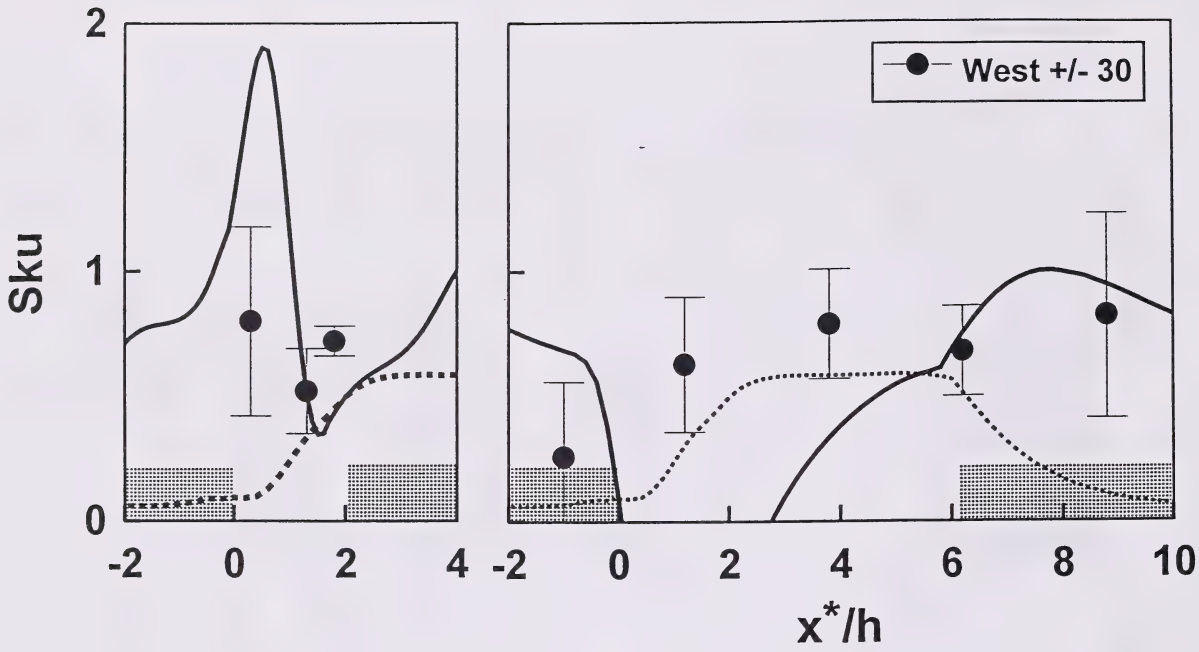

Figure 4.12. Observed versus modelled (Eq. A2) horizontal profiles of velocity skewness Sk_u at z = 9m. The dashed line results from having dropped the production term $3\ \alpha_{sk}^2\ k\ \partial_x k$, which otherwise (solid line) causes large negative Sk_u near the upwind edge of the wide clearings.

Sk_u , which cannot be explained within the scope of a 2-d flow model. This variability probably arose from our short averaging intervals (15 or 30 mins), and perhaps partly from imperfect response of the propellor anemometers. The simulation of Sk_u is disappointing, in view of the encouraging result we reported for the Abbot's Booby clearing. Fortunately, however, the variance $\sigma^2_{u|u|}$ of the wind force is much less sensitive to Sk_u than to the lower moments.

6.3.6. Wind force $\sigma_{u|u|}$ and tree sway

Figure 4.13 compares the observed spatial pattern of the normalised wind force $\sigma_{u|u|}/U_{clr}^2$ against the simulations. The velocity variance σ_u^2 was derived from the calculated TKE, assuming equilibrium partitioning, ie. $\sigma_u^2 = c_e\ c_u^2 k$. We set kurtosis $Kt_u = 4$ (a value typical of our measurements), and as anticipated (Appendix 1) found the modelled wind force was not very sensitive to the specification of skewness Sk_u, witness the small difference between the outcome using $Sk_u = 1$ and that using model-calculated skewness.

The model has captured very well the dramatic reduction of the wind forcing relative to the distant reference clearing, and has given quite precisely the local detail of the pattern of wind force within the cutblocks. Given the tight connection between $\sigma_{u|u|}$ and tree sway, we are now in the position that, once given a figure for U_{clr}, which is more or less a "weather station" windspeed, we may infer the r.m.s. sway σ_θ of a "characteristic" (remnant spruce) tree, whatever its position in the array of cutblocks.

7. Model Investigation of the Effect of Forest Border Width

As an example of the potential of a wind flow model to evaluate strategies for minimising windthrow, we shall investigate the consequence of using forest strips of *reduced width*, $X_F = 3h$ or $X_F = 1h$, to shelter remnant spruce in cutblocks of unaltered width $X_c = 6.1h$.

The sole difference between the simulations required for these three cases ($X_F/h = 6.1, 3, 1$) is the distribution of forest-drag. We made no changes to the grid distribution, to the location of the large upstream "reference clearing" wherein the velocity scale S_{clr} is "measured," nor to the input parameters ($c_d ah = ¾$, $\gamma = 0.05$). As previously, we focus on the wind properties in the downwind member of a *series* of four cutblocks, each of which is *equally* provided with a shelter-strip (of width $X_F/h = 1, 3,$ or 6.1).

Figure 4.14 shows the comparative profiles of speed, TKE and rms wind-force within the "test" cutblock (width 6.1h), as provided with either a 1h, a 3h, or a 6.1h shelter-block. According to the model, if 3h shelter blocks are provided (rather than 6h blocks), mean windspeed reduction is not so favourable, though still entirely acceptable ($S < 0.4\ S_{clr}$); while, quite unexpectedly, the TKE is *greatly* reduced over much of the cutblock, falling to about as low as only 25% of the *already* reduced TKE figure when 6h shelter was provided! The consequence is that wind protection is *markedly better* when the shelter strips are only 3h wide than when they are 6.1h wide.

Whether or not this is true, only comparative observations can decide. In the first paper of this series, we summarised observations of TKE across a number of clearings from different

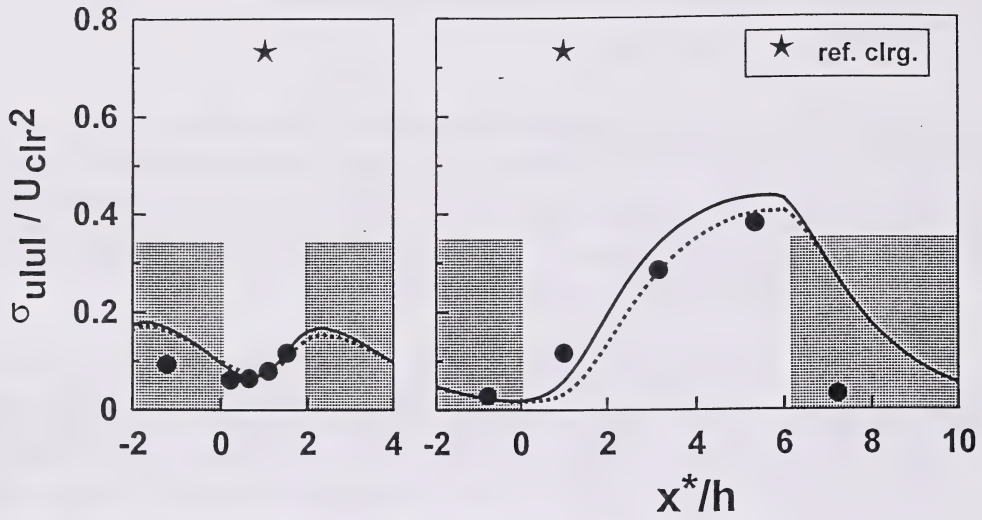

Figure 4.13. Comparison of measured and modelled spatial variation of the normalised wind force $\sigma_{u|u|}/U_{clr}^2$ across the instrumented cutblocks and in the distant reference clearing (★, actually observed far upwind on the x^*/h axis). Simulation assumes $c_d ah = ¾$, $\gamma = 0.05$. For the calculation of $\sigma_{u|u|}$ according to Eq. (1), we assumed $Kt_u = 4$ and either set $Sk_u = 1$ (solid line), or calculated Sk_u according to Appendix 3 (dashed line). Note that $\sigma_{u|u|}$ determines the standard deviation of tree sway angle σ_θ, and that U_{clr}, being measured in a large clearing, can be considered as more or less a weather station windspeed.

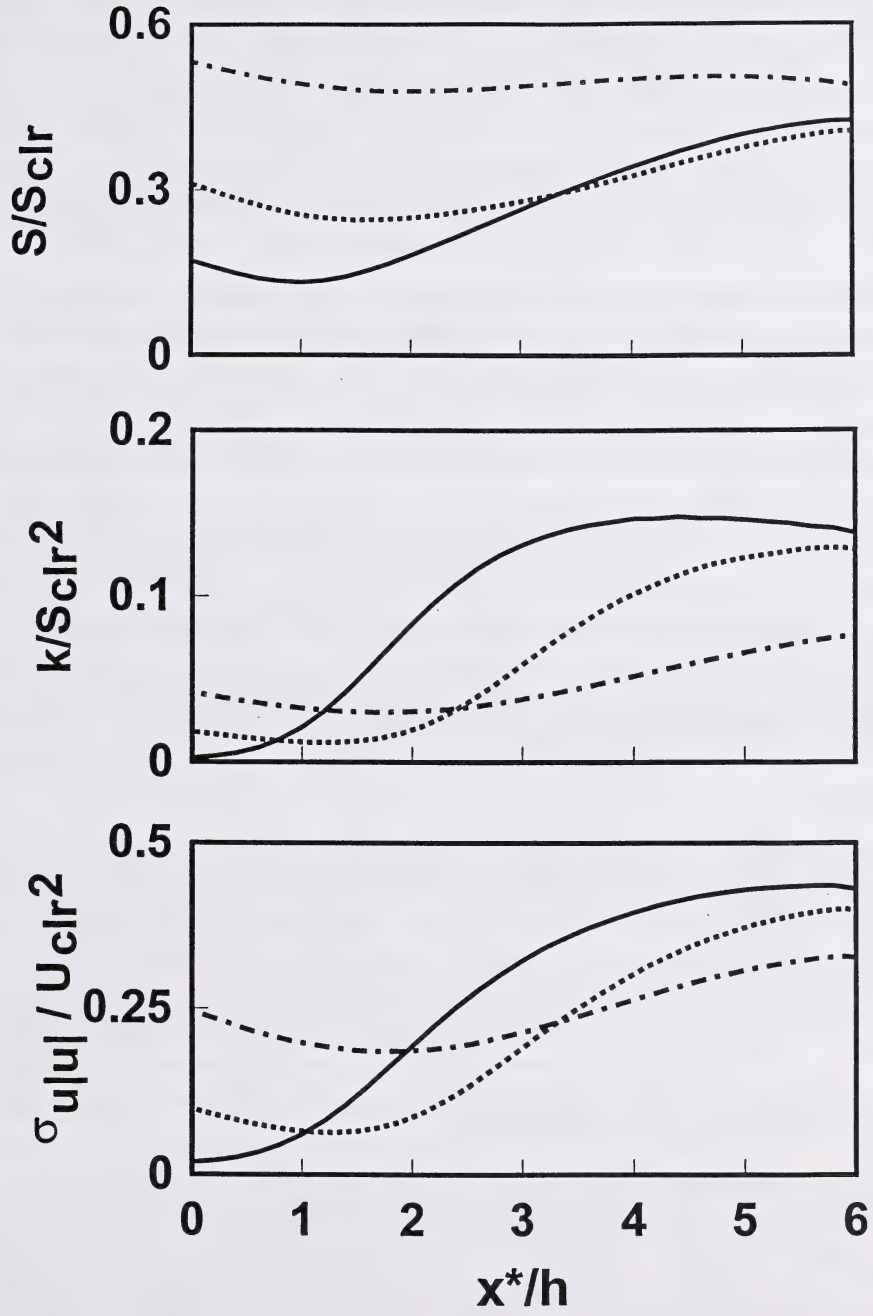

Figure 4.14. Comparative numerical simulations of the patterns of windspeed (S), turbulent kinetic energy (k) and root-mean-square wind force ($\sigma_{u|u|}$) across the fourth of a series of cutblocks, each having width $X_c = 6.1h$, and each sheltered by forest strips of width $X_F = 6.1h$ (**solid line**), $X_F = 3h$ (**dashed line**), or $X_F = h$ (**dot-dashed line**). Simulations with $c_d ah = ¾$, $\gamma = 0.05$.

experiments, and found a striking uniformity in the pattern of TKE "recovery." The present simulations (of clearings with forest borders of X_F = 3h or X_F = 1h) do not uphold the pattern: in both cases they show an initial *decrease* in TKE with increasing x across the clearing. Perhaps the explanation for this discrepancy lies in the fact that none of the experimental clearings had a geometry like that we have simulated. In any case, if the predictions of Figure 4.14 should prove to be in conflict with observation, one would be impelled to conclude that the earlier-shown concordance of the model with observations (see Sections 4-6) is largely spurious, perhaps only the fortuitous consequence of "tuning." That possibility is scarcely believable, we think: for example, there simply *was* no tuning in the case of our simulation of Abbott's Booby study.

Well, if this unexpected model result were true in reality, then why? Why would *narrower* shelter strips provide *more effective* reduction of the r.m.s. wind force? In contemplating the matter, recall that the impact of the shelter on *turbulence* is more important than its impact on the mean wind. Although the influence of porous-shelterbelt thickness (W) on *mean* wind reduction has been studied computationally (Wang and Takle, 1996) and experimentally (Takahashi, 1978), and whilst others have investigated the influence of *spacing* of successive porous barriers (screens, W≈0; or thick windbreaks of various W) on *mean* wind, we are not aware of any existing comprehensive study of the pattern of *TKE* around a sequence of porous barriers of arbitrary width (W) and spacing. In interpreting Figure 4.14, then, we can only speculate. The act of providing shelter in one region so as to reduce near-ground windspeed *causes* a downwind region of increased vertical shear, and associated turbulence (increased shear production in Eq. 12): and so perhaps the provision of *wider* forest strips leads to stronger vertical wind shear at the upwind edge of the protected zone (cutblock) than does provision of narrower shelter, causing accentuated shear production of turbulence, and the surprising r.m.s. wind-force pattern suggested by Figure 4.14.

8. Conclusions

Our aim has been to combine a high-resolution (order 1m) wind and turbulence model, with a tree-motion model, to infer statistics of remnant tree sway in forest clearings. To that end we have adapted the K-theory closure of Wilson et al. (1998; WFR), tested it against our own and others' observations of forest-edge flows, and showed it performs at least as well as the more-complex models of earlier authors. With appropriate choices of domain size, resolution, etc., simulations show quite good agreement with observations of mean windspeed and turbulent kinetic energy, without alteration of the basic closure parameters (c, α, μ) formerly optimised by WFR. The implied spatial patterns of the root-mean-square wind force $\sigma_{u|u|}$, which determine the r.m.s. tree sway σ_θ, are in excellent agreement with measurements.

But our cutblock flow observations at Hotchkiss are from a single height, so that despite the simplicity of the WFR wind model, there is an enormous disparity between the prolific model output (complete spatial fields of U, V, W, P, k, ε, λ and much more) and the available data to judge its accuracy. To some extent we addressed that deficiency by comparing simulations against the more-complete observations of Raupach et al. (1987). Nonetheless many readers, and especially those very conversant with numerical flow models, may wonder whether the ability of the model to calculate the spatial fields of the mean wind, TKE and wind-force variance represents actual skill, or just judicious selection of model output. That disquieting possibility resonates in our own minds

too, for certainly the model results shown are but the "tip of a paperberg" calculated; and we did specify $c_d ah$ and γ to optimise model agreement with our cutblock data. It may be useful, then, to address the issue of our own objectivity. *How critically* have we compared model results with data? What reassurances can we give that this model is not a slippery thing, that would conform to any data? These points are pertinent:

- We chose maximal *simplicity* in the flow modelling[3], to minimise the introduction of flexible parameters.

- We insisted on constancy of the two unknown (thus free to be optimised) parameters ($c_d ah$, γ) across both our experimental configurations.

- We acknowledged the role of those constants in adjusting "model curves" toward the data.

- We displayed the modelled and observed fields so as to clearly display *differences*.

- We used a *single normalising scale*, external to the test cutblocks, so as to avoid imparting any misleading appearance of quality to the simulations[4].

- We included *new, testable predictions* of the model.

In short, although the success of the simulations is assuredly not automatic, and depends on the experience of the user to apply the model appropriately, making necessary judgements especially where important input data are uncertain, it remains that *given* a set of inputs, the model is completely objective and reproducible.

In all probability one could invoke a more complex treatment of the Hotchkiss flow, and attain better agreement with observations. For example, there is simply no basis to insist that $c_d a$ is constant with position (except in cutblocks, where it vanishes); this was a noticeably inhomogeneous forest. At the very least, leaf area density in the aspen forest is strongly height-dependent (eg. Amiro, 1990), peaking well below mean tree height: perhaps through having adopted a height-independent (bulk) drag parameter, we should have also used an *effective* or *aerodynamic* canopy

---

[3]An exception is our having carried a full boundary-layer, and Coriolis force. Our first simulations of the Hotchkiss flow assumed shear stress to be height-independent (except where disturbed by the forest clearings) to the top of the computational domain, placed at $z/h = 40$; ie. we ignored large scale pressure gradients, and the Coriolis force, and entirely neglected the crosswind component V. Interestingly, just as WFR found it non-essential to properly model the outer region of their wind-tunnel boundary layer, we found that nothing vital was gained by adding proper PBL structure - other than the assurance we had done the right thing, and the revelation that mean wind direction may swing drastically within the canopy layer.

[4] Whereas in Wilson and Flesch (1996) we unnecessarily introduced independent normalisations for mean wind and for TKE, such that *both* quantities were forced into agreement with observation at one point *within* the cutblock.

height (h) that is lower than the "visual" or sampled tree height. It seemed to us better to neglect such options, and show these less-than-perfect outcomes, which nevertheless seem quite realistic, and useful as regards the pattern of tree sway. We look forward to experimental confirmation or contradiction of the untested prediction of Section (7) that in the context of windthrow of remant spruce, wider shelter-strips may function less-effectively than narrow.

In conclusion, given the apparent ability of our wind flow model to diagnose velocity statistics within cutblocks, and the relationship we have established between tree sway and the wind, we feel hopeful that a wind model *can* be a useful tool for identifying effective cutblock designs. No doubt mesoscale meteorological events, possibly in interaction with topographic complexities ignored here, lend a sporadic, unpredictable complexity to the pattern of windthrow. And of course, spatially-varying soil and tree properties must distort our simple picture. Nevertheless we expect that underlying such randomness, and visible in the long term, there will exist a spatial pattern in tree windthrow that is governed by "routine" wind dynamics, as captured in such models as we described. That blow-down pattern should correlate with long-term spatial trends in the central-tendency statistics we considered, the r.m.s. tree sway (σ_θ), and its surrogate the r.m.s. wind force ($\sigma_{u|u|}$).

9. References

Amiro, B.D., 1990: "Comparison of turbulence statistics within three boreal forest canopies." Boundary Layer Meteorol., **51**, 99-121.

Blakadar, A.K., 1962: "The vertical distribution of wind and turbulent exchange in a neutral atmosphere." J. Geophys. Res., **67**, 3095-3102.

Chen, J.M., T.A. Black, M.D. Novak, and R.S. Adams, 1995: "A wind tunnel study of turbulent airflow in forest clearcuts." In M.P. Coutts and J. Grace (eds.), *Wind and Trees*, Chapter 4. Cambridge University Press, London.

Delage, Y., 1974: "A numerical study of the nocturnal atmospheric boundary layer." Quart. J. R. Met. Soc. **100**, 351-364.

Finnigan, J.J., and Y Brunet, 1995: "Turbulent airflow in forests on flat and hilly terrain." Pp 3-40 in *Wind and Trees*. Eds. M.P. Coutts and J. Grace. Cambridge University Press, UK.

Gash, J.H.C., 1986: "Observations of turbulence downwind of a forest-heath interface." Boundary Layer Meteo., **36**, 227-237.

Green, S., N. Hutchings, and J. Grace, 1994: "Modelling turbulent airflow in sparse tree canopies." Preprint volume (pp86-87), 21st Conference on Agric. Forest Meteorol., Am. Met. Soc. San Diego.

Hanjalic, K., and B.E. Launder, 1972: "A Reynolds stress model of turbulence and its application to thin shear flows." J. Fluid Mech., **52**, 609-638.

Hinze, J.O., 1975: *Turbulence*. McGraw-Hill. ISBN 0-07-029037-7.

Holland, J.Z., 1989: "On pressure-driven wind in deep forests." J. Applied Meteorol. **28**, 1349-1355.

Li, Z.J., D.R. Miller, and J.D. Lin, 1985: "A first-order closure scheme to describe counter-gradient momentum transport in plant canopies." Boundary Layer Meteorol., **33**, 77-83.

Li, Z., J.D. Lin, and D.R. Miller, 1990: "Air flow over and through a forest edge: a steady state numerical simulation." Boundary Layer Meteo., **51**, 179-197.

Liu, J., J.M. Chen, T.A. Black, and M.D. Novak, 1996: "E-ε modelling of turbulent airflow downwind of a model forest edge." Boundary Layer Meteorol., **77**, 21-44.

Miller, D.R., J.D. Lin and Z.N. Lu,1991: "Airflow across an alpine forest clearing: a model and field measurements." Agricultural and Forest Meteorology **56**, 209-225.

Navratil, S., L.G. Brace, E.A. Sauder and S. Lux, 1994: "Silivicultural and harvesting options to favor immature white spruce and aspen regeneration in boreal mixedwoods." Information Report NOR-X-337, Northern Forestry Centre, Canadian Forest Service.

Patankar, S.V., 1980: *Numerical Heat Transfer and Fluid Flow*, Hemisphere Publ. Co. ISBN 0-07-048740-5

Raupach, M.R., E.F. Bradley, and H. Ghadiri, 1987: "Wind tunnel investigation into the aerodynamic effect of forest clearing on the nesting of Abbott's Booby on Cristmas Island." Internal report, CSIRO Centre for Environmental Mechanics, Canberra.

Raynor, G.S., 1971: "Wind and temperature structure in a coniferous forest and a contiguous field." Forest Sci., **17**, 351-363.

Schilling, V.K., 1991: "A parameterization for modelling the meteorological effects of tall forests - a case study for a large clearing." Boundary Layer Meteorol., **55**, 283-304.

Svensson, U., and K. Haggkvist, 1990: "A two-equation turbulence model for canopy flows." J. Wind Eng. Indust. Aero., **35**, 201-211.

Shinn, J.H., 1971: "Steady-state two-dimensional air flow in forests and the disturbance of surface layer flow by a forest wall." Ph.D. thesis, University of Wisconsin, Madison. 91pp.

Takahashi, H., 1978: "Wind tunnel test on the effect of width of windbreaks on the wind speed distribution in leeward." J. Agr. Met. (Japan). **33**, 183-187.

Wang, H. and E.S. Takle, 1996: "On three-dimensionality of shelterbelt structure and its influences on shelter effects." Boundary Layer Meteorol. **79**, 83-105.

Wilson, J.D., and T.K. Flesch, 1996: "Diagnosing wind variation in periodic forest clearcuts, in relation to tree sway," preprint volume, 22nd Conference on Agricultural & Forest Meteorology, Am. Meteorol. Soc., pp 387-390.

Wilson, J.D., J.J. Finnigan, and M.R. Raupach, 1998: "A first-order closure for disturbed plant-canopy flows, and its application to winds in a canopy on a ridge." Quart. J. R. Meteorol. Soc. 124, 705-732. See also Preprint Volume, 11th Symposium of the AMS on Boundary Layers and Turbulence, pp539-542.

Appendix 1. Relative Impact of Wind Statistics on r.m.s. Wind Force

Eq. (1) for the specification of the root-mean-square wind force $\sigma_{u|u|}$ involves the mean wind velocity U, the variance σ_u^2, the skewness Sk_u and the kurtosis Kt_u. Is it equally important to specify each of these accurately? The differential $d\sigma^2_{u|u|}$ may be expressed as

$$\frac{d\sigma^2_{u|u|}}{\sigma^2_{u|u|}} = \frac{a_U \frac{dU}{U} + a_\sigma \frac{d\sigma_u}{\sigma_u} + a_S dSk_u + a_K dKt_u}{(Kt_u - 1) + 4\left(\frac{U}{\sigma_u}\right)^2 + 4\left(\frac{U}{\sigma_u}\right) S}$$

where the coefficients of the numerator are:

$$a_U = 8\left(\frac{U}{\sigma_u}\right)^2 + 4\left(\frac{U}{\sigma_u}\right) Sk_u \quad , \quad a_\sigma = 4(Kt_u - 1) + 8\left(\frac{U}{\sigma_u}\right)^2 + 12\left(\frac{U}{\sigma_u}\right) Sk_u$$

$$a_S = 4\left(\frac{U}{\sigma_u}\right) \quad , \quad a_K = 1$$

With $Kt_u = 4$, $Sk_u = 1$, and $U/\sigma_u = 1$, values that are typical of our clearing flows, we evaluated the partial fractional changes $d\sigma^2_{u|u|}/\sigma^2_{u|u|}$ caused by 10% changes in each of U, σ_u, Sk_u and Kt_u, ie. by $dU/U = 0.1$, etc. The outcomes, in order of increasing fractional response, were as follows: 1% response to 10% in Kt_u , 4% response to 10% in Sk_u , 11% response to 10% in U, and 28% response to 10% in σ_u.

Appendix 2. Role of the Coriolis Force in Canopy Flows

The canopy "wind spiral" has received little attention despite Shinn's (1971) early recognition of it, an exception being Holland (1989). Its origin is simple to give in qualitative terms: deep enough within a dense canopy ($z<<h$) the Coriolis force and the turbulent shear-stress are "small," and it follows that the mean wind is directed *parallel* to the large scale pressure gradient, implying (up to) a full 90° swing in direction between the Geostrophic-level, where the wind blows perpendicular to the pressure gradient, and ground-level. Shinn used the term "Quasi-Geotriptic" to describe that local force-balance, "a balance of the drag force and the pressure gradient force but with residual effect of the Coriolis force evident in the direction of the wind drift with respect to the geostrophic definition of the pressure gradient direction."

Dramatic directional shear is presumably then to be regarded as *normal*, in mid- and high-latitude canopies. It will have to be accounted for in scientific descriptions of many problems, eg. short range patterns of (pollen, seed, etc.) dispersion from localised sources. As regards forest-edge flows, we infer the force-balance may involve both horizontal velocity components in an essential way, ie. changes coupled through the Coriolis force may be important even when the flow has along-edge symmetry ($\partial/\partial y = 0$).

Appendix 3. Diagnosing Velocity Skewness

Our basis for determination of the alongwind velocity skewness $Sk_u = \langle u'^3 \rangle / \sigma_u^3$ was a simplified transport equation suggested by Hanjalic and Launder (1972, Appendix A; hereafter HL). Our disturbed canopy flow is more complex than the wall boundary-layer flow considered by HL, but we nevertheless adopted their analysis without change. As our closure resolved total TKE (k), but not the separate the components σ_u^2 (etc.), we assumed that *equilibrium* partitioning of TKE prevailed throughout our disturbed flow, ie. that everywhere

$$\sigma_u^2 \equiv \overline{u'^2} = \alpha_u \, k \qquad \textbf{(A1)}$$

Here $\alpha_u = c_e \, c_u^2$, $c_u \approx 2$ being the equilibrium value of the ratio σ_u / u_{*0}. The HL analysis, so simplified, results in the following transport equation for our two-dimensional, steady state case

$$U \frac{\partial \overline{u'^3}}{\partial x} + W \frac{\partial \overline{u'^3}}{\partial z} = -3 \, \alpha_u^2 \, k \frac{\partial k}{\partial x} - 3 \, \alpha_u \, \overline{u'w'} \frac{\partial k}{\partial z} - \frac{}{} \qquad \textbf{(A2)}$$

and implies that in undisturbed flow (ie. setting $\partial / \partial x = 0$),

$$Sk_u = - \kappa \frac{\overline{u' \, w'}}{\varepsilon \sqrt{k}} \frac{\partial k}{\partial z} \qquad \textbf{(A3)}$$

where $\kappa = 3 \, c_s' \, \alpha_u^{-1/2}$. According to Eq. (A3), the sign of Sk_u is controlled by the vertical gradient in TKE. This is surely an oversimplification, but we found that with $\kappa = 1$ (ie. $c_s' = \alpha_u^{1/2}/3$), Eq. (A3) gives a good prediction of the equilibrium velocity skewness in and above a model canopy in a wind tunnel.

For disturbed flows, after first obtaining the velocity and TKE fields, we solved Eq. (A2) for skewness. We added small artificial diffusion terms to Eq. (A2) and followed the numerical practise that is standard under SIMPLE.

Here the shear stress is assumed to be determined by the mean strain, in analogy with Newton's law for the *viscous* shear stresses. K is the "eddy viscosity," and may always be regarded as the product ($K = \lambda \Gamma$) of a turbulence lengthscale (λ) and velocity scale (Γ). Its specification, auspicious or otherwise, is often the key to success of a flow simulation. In the simplest flows, it can be prescribed algebraically. For example in the neutrally-stratified and undisturbed atmospheric surface layer (NSL), at heights $z >> z_0$, z_0 being the roughness length, it is well established that $K = k_v u_* z$, where $k_v \approx 0.4$ is von Karman's constant, and u_* is the friction velocity; ie. in the ideal NSL, $\lambda = k_v z$ and $\Gamma = u_*$. In more complex flows, one might obtain the velocity scale Γ from the mean velocity shear ($\Gamma = \lambda \partial U/\partial z$; Prandtl's closure); or, one might assume Γ to be proportional to $k^{1/2}$, and so obtain it by including (as one of the equations integrated) the transport equation for k (Prandtl-Kolmogorov closure). One step higher in closure-complexity, falls the popular "k-ε" model, wherein the lengthscale λ too is *calculated*, as $\lambda \propto k^{3/2}/\varepsilon$, by also including a transport equation for the rate (ε) of dissipation (by viscous forces) of TKE to heat. Or, one may abandon K-theory altogether, and include a simplified budget equation for τ , which can be derived from the Navier-Stokes equations ("higher-order closure"). For reasons discussed by Wilson et al. (1998), our preference in treating disturbed canopy flows is to use their variant of the K-closure, arguably the simplest applicable.

2.2. Simulations of Forest Edge Flow

Apparently the earliest numerical simulations of wind flow through a forest edge were by Li et al. (1990; hereafter LLM), and by Svensson and Haggkvist (1990). In both cases K-theory was used to relate the shear stress τ to the mean velocity gradients. However to introduce the possibility of counter-gradient turbulent momentum transport (ie. to allow that τ may transport mean momentum from regions of *low* mean speed to regions of *high* mean speed, which can happen in a flow of this type and is disallowed by K-theory), LLM used a heuristic modification of Eq. (5), first given by Li et al. (1985). The shear stress gradient in Eq. (4) was parametrized as:

$$\frac{\partial \tau}{\partial z} = - \frac{\partial}{\partial z} \left(K \left(\frac{\partial U}{\partial z} + \frac{\partial W}{\partial x} \right) \right) - c \left(U(h) - U(z) \right) \qquad \textbf{(6)}$$

where c is an empirical coefficient (presumably this additional term was included only within the canopy). The eddy viscosity was calculated using Prandtl's mixing-length formulation.

LLM simulated the field experiments of Raynor (1971), who reported cup windspeeds measured near the edge (x = 0) of a pine forest of height h = 10.5 m. For flow *into* the forest, the model replicated generally to within a few percent the observed windspeeds, which showed an abrupt but regular transition from the open-field profile-form ($U \propto \ln_e z$), to a canopy-type (inflexion-point) wind profile. The model reproduced an observed jet of high windspeeds penetrating into the canopy at low level (where the leaf area density was small) and visible as a secondary maximum in windspeed even at a distance 10h into the forest from the edge, but the authors did not state whether this feature depended on their having included the extra source in the U-mtm equation. In the case of flow *from* the forest, again model performance was excellent, reproducing the canopy wind profiles upstream from the edge, which though self-similar in form showed slight acceleration as the edge was approached. For both directions of flow, the authors emphasized the sizeable pressure

gradients affecting the flow near the forest edge (such pressure gradients apparently exert a large influence on the flow in our periodic cutblocks). The LLM model was later applied by Miller et al. (1991) to simulate forest clearings.

In a study concerned with efficient parametrization of forest effects in mesoscale models, Schilling (1991) reported the results of a low-resolution ($\Delta x = 500m$) simulation of flow through a wide clearing (width $X_C = 8$ km). Schilling adopted the Prandtl-Kolmogorov form of K-theory, ie. $K \propto \lambda k^{1/2}$ (velocity scale from TKE budget; imposed-lengthscale λ), but without adaptation of the lengthscale to account for the presence of the canopy. As our instrumented clearings are typified by X_C/h = 2-6, whereas Schilling's clearing is of entirely different aspect ratio $X_C/h = 400$, our simulations are completely different in scale.

Green et al. (1994) studied the flow through a stand of forest whose crosswind extent was 10h. They reported qualitative agreement between the mean velocity and the TKE as observed in a wind tunnel simulation, and as according to a numerical model based on a modified k-ε closure. Owing to the drag of vegetation, application of the k-ε model in presence of a canopy requires specification of the scale-range covered by TKE, and entails heuristic modifications of the k- and ε-equations. Such adjustments are arbitrary and ambiguous, and can have a large (100% or more) impact on numerical results, particularly for TKE (see Green et al.,1994, and Liu et al., 1996, for forest edge flow; and Wang and Takle, 1995, for windbreak flow).

Liu et al. (1996; hereafter LCBN) used the k-ε model to simulate the flow from a uniformly forested region into a clearing, comparing their model with wind-tunnel observations of Chen et al. (1995). Like Green et al. (1994), but slightly differently, they modified the TKE and dissipation equations of the standard k-ε model, in order to account for the influence of vegetation. Viewed on the large scale (5h x 35h; their Figures 2 and 3), the modelled mean velocity field (U) appears to be in excellent agreement with the observations, though it is the nature of side-by-side vector plots and contour plots to emphasize similarity rather than difference. Their Figure 4 compares modelled and measured vertical U-profiles, showing excellent quantitative conformity of model and data, except for sizeable discrepancies (order 100%) within about 3h from the forest edge. In that region the numerical model produced mean flow reversal near ground, while flutter-flags in the wind tunnel indicated intermittently reverse flow. The hot-film anemometers rectify reverse-velocities, so were in error in this region. Turbulent kinetic energy was also simulated well, but only provided that sources in the k- and ε-equations were adjusted. Without that step errors in k of order 100% occurred (their Figure 9). LCBN concluded their model was "less satisfactory in describing turbulent airflow over short distances downwind of forest edges."

Relative to the work described above, our present examination of flow in discontinuous forests has a more specific end in view: can we model the spatial variation of the lower order wind statistics sufficiently well that the implied spatial patterns in the r.m.s. wind force $\sigma_{u|u|}$ and (by virtue of our tree-sway model) tree sway σ_θ are realistic? While to all appearances the LCBN model may be quite capable of answering the question, we chose to investigate the matter using a model based on the simplest workable turbulence closure for disturbed canopy flows (Wilson et al., 1998; hereafter WFR), which through direct algebraic specification of the lengthscale, sidesteps the ambiguities of sources in the k- and ε- equations. The WFR model has already been tested, for both

uniform and disturbed canopy flows, more exhaustively than modified k-ε type models. In Section (3) we shall briefly describe the WFR model. In Sections (4,5) we show that without alteration, other than to parametrize the lengthscale adjustment withing clearings, the WFR model provides good simulations of others' experiments on clearing flows. In Section (6) we compare the WFR model against our measurements in the Hotchkiss cutblocks.

3. Wind Flow Model

We consider only flows whose mean properties are constant along an axis (y) oriented parallel to forest edges, and assume the mean wind is oriented approximately perpendicularly across the edges, ie. along the x-axis. When we apply our model to simulate our cutblock flows at Hotchkiss, that symmetry assumption is not exactly valid, for if X_C, Y_C denote the alongwind- and crosswind-widths of the cutblocks, then the aspect ratio Y_C/X_C was not very large (3, 15 for the wide and narrow cutblocks, respectively). However exploratory simulations with a 3-dimensional generalisation of our model (A. Tuzet, pers. comm.), permitting to account for finite aspect ratio of the clearing and/or for winds at oblique incidence, suggest our present neglect of y-dependence is not very consequential.

The wind flow model is a straightforward adaptation of that applied by Wilson et al. (1998; hereafter WFR) to calculate variation of the wind and turbulence in a model plant canopy on a wind-tunnel ridge. Finding it the simplest adequate treatment of disturbed canopy flow, WFR chose a first-order turbulence closure which has seen use in just about every type of micrometeorological flow (eg. the nocturnal boundary layer; Delage, 1974); the eddy viscosity is written $K \propto k^{1/2} \lambda$, where the turbulent kinetic energy (k) is obtained from a simplified transport equation, and the turbulence lengthscale λ is specified algebraically. Changes to the WFR model necessary for our present purposes are twofold in origin. Firstly, we require a flow domain extending several kilometers alongwind over the periodic cutblocks, and so must simulate a deep layer of the Planetary Boundary Layer (PBL): thus Coriolis effects couple the mean alongwind velocity component (U) to the crosswind velocity (V). Secondly, variation of the lengthscale across the cutblock-forest block boundaries must be parameterised. In addition to these changes, because the skewness of windspeed influences tree motion, we added an approximate transport equation for the third moment of the velocity fluctuation (Appendix 3).

Detailed explanation of the model equations and numerical procedure is given by WFR, and so we shall give only a brief description here. As our ultimate objective is the understanding or interpretation of patterns of tree windthrow, and (our own) observations are from periods of strong winds, we need not be concerned with temperature-stratification. We solved simplified U, V, W - momentum equations, that represent only what are (according to experience) the dominant terms (advection by the mean flow; pressure gradient; drag on trees; and divergence of the vertical turbulent momentum flux). These equations, cast in dimensionless form (using lengthscale h, and a velocity scale U_G defined below) are:

$$\frac{\partial}{\partial x}\left(U^2 - K_a \frac{\partial U}{\partial x} \right) + \frac{\partial}{\partial z}\left(UW - K \frac{\partial U}{\partial z} \right) = f\,(V - V_G) - \frac{\partial P}{\partial x} - c_d\, a^*\, U \sqrt{U^2 + V^2} \qquad (7)$$

$$\frac{\partial}{\partial x}\left(U\,V - K_a \frac{\partial V}{\partial x} \right) + \frac{\partial}{\partial z}\left(VW - K \frac{\partial V}{\partial z} \right) = f\,(U_G - U) - \frac{\partial P}{\partial y} - c_d\, a^*\, V \sqrt{U^2 + V^2} \qquad (8)$$

$$\frac{\partial}{\partial x}\left(UW - K_a \frac{\partial W}{\partial x} \right) + \frac{\partial}{\partial z}\left(W^2 - K_a \frac{\partial W}{\partial z} \right) = - \frac{\partial P}{\partial z} \qquad (9)$$

The incompressible continuity equation

$$\frac{\partial U}{\partial x} + \frac{\partial W}{\partial z} = 0 \qquad (10)$$

also applies ($\partial_y V = 0$ by assumption). In the momentum equations P is the local mean pressure perturbation (normalised on ρU_G^2); $f^* = fh/U_G$, where f is the Coriolis parameter; fU_G, fV_G are the components of the large-scale background pressure gradient, where (U_G, V_G) are the components of a nominal "Geostrophic" wind aloft; c_d is the bulk drag coefficient of trees; and $a^* = ah$, where a is the area density ($m^2.m^{-3}$) of tree parts (variable through cutblocks and forest blocks). K_a is a small artificial viscosity/diffusivity, included to ensure numerical stability, while K is the "true" eddy viscosity, estimated as

$$K = \lambda(x,z)\, \sqrt{c_e\, k(x,z)} \qquad (11)$$

In Eq. (11) the constant $c_e = u_{*0}^2/k_0(h)$, where $-u_{*0}^2$, $k_0(h)$ are the shear stress and the TKE at height $z = h$ under the reference condition of a uniform forest canopy; $\lambda(x,z)$ is a turbulence lengthscale; and k(x,z) is the TKE determined from the approximate TKE budget:

$$\frac{\partial}{\partial x}\left(U\,k - K_a \frac{\partial k}{\partial x} \right) + \frac{\partial}{\partial z}\left(W\,k - \mu\, K \frac{\partial k}{\partial z} \right) = K\left(\left(\frac{\partial U}{\partial z} \right)^2 + \left(\frac{\partial V}{\partial z} \right)^2 \right) - \varepsilon \qquad (12)$$

The constant μ represents the ratio of the effective eddy diffusivity for TKE to the eddy viscosity. The TKE dissipation rate (ε) was specified as

$$\varepsilon = \max \left[\frac{(c_e k)^{\frac{3}{2}}}{\lambda} , \alpha c_d a^* \sqrt{U^2 + V^2}\, k \right] \quad (13)$$

where within the canopy the wake conversion term dominates. The rationale for this closure is given by WFR.

3.1. Specification of the lengthscale

Like Li et al (1990), we anticipated it would be necessary for forest-edge flows to interpolate for the lengthscale between two limiting cases: the infinite open plain lengthscale λ_P , and the infinite-forest lengthscale λ_F. However our specification of λ_F differs from theirs, and we interpolated differently. Over flat, open ground during neutral stratification, the lengthscale may be parameterised as

$$\frac{1}{\lambda_P} = \frac{1}{k_v z} + \frac{1}{L_\infty} \quad (14)$$

where L_∞ is Blakadar's (1962) lengthscale, limiting growth of the lengthscale in the PBL. In dimensional terms, L_∞ is often estimated (eg. Delage, 1974) as approximately

$$L_\infty = 0.0004 \frac{U_G}{f} \quad (15)$$

Rather than use (as did Li et al.) an in-forest lengthscale (λ_F) based on an equilibrium parametrization tuned to canopy area density, we followed WFR and wrote $\lambda = \max(\lambda_i, \lambda_o)$, where

$$\frac{1}{\lambda_i} = \frac{1}{k_v z} + \frac{1}{\lambda_c} , \quad \frac{1}{\lambda_o} = \frac{1}{k_v (z - d)} + \frac{1}{L_\infty} \quad (16)$$

λ_c is a canopy "shear length scale,"

$$\lambda_c = c \sqrt{k(h)} \left(\frac{\partial S}{\partial z} \right)_h^{-1} \quad (17)$$

where $S = (U^2+V^2)^{1/2}$ is the "cup" windspeed; this parametrization links the lengthscale in and near the canopy to the wind shear at canopy top, which may vary substantially across forest blocks.

These two limiting expressions for the lengthscale (infinite clearing, infinite forest) may be conveniently blended into a universal expression valid at all locations, simply by replacing the displacement length d in Eq. (16) with an effective displacement length d_e,

$$d_e = \frac{d}{1 + \gamma (x - x_0)} \qquad \textbf{(18)}$$

where d ($\approx$⅔h) is the equilibrium displacement length, x_0 ($\leq$x) denotes the leeward edge of the forest block lying immediately upwind of the clearing in question, and γ is an empirical constant. Upon passage from clearing back into forest, we immediately restored the equilibrium displacement length, $d_e = d$. In general, our simulations were rather insensitive to our treatment of the lengthscale transition, although the calculated pattern of TKE for the Hotchkiss cutblock flow showed some reaction to the choices made.

3.2. Specifying adjustable constants

The artificial diffusivity was set at $K_a = 0.001 h U_G$, and had insignificant effect on the simulations other than to ensure numerical stability.

The WFR closure involves three closure constants. These were optimised by WFR ($c = \alpha = 1$, $\mu = 0.2$) by matching equilibrium solutions of the equations to wind tunnel observations in and above a uniform model canopy, and were not changed in the present work. Well above the canopy it would be more consistent with others' shear layer simulations to set the ratio (μ) of the diffusivity for TKE to the eddy viscosity as $\mu = 1$; but our simulations are focused on flow changes very near ground, and we incorporated the outer boundary-layer simply as an appropriate domain within which those changes occurred, not as an end in itself.

Other rather familiar parameters have appeared in our model equations, as constants which we want to clearly distinguish from the closure parameters - to emphasize that the success of our simulations does not depend on any flexibility in their specification: they are c_e, and the Coriolis parameter, f. Typically in flow above a uniform canopy, $\sigma_{u,v,w}/u_{*0} \approx 2,2,1.3$, implying $c_e \approx 0.2$: we used $c_e = 0.18$. And we set $f^* = (hf/U_G) = 1.5 \times 10^{-4}$, which represents moderately windy conditions at middle lattitudes over a tall forest.

It only remained in our present applications of the wind flow model to specify the lengthscale adjustment parameter (γ); and the forest-specific canopy area density a(z), and drag coefficient $c_d(z)$. These choices will be given for each case study.

3.3. Numerical details & boundary conditions

Numerical details specific to each case-study will be given in following sections, but we shall here cover the general scheme we employed in integrating the governing equations. We used Patankar's (1980) well-documented **S**emi-**I**mplicit **M**ethod for **P**ressure-**L**inked **E**quations (SIMPLE) to solve the equations. Inflow profiles of U, V, k were obtained as equilibrium ($\partial/\partial x = 0$) solutions

of the equations (with or without a forest, as appropriate), and imposed far upwind from the region of interest. Far downwind, at the outflow boundary, we set $\partial U/\partial x = \partial V/\partial x = \partial k/\partial x = W = 0$.

3.3.1. Upper boundary conditions

For the Hotchkiss simulations, we set $U = U_G = 1$, $V = V_G$, $W = k = 0$. All velocities were scaled on U_G, thus the specification $U_G = 1$; V_G was adjusted so that near the top of the canopy, $V \approx 0$. For simulation of the wind-tunnel flow, we placed the uppermost W gridpoint at the top of the domain, so that the shear stress along that boundary is the required condition on the U-momentum balance. Either we specified that shear stress aloft as undisturbed (u_{*0}^2) and constituting the velocity scale for the simulation; or, if we wished to properly account for stress and TKE gradients at $z>h$ in the incident flow, we incorporated an effective background pressure gradient, and specified the stress aloft as vanishing; ie. if the measured stress gradient above the canopy was $(\partial\tau/\partial z)_0$ then we applied a background pressure gradient $(1/\rho)(\partial P/\partial x)_0 = (\partial\tau/\partial z)_0$ throughout the layer $z \le z_{mx} = h+\tau(h)/(\partial\tau/\partial z)_0$ so as to give rise to a linear variation of shear stress from 0 at $z = z_{mx}$ to $\tau(h)$ at $z = h$.

3.3.2. Lower boundary conditions

Two choices were explored for the lower boundary conditions. Initially, we set the lowest U,V gridpoints on ground, where $U = V = 0$. Then the lowest vertical velocity and TKE gridpoints lie above ground, within normal control volumes, for which the required boundary condition is a specification of the *flux* to ground. We set those fluxes to zero. This direct imposition of the no-slip condition obviates necessity to assume a "wall function" relationship between surface shear-stress and near-wall windspeed, and seems the better choice within a fully forested domain.

However far downwind in sufficiently wide clearings, naturally one expects any reasonable model to develop the usual semi-logarithmic equilibrium wind profile; and if one did not *impose* a roughness length in the clearings, then a value implicit to the model itself, but which is unknown *a priori*, must eventuate. To circumvent that curious ambiguity, in all reported simulations we have set the lowest vertical velocity and TKE gridpoints on ground. Consequently the lowest U,V gridpoints lay above ground, at $z = z_P$, and a condition on the corresponding vertical momentum fluxes to ground was required. We specified $\langle u'w' \rangle = -u_{*u}^2$, $\langle v'w' \rangle = -u_{*v}^2$, where:

$$
\begin{aligned}
u_{*u} &= k_v \, U_P / \ln\left(\frac{z_P}{z_0}\right) \\
u_{*v} &= k_v \, V_P / \ln\left(\frac{z_P}{z_0}\right) \\
u_*^2 &= u_{*u}^2 + u_{*v}^2
\end{aligned}
\qquad \textbf{(19)}
$$

Of course, these wall relationships are not valid within the canopy (nor for that matter in regions of highly-disturbed flow), but as the shear stress on ground beneath a dense canopy is very small, its miscalculation (by the above relationships) is expected to carry negligible penalty. It is interesting

CHAPTER 5

USING A WIND FLOW MODEL TO IDENTIFY HARVEST DESIGNS THAT REDUCE WINDTHROW

T.K. Flesch[1], J. D. Wilson[1], D.A. MacIsaac[2], and S.J. Lux[2]
[1]University of Alberta and [2]Canadian Forest Service, Edmonton, Canada

1. Introduction

Reducing the risk of windthrow can be an important criterion in designing a partial-cut forest harvest system. Yet our understanding of how harvesting patterns influence the risk of subsequent windthrow of unharvested trees is incomplete. How might a forest manager identify a harvest design that provides effective wind protection?

Computer wind flow models are a potential means of investigating the wind pattern associated with a harvest design. The cost is negligible relative to that of full scale or wind tunnel trials, and the number of harvest configurations that can be simulated is limitless. The objective of this study is to demonstrate the use of a wind model for identifying harvest systems that minimize windthrow. Our context, and observational basis, is a management trial under way in Alberta, Canada, at a location called Hotchkiss (Navratil et al., 1994).

2. Shelterwood Harvesting System

In the aspen (*Populus tremuloides*) and white spruce (*Picea glauca*) dominated boreal mixedwoods of western Canada, researchers and foresters are investigating harvesting techniques that preserve the immature spruce understory, with a goal of perpetuating a healthy mixedwood. One approach is the "two-stage" harvesting and stand tending model (Brace and Bella 1988) in which the overstory aspen is harvested at 60 years, leaving the immature understory spruce (Figure 5.1). Sixty years later a second harvest is scheduled to remove the spruce that has grown to maturity, as well as a second cohort of regenerated aspen.

An obstacle to this two-stage harvest is the susceptibility of the immature spruce to windthrow after aspen removal. One approach is to employ a one-pass modified uniform shelterwood (hereafter referred to as a shelterwood design). In this system the aspen is harvested in narrow cutblock strips that are left surrounded by unharvested "shelterwood" (Figure 5.2). These shelterwood strips provide wind shelter for immature spruce in the cutblocks. Flesch and Wilson (1999a) found the average wind velocity (U) and the turbulent kinetic energy (k) were strongly reduced along the upwind edge of these cutblocks, and field observations confirm this translates into reduced windthrow.

The question that immediately arises is, how wide ought the cutblocks and protecting shelterwood strips be, relative to forest canopy height (h), for adequate wind protection?

3. Predicting Wind Shelter

3.1. *Relating Wind Statistics to Windthrow*

We consider the instantaneous wind "force" acting on a tree as (proportional to) $u|u|$, where u is the instantaneous horizontal wind velocity (in the x, i.e., alongwind, direction) at a nearby point. Flesch and Wilson (1999b) noted that the variance of the wind force ($\sigma^2_{u|u|}$), observed at height $z = 0.4h$, correlated closely with the variance (σ_θ^2) of the sway angle of a sample of remnant spruce (of

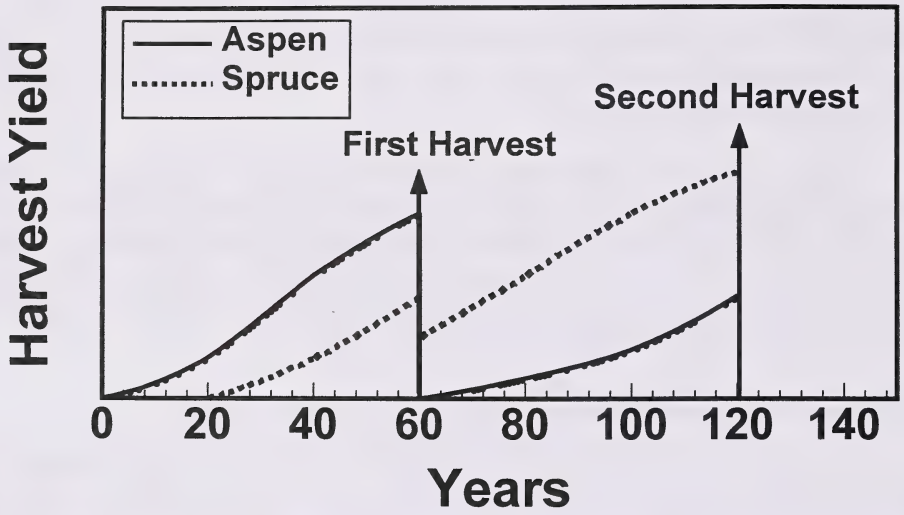

Figure 5.1. Generalized two-stage harvest model for an aspen-spruce mixedwood forest (from Brace and Bella 1988).

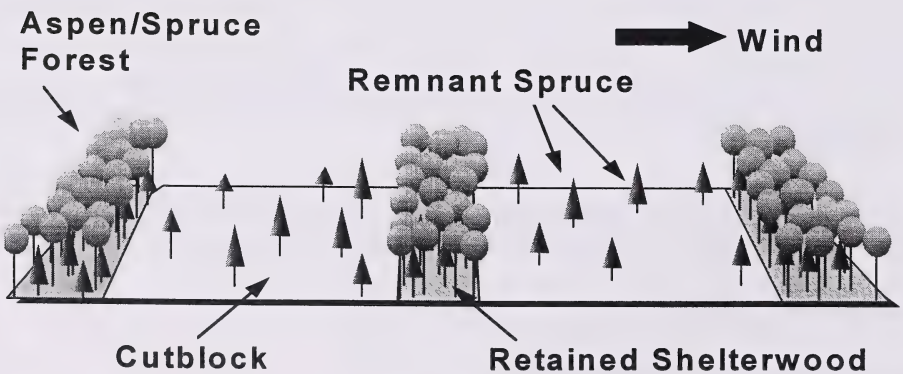

Figure 5.2. Idealised view of cutblocks

height $h_r \approx 0.5h$) surveyed at the Hotchkiss site. While this correlation may not be universally true, it can be exploited at Hotchkiss: by assuming greater sway means greater strain on the tree/soil complex, and greater likelihood of windthrow, we may use $\sigma_{u|u|}$ as a "flag" to identify zones of likely windthrow. We approximate $\sigma_{u|u|}$ as

$$\sigma_{u|u|} \approx \sqrt{3(c_u k)^2 + 4U^2(c_u k) + 4U(c_u k)^{3/2}} \quad , \tag{1}$$

by assuming $\sigma_u^2 \propto k$ (with fixed proportionality constant), and setting skewness $Sk_u = 1$ and kurtosis $Kt_u = 4$ (values representative of the Hotchkiss flows; Chapter 2). Taking typical k partitioning $\sigma_u:\sigma_v:\sigma_w = 2:2:1.3$, we have $c_u = 0.82$. We may now map the relative probability of windthrow using a wind model which diagnose the spatial pattern of U and k across a harvest design.

3.2. Wind Flow Model

Our wind model, shown in Chapter 4 to agree well with measurements of U, k in cutblocks at Hotchkiss, is based on the mean momentum equations, closed using eddy viscosity $K \propto k^{1/2} \lambda$; k is obtained from a simplified transport equation, and the turbulent lengthscale λ is specified algebraically. For the present work crosswind (y) symmetry is assumed, and a flow near-normally incident to the forest edges is simulated by varying the tree drag coefficient with along-wind position (x), the drag coefficient vanishing within cutblocks.

Being only local in its scope, i.e., covering a horizontal domain of only a few kilometers, a wind model is able to diagnose not $\sigma_{u|u|}$, but only a ratio $\sigma_{u|u|}/U^2_{clr}$, where U_{clr} is a normalising reference velocity. This was chosen to be the average windspeed as specified/measured in a nearby "reference clearing," large enough to be considered as approximating a local "weather station." Given a history of average windspeed (and direction) at such a station, *and* if it were the case that our model was properly three-dimensional, *and* if we had specified (mechanically) each of the remnant trees in question, *and* if knew what threshold value for $\sigma_{u|u|}$ would suffice to "knock down" such trees, then we could interpret on a theoretical basis the windthrow losses, hour by hour, over that season, at that location, of that tree-type.

The trees actually blown down at Hotchkiss over the period of record available to us were variable in their particulars; having blown down at unknown times, during unknown winds, and wind directions. Thus several circumstances prevent us from testing our theory in a rigorous manner, though none compromise the methodology we suggest - for the model *can* be extended to three dimensions, linked to an actual climatology, and tested relative to data gathered storm-by-storm.

Here we resorted to a "calibration," in the following sense. We noted that two years after aspen harvest at Hotchkiss, remnant spruce windthrow in a particular cutblock (width $X_c = 6.1h$) was common beyond distances 2.5h downwind from the forest edge. A wind simulation for that cutblock suggested that beyond x = 2.5h, the normalised wind force $\sigma_{u|u|}/U^2_{clr}$ (hereafter labeled Φ) exceeded 0.25. So we defined as a threshold for severe incidence of windthrow, the value $\Phi = 0.25$. Of course the criterion is strictly valid (if at all) specifically for that 2 year wind climatology, and the particular tree characteristics at Hotchkiss.

4. Accuracy of Model Predictions

We investigated five of the harvest designs at Hotchkiss, each "design" being a periodic series of cutblocks and forest blocks, of proportions (X_c, X_f). For each of these cases we used the flow model to create a dichotomous risk map: identifying the risk zone(s) where $\Phi > 0.25$. To each harvest design we assigned a windthrow severity rating, based on the fractional area with $\Phi > 0.25$ (see Table 5.1). These were subsequently (and independently) compared with "observed" ratings, based on the actual proportion of remnant spruce losses.

Table 5.1. Definition of windthrow ratings

Model Rating	
% area with $\Phi > 0.25$	rating
< 10	1
10 - 30	2
30 - 50	3
50 - 70	4
> 70	5

Observed Rating	
% uprooted trees	rating
< 5	1
5 - 10	2
10 - 15	3
15 - 25	4
> 25	5

According to Figure 5.3, modelled and observed-ratings compare quite well. The model correctly predicted the increased risk as cutblock widths increased from X_c = 2h to 4h to 6h. We acknowledge the ambiguity inherent in our using different (and rather loose) criteria to arrive at model- and observed- ratings of windthrow. Nevertheless, we do not think Figure 5.3 is just a spurious result of the respective (and independent) choices made by the two teams (University of Alberta, wind model; Canadian Forest Service, windthrow survey).

5. Investigating an Optimum Design

One might ideally define an optimum shelterwood design as one eliminating windthrow while minimizing the percentage of forest retained as windbreak strips (maximizing aspen harvest), and maximizing the width of the individual cutblocks (for efficient use of harvest equipment). The wind model was used to search for an optimum design (for the circumstances at Hotchkiss).

Designs were examined in which the harvest domain (sequence of cutblocks and shelterwood strips) spanned approximately 40h. We simulated designs where 10%, 20%, 25%, 30%, and 35% of the forest was retained as shelterwood strips (of varying width X_f). For each retention level, cutblock width was varied from X_c = 1 to 6h. The resulting cutblock/shelterwood strips were distributed across the harvest domain. For example, a 20% forest retention with X_c = 2h would have a recurring pattern X_c, X_f = (2h, 0.5h).

Figure 5.4 shows the predicted patterns of U, k, and the normalised wind force Φ, for a design in which only 10% of the forest was retained, and X_c = 2h. In this case both U and k were high compared with designs retaining more forest, but the overall wind pattern was common to all

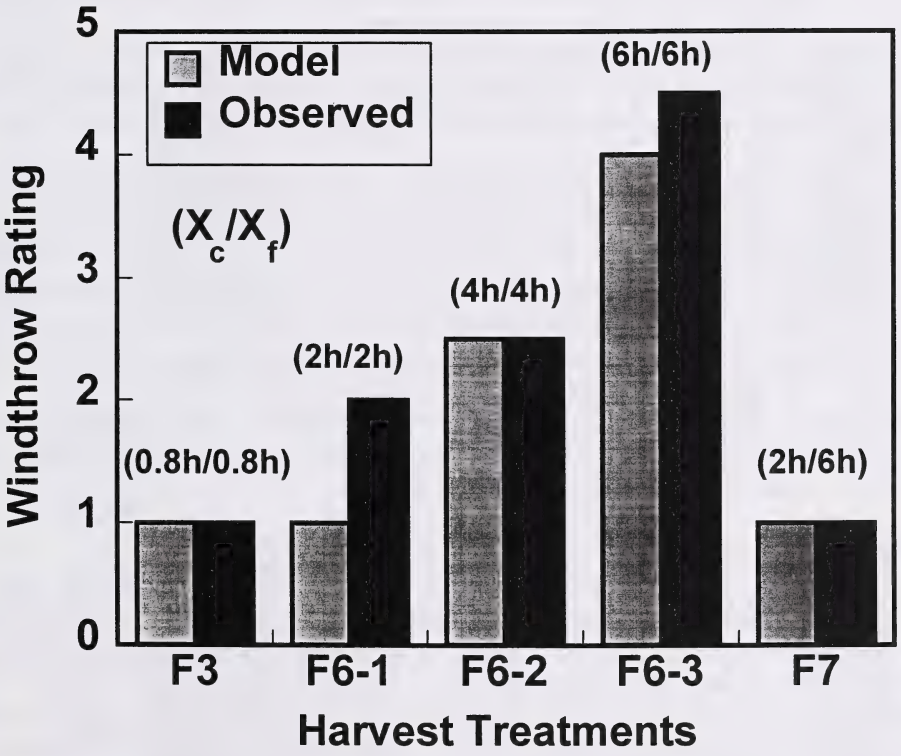

Figure 5.3. Comparison of windthrow risk rating from the wind model ("model") with the rating based on observed windthrow ("observed"), for five harvest designs. A rating of 1 is low risk and 5 is high risk. The ratio of the cutblock width (X_c) to forest width (X_f) is given above the bars.

the designs. In all cases U and k were low at the upwind edge of the harvest domain, and initially increased as x increased. Maximum U occurred between x = 10h and 15h, while the maximum k was between x = 3h and 6h. This gave a maximum Φ between x = 3h and 10h. We conclude therefore, that the maximum likelihood of windthrow will be in the area between x = 3 and 10h, regardless of the design. For locations x > 20h, there was a plateau in Φ, with succeeding cutblocks being essentially identical to each other.

In Figure 5.5 we plot the percentage of risk area (where $\Phi > 0.25$) associated with our hypothetical designs, showing the effect of forest retention and cutblock width. Several conclusions are evident. First, the greater the amount of retained forest, the greater the wind protection. This is intuitive: the more forest, the greater the wind drag, and the lower are U and k. Particularly impressive was the large drop in risk area as the retained forest increased from 10 to 20%. Our predictions indicate that a 10% level of forest retention is inadequate to provide effective wind shelter (for typical remnant spruce under the recent Hotchkiss wind climatology).

The second conclusion we draw from Figure 5.5 is that the risk area increases as the cutblock width increases. Looking at the 30% forest retention curve we see that the risk area increased from 0 to 49% as X_c increased from 1h to 6h. Most of this increase occurred as X_c increased beyond 2h: in other words X_c = 1h was not greatly superior to X_c = 2h. This suggests that cutblock width should not much exceed X_c = 2h, in order to minimize windthrow risk. Delineation of a truly optimal design requires economic and engineering judgements to supplement these "environmental" calculations. But Figure 5.5 does lay out likely bounds to an optimum design. Clearly 10% forest retention does not provide adequate wind protection, while retaining more than 30% is unnecessary. Cutblocks with $X_c > 3h$ are at significantly higher risk than narrower cutblocks, while little benefit comes from using cutblocks narrower than X_c = 2h.

6. Conclusions.

We used a wind flow model (and a supplementary site-, season-, tree-specific criterion) to predict windthrow likelihood in various shelterwood harvest designs, demonstrating the potential of wind models as an easy, inexpensive, and quick means of assessing harvest designs. We consider the risk area percentages we have cited as carrying some uncertainty, and one ought certainly to be cautious about assuming them broadly valid (i.e., as covering other sites with other tree types and wind climatologies). We reiterate the principal approximations and restrictions introduced: that winds in the y direction are unimportant in these designs; that $\sigma_{u|u|}$ at z = 0.4 h is well correlated with tree sway; that tree sway is an adequate index for windthrow; and that regions where $\Phi > 0.25$ correspond categorically to "severe" long term windthrow.

We consider that the proper role for a wind flow model is in guiding field trials. A wind model allows the testing of large numbers of possible harvest configurations, from which a set of promising designs could be chosen. The end result would be a smaller and less costly experiment than would otherwise be the case.

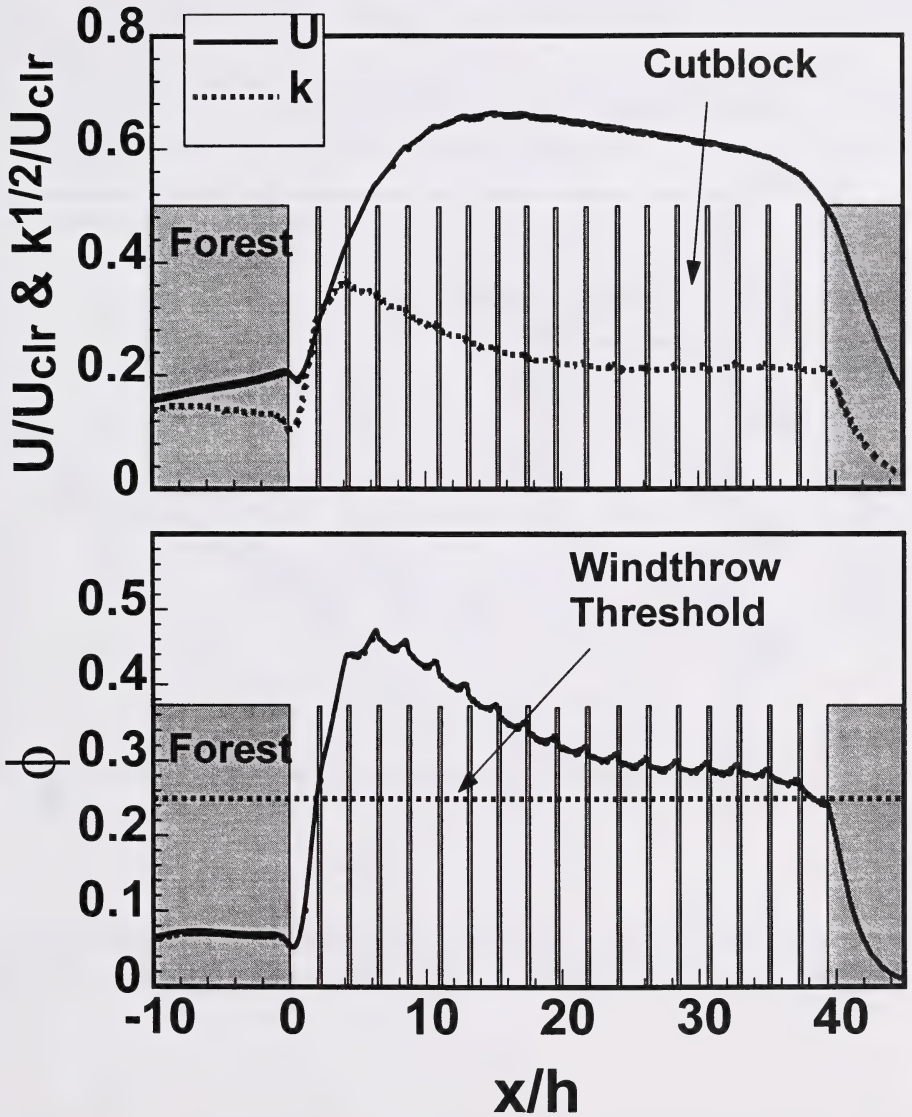

Figure 5.4. Predicted average wind velocity (U), turbulent kinetic energy (k), and normalised wind force (φ) across a harvest design ($X_c = 2h$, $X_f = 0.2h$). Shaded areas are unharvested forest.

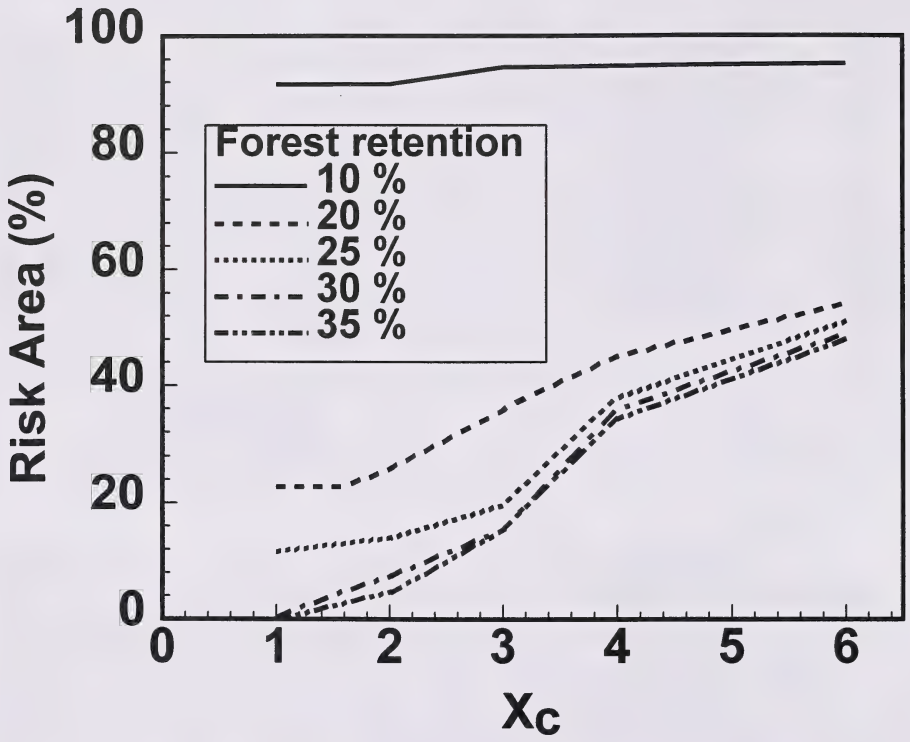

Figure 5.5. Predicted windthrow risk area in harvest domain (40h in width) plotted as a function of cutblock width (X_c), for five forest retention levels (10, 20, 25, 30, and 35%).

7. References

Brace, L.G; Bella, I.E. 1988. Understanding the understory: dilemma and opportunity. Pages 69-86 *in* J.K. Samoil, ed. Management and Utilization of Northern Mixedwoods. Proc. Symp., April 11-14 1988, Edmonton, Alberta, Can. For. Serv., North. For. Cent. Edmonton, AB, NOR-X-296.

Navratil, S., Brace, L. G., Sauder, E. A., and Lux, S. 1994. Silvicultural and harvesting options to favor immature white spruce and aspen regeneration in boreal mixedwoods. Can. For. Serv., Northern Forestry Centre, Edmonton, AB. Info. Rep. NOR-X-337. 74 p. + appendices.